An organelle pathogen sensor reveals factors required for mediating trans-kingdom membrane contact sites

Dissertation
zur
Erlangung des Doktorgrades
der Mathematisch-Naturwissenschaftlichen Fakultät
der Universität zu Köln

vorgelegt von

Chahat Mehra
aus Varanasi, Indien

Accepted in the year 2025

Abstract

Toxoplasma gondii (*Toxoplasma*) is a human parasite that establishes a life-long infection in one-third of the world's population although prevalence can vary depending on the country. In Germany for example more than 50% of the population over age 50 are estimated to be seropositive for *Toxoplasma*. Thus, defining the mechanisms by which *Toxoplasma* engages with the host cells can lead to the development of better therapeutics. A common consequence of infection with *Toxoplasma* is the formation of trans-kingdom membrane contact sites (MCS) between the vacuole of *Toxoplasma* and host mitochondria and host endoplasmic reticulum (ER). Although the association of host ER with the vacuole was first described in the early 1970s neither of the molecular components that mediate this interaction have been identified thus far.

Here, we investigated the molecular machinery that mediates the MCS between *Toxoplasma* and ER. To this end, we developed a split-GFP based sensor where GFP reconstitution indicates successful formation of MCS between the pathogen and host organelles. To validate our sensor for FACS based CRISPR-Cas9 screening, I first applied it to monitor the known mitochondria- *Toxoplasma* MCS. As expected, GFP reconstitution occurred at these contact sites but failed to do so in the absence of the *Toxoplasma* tether TgMAF1 or the host counterpart TOM70, confirming the sensors specificity. I then adapted our sensor to study host ER-*Toxoplasma* MCS and performed a *Toxoplasma* effector protein targeted loss-of-function CRISPR screen. I found that *Toxoplasma* rhoptry protein 1 (TgROP1) is required for mediating *Toxoplasma*-ER MCS. Interestingly, TgROP1 contains putative FFAT [(two phenylalanines (FF) in an acidic tract (AT)] motifs, that are regions known to interact with ER membrane proteins VAPA/VAPB (VAPs). Subsequent work identified VAPs as required to mediate MCS with the *Toxoplasma* vacuole and mutating the FFAT-binding domain of VAPs reduced this interaction.

Our findings reveal that *Toxoplasma* exploits a mechanism like host proteins to establish MCS with host organelles. This work advances our current understanding of host

pathogen MCS and lays the foundation for future studies investigating their functional consequences on infection outcomes.

Table of contents

Abstract II
1 Introduction 1
1.1 Membrane contact sites 1
1.2 MCS proteome 2
1.3 Methods to identify proteins at MCS 5
1.4 Functions of membrane contact sites 8
1.5 Host-pathogen membrane contact sites 14
1.6 *Toxoplasma gondii*- a brief history 14
1.7 The intracellular niche of *Toxoplasma gondii* 16
1.8 Two *Toxoplasma* organelles that affect host functions 18
1.9 Host mitochondrial association 19
1.10 Host endoplasmic reticulum association 22
2 Aims of the thesis 27
3 Results 28
3.1 Identification of proteins mediating host ER- *Toxoplasma* MCS. 28
3.2 Further characterization of the host-microbe split-GFP system 82
4 Discussion 88
4.1 The molecular nature of the interaction between TgROP1 and VAPs 89
4.2 What is the function of the host ER-*Toxoplasma* MCS- friend or foe? 91
4.3 Why are host MCS proteins targeted by pathogens? 94
4.4 Tug of war- hERa versus HMA 95
4.5 Can our host-microbe sensor be used to study MCS with other pathogens? 96
5 List of abbreviations 99
6 References 102

1 Introduction

1.1 Membrane contact sites

Eukaryotic cells are arranged in membrane-bound organelles (such as mitochondria, endoplasmic reticulum, lysosomes and the Golgi apparatus), and communication between organelles is crucial to maintain cellular physiology (Scorrano et al., 2019; Voeltz et al., 2024). Organelles communicate in two main ways: via vesicular trafficking pathways and membrane contact sites (MCS). MCS are defined as two membranes typically within a 10-30 nm distance (ranging up to 80 nm) and held together by tethers on juxtaposed membranes (Scorrano et al., 2019). The first observations of a MCS dates to 1956, where in liver cells tubule-like structures which, we now know to be the endoplasmic reticulum (ER) (formerly called ergastoplasm) were observed organizing near the mitochondria (Bernhard & Roullier, 1956). However, due to a lack of biological relevance associated with this observation the organelle-organelle MCS field stagnated.

This field began to gain momentum upon publication of two landmark papers that suggested that mitochondria-ER MCS are sites of lipid synthesis and calcium transfer (Rizzuto et al., 1998; Vance, 1990). The first study to report a function associated to a contact site was from biochemical experiments where a fraction of rat liver mitochondria was enriched with lipid synthesis enzymes belonging to the ER (Vance, 1990). Subsequently, mitochondria-ER MCS were reported to allow Ca^{2+} transfer from the ER to the mitochondria (Rizzuto et al., 1998). For a long time, the view in the field was that the ER is at the center of MCS formation in a eukaryotic cell (H. Wu et al., 2018). Further breakthrough in our understanding of MCS came from the advent of fluorescence microscopy approaches that have now revealed the extent to which virtually all organelles are in contact with one another (Fig. 1.1) (X. Huang et al., 2020; Valm et al., 2017). Generally, four main characteristics are associated with a contact site: protein tethers that hold the membranes together, lack of fusion between the two membranes, the contact site mediates a specific function in the cell, and it has a defined proteome/lipidome (Scorrano et al., 2019). This section will discuss protein composition

of membrane contact sites, their functions, methods to investigate new MCS and the advances in the emerging field of host pathogen MCS, all with a focus on MCS with the endoplasmic reticulum.

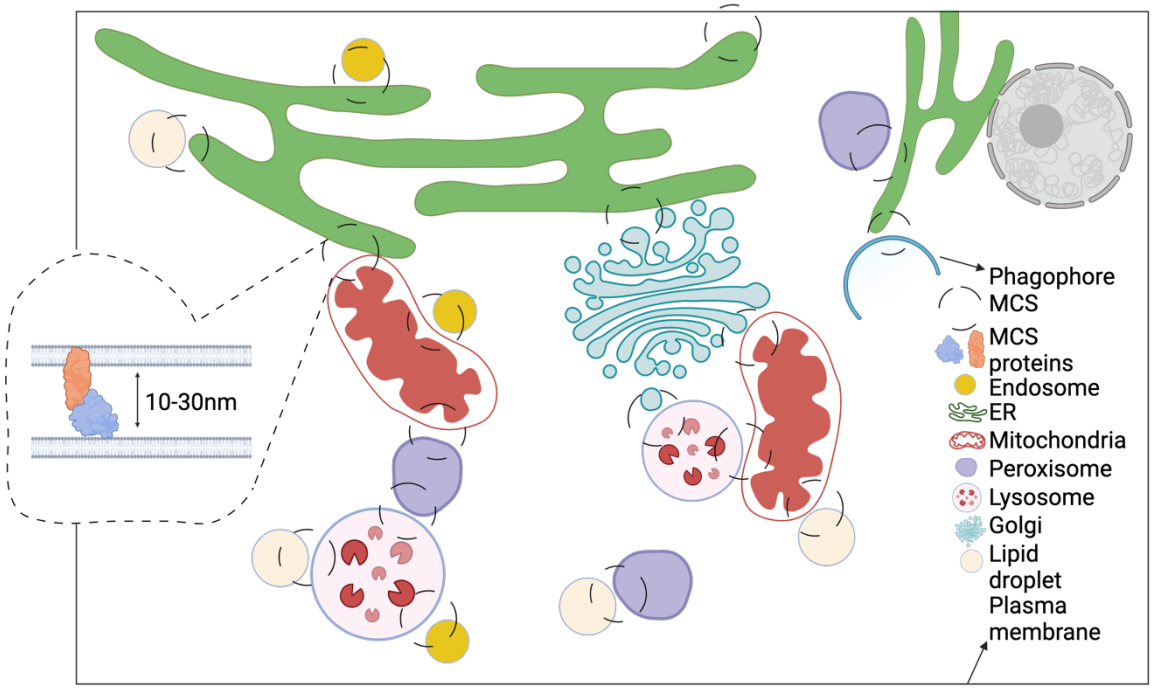

Fig. 1.1: Inter-organellar membrane contact sites (MCS) in a cell. The figures made in this chapter were generated with biorender.com.

1.2 MCS proteome

MCS can be homotypic (same membranes) or heterotypic (between two different membranes) and static or dynamic in nature. MCS formation is not a random event but is defined by the presence of specialized proteins at these regions (Eisenberg-Bord et al., 2016; Scorrano et al., 2019). Furthermore, the proteome of a contact site is of great importance as it can provide insights into the functions associated with it. The three main types of proteins found at MCS are molecular tethers, functional and regulatory proteins (Eisenberg-Bord et al., 2016). Briefly, molecular tethers physically bring the membranes together. The functional proteins may execute specific roles such as non-vesicular transfer of lipids. Last, the regulatory proteins can integrate environmental signals to

regulate the size/ number of contacts based on cellular need (Eisenberg-Bord et al., 2016; Scorrano et al., 2019). These roles are not mutually exclusive and MCS-resident proteins can exert more than one of these functions. For example, yeast protein Lam6 is a member of many MCS and works both as a tether and a functional protein due to its role in facilitating sterol transfer at mitochondria-ER MCS (Elbaz-Alon et al., 2015; Kornmann et al., 2009). While some MCS proteins mediate several functions at different MCS, sometimes at a MCS a combination of proteins can be found. A notable example of this are mitochondria associated membranes (MAMs) that are regions of membrane continuity between ER and mitochondria where several proteins have been identified enabling a multitude of functions at these sites (Barazzuol et al., 2021).

1.2.1 Definition of a MCS tether

The primary function of protein tethers at MCS is to bring two membranes in close apposition preventing membrane fusion (Eisenberg-Bord et al., 2016; Scorrano et al., 2019). Therefore, protein tethers need to be targeted to specific membranes to exert their functions. Thus, they usually contain either transmembrane domains (TM) or membrane targeting domains such as a pleckstrin homology (PH) domain that can bind phosphatidylinositides (PI) in membranes (Eisenberg-Bord et al., 2016). Generally, to define a protein as a tether it must fulfil one or more of the following criteria: 1) localize and be enriched at the MCS, 2) its loss must reduce the extent of MCS formation, 3) its deletion should affect the physiological processes associated with the MCS, 4) its overexpression may increase the number and/or size of MCS and 5) either as a single protein or in a complex it brings the two membranes in close proximity (Eisenberg-Bord et al., 2016; Scorrano et al., 2019).

1.2.2 VAP proteins- promiscuous ER tethers

The most common tethers are ER-localized vesicle-associated membrane protein (VAMP)-associated proteins (VAPs) that mediate MCS formation between ER and various organelles (Fig. 1.2) (Murphy & Levine, 2016; Obara et al., 2024; H. Wu et al., 2018). VAP proteins are conserved across all eukaryotes and the two most widely studied VAP

proteins are: VAPA and VAPB. These proteins are highly homologous and often have redundant functions in mediating MCS with the ER (James & Kehlenbach, 2021; Murphy & Levine, 2016). Both VAPA and VAPB (hereafter collectively referred to as VAP) are tail anchored proteins containing a N-terminus major sperm protein (MSP) domain, a predicted coiled-coil domain and a transmembrane domain (Fig. 1.2) (James & Kehlenbach, 2021; Nishimura et al., 1999).

Most interactions of VAP proteins occur with proteins containing a 7 amino acid sequence, known as the FFAT [two phenylalanines (FF) in an acidic tract (AT)] motif (Loewen et al., 2003; Murphy & Levine, 2016). The FFAT motif contains a core defined by the following amino acids: E_1-F/Y_2-F_3-D_4-A_5-x-E_7 (where x can be any amino acid, and the numbers indicate the amino acid positions). The residues immediately adjacent, particularly upstream to the core sequence comprises typically of acidic amino acids (Loewen et al., 2003; Murphy & Levine, 2016). Furthermore, it is now known that only position two in the core sequence of the original motif is essential and amino acid substitutions are tolerated at most positions in the original FFAT sequence (Murphy & Levine, 2016). This is best illustrated by the finding that interaction between VAPA and oxysterol binding protein (OSBP)-related protein (ORP) 3 (ORP3), is dependent on both the canonical and modified FFAT motifs of ORP3, and mutations in both motifs is required to reduce interaction with VAPs (Weber-Boyvat et al., 2015). Identification of the FFAT or modified FFAT motifs have allowed finding a plethora of VAP-dependent MCS with the ER (Murphy & Levine, 2016; H. Wu et al., 2018). Furthermore, most VAP interaction with FFAT-containing proteins can be hindered by introducing a double charge substitution in residues Lysine (K) at position 94 and methionine (M) at position 96 both to an aspartic acid (D) in VAPA or by mutating K87 to D and M89 to D of VAPB and is a common way to test FFAT dependent binding (James & Kehlenbach, 2021; Kaiser et al., 2005). Collectively, many ER-MCS are VAP-mediated, and this generally involves binding FFAT or FFAT-like motifs on the partnering organelles (Murphy & Levine, 2016; H. Wu et al., 2018).

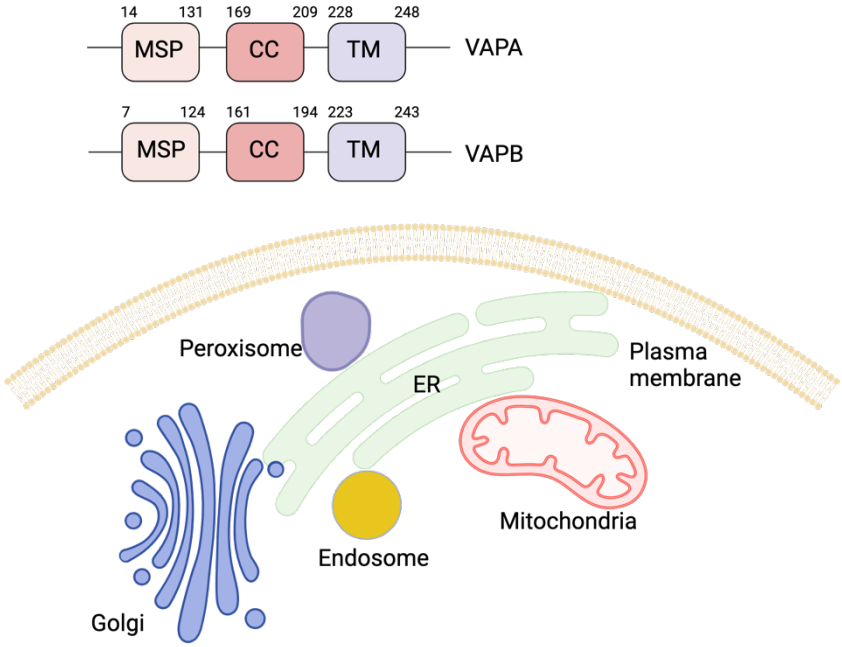

Fig. 1.2: VAPA and VAPB establish MCS between the ER and various organelles. Domain organization (top) of vesicle-associated membrane protein (VAMP)-associated protein (VAP) VAPA and VAPB (VAP). Schematic of contact sites (bottom) mediated by VAP proteins between the ER and the following organelles: Golgi, endosome, peroxisome, mitochondria and plasma membrane (James & Kehlenbach, 2021). MSP: Major sperm domain; CC: Coiled coiled; TM: transmembrane domain.

In recent years considerable work has been performed in identifying the tethers of many MCS. This progress in our understanding can be largely attributed to the powerful molecular and biochemical approaches that have been employed to investigate MCS (X. Huang et al., 2020; Scorrano et al., 2019). The next section will briefly discuss the tools to identify new tethers mediating MCS.

1.3 Methods to identify proteins at MCS

The traditional and most reliable method to report on MCS is by visualizing them via classical electron microscopy (EM) and its various variants such as electron tomography (ET) and focused ion beam-scanning EM (FIB-SEM) (X. Huang et al., 2020). While providing excellent resolution at the nanometer scale, EM is a snapshot of the biological process showcasing the biology at the time of fixation (Scorrano et al., 2019). Over the last few decades, with the breakthroughs in the field of fluorescence microscopy such as

the development of the large spectrum of fluorophores, live-cell microscopy and super resolution approaches, has dramatically increased our understanding of the dynamics and frequency of MCS (X. Huang et al., 2020; Valm et al., 2017; H. Wu et al., 2018). In addition, there are several proximity-based approaches that have been employed to successfully identify MCS proteins (X. Huang et al., 2020; Scorrano et al., 2019).

1.3.1 Proximity-driven reporters

Some methods to detect MCS proteins by utilizing fluorescence signal-based proximity approaches includes proximity ligation assay (PLA), fluorescence resonance energy transfer (FRET), bimolecular complementation (BiC) systems involving split-fluorescent protein-based approaches and dimerization dependent fluorescent protein (ddFP) techniques (Fig. 1.3) (X. Huang et al., 2020). Briefly, PLA utilizes antibodies against endogenous proteins that express oligonucleotide probes which are detected by rolling-circle amplification when the probes are in proximity (Söderberg et al., 2006). This method requires access to antibodies against proteins of interest and some pre-existing information of the MCS proteome (Scorrano et al., 2019). FRET relies on the transfer of energy from one fluorophore to another in a distance of 1- 10 nm (Pietraszewska-Bogiel & Gadella, 2011). Indeed, FRET has high sensitivity for extremely close MCS, but this technique requires equimolar expression of the probes and may be technically challenging (Scorrano et al., 2019). Split-fluorescent based approaches such as split-GFP or split-Venus are based on the principle that there are two non-fluorescent halves of the fluorophore- for GFP the amino acids 1–214 (GFP 1–10) and 214–230 (GFP 11) (Cabantous et al., 2005). The two halves can be targeted to separate membranes which reconstitute a signal only when in proximity (Cieri et al., 2018). These artificial tethers are extremely useful to identify novel MCS tethers because they require no prior knowledge of the proteins mediating these MCS. A caveat is that they stabilize the extent of contact so these methods cannot be employed to study MCS dynamics (Scorrano et al., 2019). In contrast, ddFP circumvents this and is based on reversibility. However, these probes have low fluorescence which is a limiting factor in their usage (X. Huang et al., 2020). All these methods have been used to reliably study MCS in cells (Cieri et al., 2018; Csordás et al., 2010; Tubbs & Rieusset, 2016). In addition, some non-fluorescent based proximity

techniques to investigate MCS include proximity-based biotin identification (BioID) and ascorbate peroxidase (APEX). Briefly, these enzymes are targeted to the membrane of interest where upon activation they can biotinylate proteins spatially proximal to them in a short span of time and then these proteins can be identified in combination with mass spectrometry (X. Huang et al., 2020). This method can capture dynamic MCS and reveal the entire proteome of the MCS landscape in cells (Hung et al., 2017).

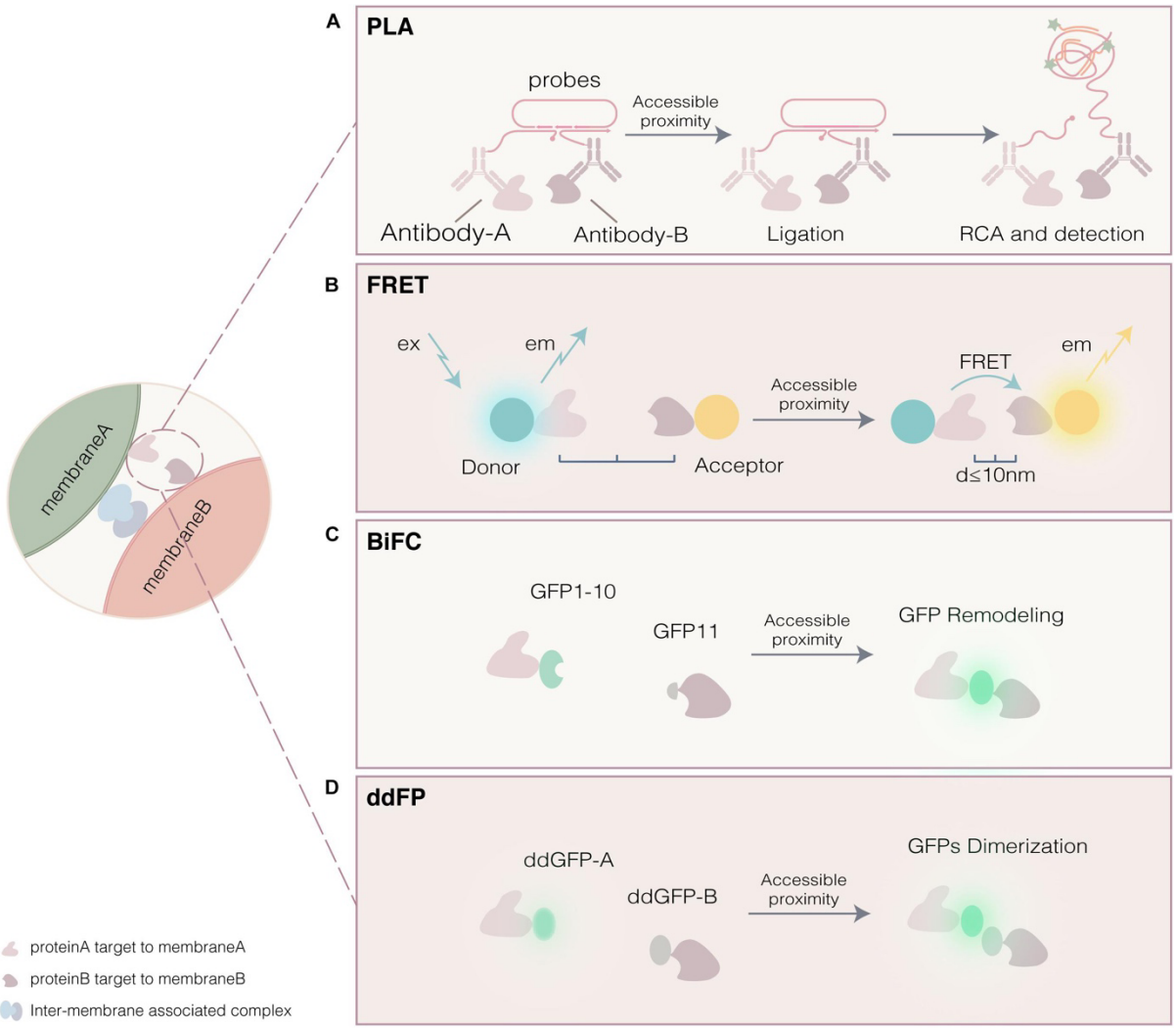

Fig. 1.3: Approaches to study MCS. (A) Schematic of the different techniques used to study membrane contact sites includes: (A) Proximity ligation assay (PLA); (B) Fluorescence resonance energy transfer (FRET); (C) Bimolecular fluorescence complementation (BiFC); (D) Dimerization-dependent fluorescent proteins (ddFP). Copyright © 2020 Huang, Jiang, Yu and Yang. Republished with permission (Huang et al., 2020).

1.3.2 Genetic screen-based identification of MCS proteins

Many genetic screens have also successfully identified MCS proteins. A prime example is the RNA interference screens that identified the key players of store-operated Ca^{2+} entry (SOCE) mechanism in cells (Liou et al., 2005; Zhang et al., 2005, 2006). Furthermore, in yeast the factors mediating ER–mitochondria MCS that is called the ER-mitochondria encounter structure (ERMES) were identified by a screening approach (Kornmann et al., 2009). Moreover, recent studies combine fluorescent readouts with clustered regularly interspaced short palindromic repeats (CRISPR)–Cas9 technology. Briefly, Cas9 induces targeted double-stranded DNA breaks which, results in the knockout of the gene of interest. Such an approach allows to test several genes simultaneously (Shalem et al., 2015). Indeed, using such a split-GFP based loss of function CRISPR-Cas9 screening approach the protein guided entry of tail anchored protein factor 4 (GET4) was suggested to mediate ER-mitochondria MCS (Wilson et al., 2024).

It is evident that each technique has its pros and cons. Therefore, to identify proteins mediating a MCS generally a combination of electron microscopy, confocal microscopy and biochemical techniques is employed. This combination of strategies has made it possible to reliably report on many new MCS tethers and proteins in recent years (Eisenberg-Bord et al., 2016; X. Huang et al., 2020; Scorrano et al., 2019).

1.4 Functions of membrane contact sites

Once the proteins mediating a MCS have been identified, the next step is usually to understand the function and physiological relevance of the MCS. Over the years several functions have been associated with MCS such as lipid metabolism, calcium signalling, regulation of organelle dynamics and organelle biogenesis (Voeltz et al., 2024). In the next section, I will give key examples of each of these functions to shed light on the various functions that MCS regulate in cells with a focus on MCS between ER and host organelles.

1.4.1 MCS regulate lipid exchange

The most common function ascribed to a MCS is its ability to facilitate the transport of ions and metabolites, especially lipids and Ca^{2+} (Voeltz et al., 2024). In the eukaryotic cell the coordinated efforts of many organelles allow lipid biosynthesis (Osman et al., 2011; Voeltz et al., 2024). Although the synthesis of many lipids begins in the ER, they must often be transported to various other organelles for completion of synthesis. This can occur via vesicular transport or at MCS (Voeltz et al., 2024). One of the first reports suggesting the latter was when MAMs were reported to mediate lipid transfer (Vance & Shiao, 1996). Phosphatidylserine is synthesized at the ER and then transported to the mitochondria utilizing MAMs where it is converted into phosphatidylethanolamine and then sent back to the ER which in turn generates phosphatidylcholine (Osman et al., 2011). Similarly, cardiolipin, a phospholipid exclusive to the mitochondria, is synthesized from phosphatidic acid which, is mostly delivered from the ER (Osman et al., 2011).

Lipids can also be transferred via lipid transfer proteins (LTPs) at MCS (Voeltz et al., 2024). Interestingly, several LTPs express an FFAT or FFAT-like motif that enables interaction with VAPs and this allows the transfer of lipids between organelles (Loewen et al., 2003; Murphy & Levine, 2016). An example of this is the transport of ceramide that is synthesized in the ER and transported to Golgi at ER-Golgi MCS where it is converted to sphingomyelin (Fig. 1.4). Briefly, LTP ceramide transfer protein (CERT) contains a PH domain that allows it to bind phosphatidylinositol-4-phosphate (PI4P) at the Golgi and contains an FFAT motif which allows interaction with VAPs on the ER, thus establishing MCS and transporting ceramide to the Golgi via its steroidogenic acute regulatory transfer (StART) domain (Hanada et al., 2003; Peretti et al., 2008; Voeltz et al., 2024). Another mechanism by which cells can mediate lipid transfer involving LTPs is mediated by a process called countertransport that utilizes differing PI phosphate (PIP) gradients that drive the exchange of a second lipid against its concentration gradient (Voeltz et al., 2024). A few examples of this process include the bona-fide LTPs OSBPs and OSBP-related (ORP) or OSBP-like (OSBPL) proteins (Olkkonen & Ikonen, 2024). For example, cholesterol is exchanged with PI4P from the ER to Golgi at ER-Golgi MCS via OSBP, despite the concentration of cholesterol being lower in the ER (Mesmin et al., 2013). A similar

mechanism was reported for the exchange of PS against its concentration gradient from the ER to the plasma membrane (PM) by ORP5 and ORP8 proteins fueled by the counter exchange of PI4P at ER-PM MCS (Chung et al., 2015).

1.4.2 The role of MCS in ion exchange

In addition to lipids, Ca^{2+} exchange is also a central feature of many membrane contact sites in a cell. ER is an important intracellular calcium store (Clapham, 2007). There are two prime sites of Ca^{2+} exchange with the ER mainly at ER-PM and ER-mitochondria MCS. The ER-PM MCS is the site of SOCE which is orchestrated by ER Ca^{2+} sensor stromal interaction molecule 1 (STIM1) and PM protein calcium release-activated calcium channel protein 1 (ORAI1). Briefly, when luminal levels of ER Ca^{2+} are depleted STIM1 oligomerizes and localizes specifically to the ER-PM MCS and activates ORAI1. Ca^{2+} is then transported to the ER lumen through the sarcoplasmic reticulum (SR)/ER Ca2+–adenosine triphosphatase (SERCA) channel (Fig. 1.4) (Helle et al., 2013; Liou et al., 2005; Park et al., 2009; M. M. Wu et al., 2006; Zhang et al., 2005, 2006; Zhou et al., 2013). This process is important to ensure optimal concentrations of Ca^{2+} in the ER, thus proximity of the two membranes is essential for the process to occur smoothly. Given the importance of this, it can be envisioned that other mechanisms exist to mediate ER-PM MCS. Indeed, upon increased cytosolic Ca^{2+} the ER-protein extended synaptotagmin 1 (E-Syt1) interacts with the PM forging ER-PM MCS (Giordano et al., 2013).

Another site of Ca^{2+} exchange is the ER–mitochondria junction. Here, Ca^{2+} exits the ER via the channel inositol-1,4,5-trisphosphate receptor (IP3R) and is taken up first by the outer mitochondrial membrane (OMM) protein voltage-dependent anion channel (VDAC) and then travels to the mitochondrial Ca^{2+} uniporter (MCU) on the inner mitochondrial membrane (Baughman et al., 2011). Several decades ago, it was hypothesized that ER-mitochondria MCS mediate Ca^{2+} transfer, but the mechanism remained unknown. It has since been characterized that the protein glucose-regulated protein 75 (GRP75) interacts with VDAC and IP3R to hold the OMM and ER, respectively, together and this facilitates calcium exchange (Rizzuto et al., 1998; Szabadkai et al., 2006). Much like the PM-ER MCS, the mito-ER MCS also have several forms of regulation with many players

suggested to participate to maintain Ca^{2+} exchange. More recently, it was suggested that OMM protein translocase of the outer membrane 70 (TOM70) interacts with IP3R and enhances its localization close to the mitochondria, promoting Ca^{2+} dynamics at the ER-mitochondria interface (Filadi et al., 2018). Other than Ca^{2+}, iron was reported to be exchanged at endosome-mitochondria MCS; however, the tethers and mechanism still needs to be identified (Das et al., 2016).

1.4.3 MCS regulate organelle dynamics and biogenesis

Several lines of evidence suggest that MCS influence organelle dynamics. Mitochondria are highly dynamic undergoing fission and fusion. A key protein orchestrating mitochondrial fission is dynamin-related protein 1 (DRP1) (Smirnova et al., 2001). Live-cell microscopy revealed that MCS with the ER determine the points of constriction on the mitochondria where DRP1 is recruited followed by mitochondrial division (Fig. 1.4) (Friedman et al., 2011). Similarly, ER-endosome MCS define the position of endosome fission by establishing contacts with early endosomes leading to fission (Rowland et al., 2014). Furthermore, membraneless organelles: processing bodies (P-bodies) and stress granules also undergo ER-contact site regulated fission (J. E. Lee et al., 2020). In addition to fission, the ER-endosome MCS regulate endosomal positioning. Oxysterol binding protein-related protein 1 Long (ORP1L) senses low levels of cholesterol in a cell inhibiting the recruitment of motor protein dynein to endosomes and instead promoting ER-endosome MCS formation via interaction of the FFAT-motif of ORP1L with ER proteins VAPs (Rocha et al., 2009). Consequently, the formation of MCS with the ER then halts endosomes in their location. By contrast, when the levels of cholesterol are high, ORP1L changes conformation which favors the recruitment of dynein to endosomes. Then, dynein interacts with microtubules transporting endosomes in the cell (Rocha et al., 2009). Peroxisome-ER MCS are mediated by acyl-coenzyme A–binding domain protein 5 (ACBD5) and VAPB, respectively. It was reported that loss of this MCS affects peroxisome membrane expansion and results in increased movement of peroxisomes in a cell (Costello et al., 2017).

There are a few notable examples of MCS regulating organelle biogenesis. First, MCS regulate mitochondrial inheritance. In yeast, a putative tether mitochondrial Myo2 receptor-related protein 1 (Mmr1) localizes to ER-mitochondria MCS and its loss causes defects in mitochondrial inheritance without affecting ER inheritance (Swayne et al., 2011). Second, many aspects of autophagy are also regulated by MCS (Capitanio et al., 2023). Autophagy is the cellular process by which double membrane vesicles termed autophagosomes either degrade or recycle material in the cell (Ryter et al., 2013). In yeast and mammalian cells the autophagosome forms in proximity to the ER. The protein autophagy related gene 2 (ATG2) in yeast or ATG2A in mammalian cells was reported to tether the ER to the developing phagophore and mediate lipid transfer at these MCS (Dabrowski et al., 2023; Valverde et al., 2019). Interestingly, in yeast it was reported that ATG2 transfers approximately 200 lipids per ATG molecule per second underscoring the remarkable efficiency of MCS in facilitating lipid transfer (Dabrowski et al., 2023). Additionally, another LTP vacuolar protein sorting 13 (VPS13) was also reported to transfer lipids from the ER to the phagophore (Fig. 1.4) (Dabrowski et al., 2023). In mammalian cells, two studies reported a role of mitochondria-ER and PM-ER MCS in autophagosome biogenesis suggesting that beyond the ER itself, MCS between the ER and other organelles also contributes to autophagosome biogenesis (Hamasaki et al., 2013; Nascimbeni et al., 2017).

The array of roles associated with MCS underlines their importance in maintaining cellular physiology. Thus, it is no surprise that MCS also play a role during host-pathogen interactions. In fact, MCS formation is not limited to organelles but has now been reported for several intracellular microbes and pathogens (Medeiros et al., 2021; Mehra & Pernas, 2023; Vormittag, Ende, et al., 2023a).

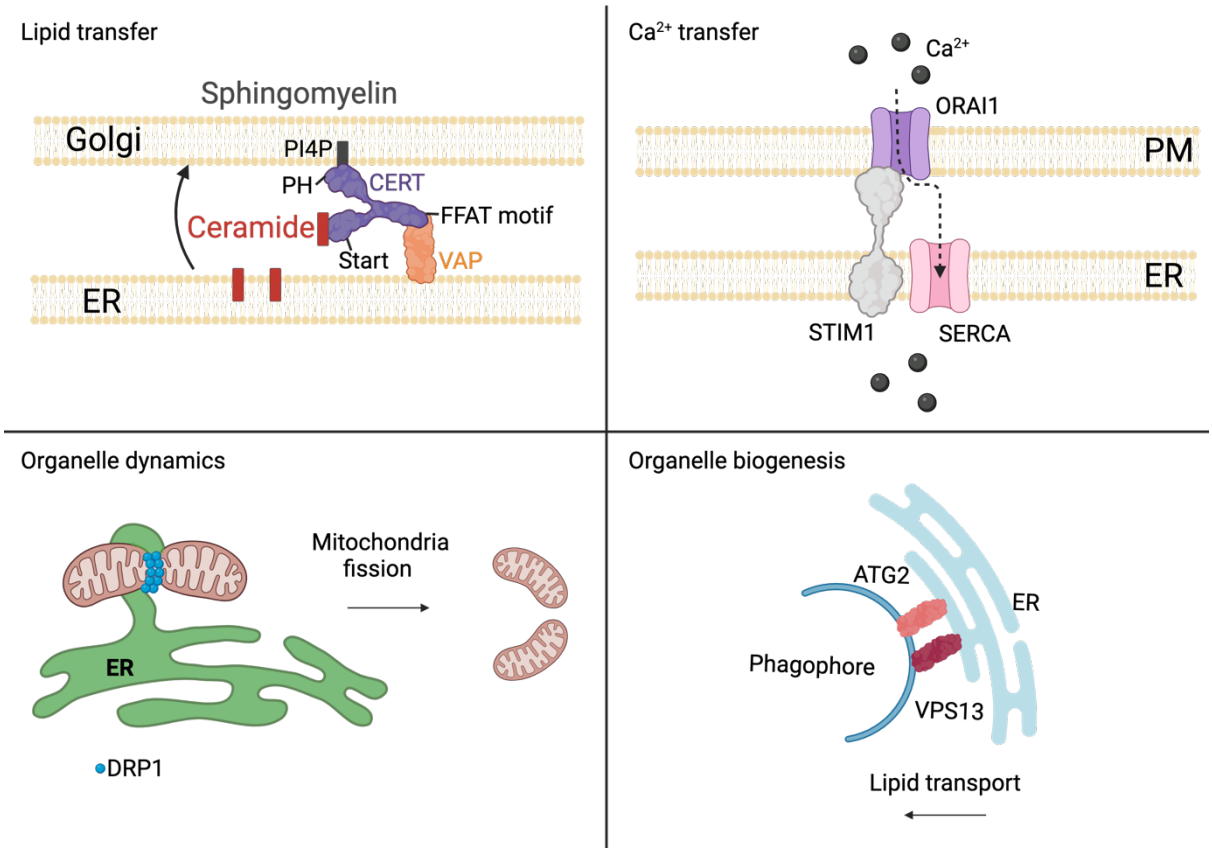

Fig. 1.4: Membrane contact sites mediate diverse functions. Key examples of functions supported by MCS includes lipid and Ca 2+ transfer, organelle dynamics and biogenesis. CERT (ceramide transfer protein); PH (pleckstrin homology); Phosphatidylinositol-4-phosphate (PI4P); Start (steroidogenic acute regulatory transfer); FFAT [two phenylalanines (FF) in an acidic tract (AT)]; VAP (Vesicle-associated membrane protein (VAMP)-associated protein); STIM1 (Ca^{2+} sensor stromal interaction molecule 1); ORAI1 (PM protein calcium release-activated calcium channel protein 1); SERCA (sarcoplasmic reticulum (SR)–ER Ca2+–adenosine triphosphatase); DRP1 (dynamin-related protein 1); ATG2 (Autophagy related gene 2); VPS13 (vacuolar protein sorting 13).

1.5 Host-pathogen membrane contact sites

A pathogen and its host are constantly communicating (Medeiros et al., 2021). This communication can be indirect such as the release of pathogen effector proteins that manipulate host functions or the production of host antimicrobial peptides that restrict pathogen growth. An example of the former is the targeting of OMM protein TOM70 by Severe acute respiratory syndrome coronavirus 2 (SARS- CoV-2) effector protein Orf9 to suppress the interferon-I response in cells (Jiang et al., 2020). An example of the latter is the release of itaconate that restricts the growth of pathogens *Salmonella enterica* and *Mycobacterium tuberculosis* (Michelucci et al., 2013).

A means of direct communication between the host and pathogen can occur via formation of trans-kingdom membrane contact sites (Medeiros et al., 2021; Mehra & Pernas, 2023; Vormittag, Ende, et al., 2023b). This interaction is less studied and whether host pathogen MCS are beneficial to the microbe or host remain open questions. In 1954, the first microscopic evidence of mitochondria present near a pathogen vacuole was observed upon infection with human parasite *Toxoplasma gondii* (Gustafson et al., 1954). Interestingly, this is around the same time that MCS were observed in uninfected cells (Bernhard & Roullier, 1956). Much like there, the relevance of host-pathogen MCS formation and further characterization took decades to understand. In the next section we will introduce *Toxoplasma gondii*, host organellar-pathogen association and, currently open questions in the field of host pathogen membrane contact sites.

1.6 *Toxoplasma gondii*- a brief history

Toxoplasma gondii (*Toxoplasma*) is an obligate intracellular parasite belonging to the phylum apicomplexan. This phylum is also home to the parasite species *Plasmodium* that is the causative agent of malaria disease in humans (Janouskovec et al., 2019). The discovery of *Toxoplasma* dates back more than 100 years ago when two groups reported its existence within the same year –in one study about a North African rodent called Ctenodactylus gundi and another study about a rabbit from Brazil (Nicolle & Manceaux, 1908; Splendore, 1908). *Toxoplasma* gets its name from Nicolle and Manceux due to its

unique crescent shape, deriving from the word *Toxon* meaning "arc" in the Greek language and "*plasma*" which means form. Clinical cases in the 1930's reported that *Toxoplasma* can be congenitally passed from a mother to their unborn child which were the first reports suggesting its importance in human health (Weiss & Dubey, 2009; a Wolf et al., 1939; A. Wolf et al., 1939). It is now common knowledge that unborn children in pregnant mothers and immunocompromised individuals are at the highest risk of *Toxoplasma* infection and fatality (Blader et al., 2015). Furthermore, it is estimated that about one-third of the world's population is infected with *Toxoplasma*, but many remain asymptomatic (Blader et al., 2015; Carruthers, 2002). Interestingly, this depends on the country as in Germany 77% of the tested population in the age group of 70–79 years old were reported as seropositive for *Toxoplasma*, thus making it an important parasite to investigate (Wilking et al., 2016).

Toxoplasma life cycle alternates between two main stages: the sexual stage that occurs only in intestines of their definitive hosts belonging to members of the feline species and the asexual stage which, occurs in the intermediate hosts such as humans (Robert-Gangneux & Dardé, 2012). Furthermore, *Toxoplasma* can cause three types of infections in their hosts. An acute infection characterized by their fast-dividing haploid tachyzoite stage, a chronic infection where the tachyzoite parasite is converted into the slow-replicating bradyzoite cyst stage and the oocyst-containing sporozoite, a stage only present in the definite hosts such as cats (Robert-Gangneux & Dardé, 2012). For *Toxoplasma* transmission to occur between two hosts the parasite is not required to complete a sexual cycle in cats (Su et al., 2003). It can be easily transmitted orally such as through consumption of contaminated water and raw or uncooked meat, and this is speculated to be the reason behind the global expansion of *Toxoplasma* (Su et al., 2003).

Most studies investigating *Toxoplasma* biology utilize the three predominant *Toxoplasma* clonal lineages which are characterized based on their genotypes as Type I, Type II, and Type III (Howe & Sibley, 1995). These strains differ in their migration, growth, host-pathogen interaction, virulence and production of cytokines in their hosts (Pernas et al., 2014; Saeij et al., 2005). The most used strain in laboratory settings is the *Toxoplasma* Type I which, is highly virulent whereas Types II and III are less virulent (Howe & Sibley,

1995; Saeij et al., 2005). The ability to isolate different *Toxoplasma* strains and adapt them to culture *in vitro* has allowed scientists to use this organism to study many questions pertaining to host-pathogen interactions. Intracellular *Toxoplasma* in cells is either in the tachyzoite stage where the parasite undergoes a lytic cycle or the dormant bradyzoite cyst stage (Blader et al., 2015). The lytic cycle comprises of several rounds of replication in a sequential process of gliding, invasion, intracellular replication and egress (Blader et al., 2015; Frénal et al., 2017).

1.7 The intracellular niche of *Toxoplasma gondii*

As a eukaryote *Toxoplasma* possesses many organelles common to a eukaryotic cell such as a nucleus, mitochondria, ER and some unusual organelles such as the apicoplast (Joiner & Roos, 2002). In addition, *Toxoplasma* contains three secretory organelles called micronemes, rhoptries and dense granules, which play a key role in coordinating the lytic cycle of the parasite (Joiner & Roos, 2002). The lytic stage of the *Toxoplasma* lifecycle begins when the tachyzoite form of the parasite finds a host cell via a process called gliding motility (Frénal et al., 2017). Once the cell is located, the parasites discharge their first secretory organelles: the micronemes that allows the parasite to reorient and to anchor itself to receptors on the host cell plasma membrane (Frénal et al., 2017; Rastogi et al., 2019). The parasites then sequentially discharge the second secretory organelle-rhoptries that are further divided into two groups: *Toxoplasma gondii* rhoptry neck (TgRONs) and bulb proteins. TgRONs are discharged first and interaction between key microneme and RON proteins enables formation of the moving junction (Alexander et al., 2005; Besteiro et al., 2011; Frénal et al., 2017). This initiates the invasion process, and the parasite actin-myosin complex pushes the parasite into the host (Frénal et al., 2017). The invasion process is remarkably rapid, occurring within 15-30 seconds (Morisaki, Heuser et al. 1995). As the parasite enters, the parasitophorous vacuole (PV) is formed which is derived from the invagination of the plasma membrane of the host (Suss-Toby et al., 1996). The PV membrane (PVM) is modified throughout infection and is the interface between the host cell cytoplasm and the parasite (Clough & Frickel, 2017; Rastogi et al., 2019). The parasite resides in the PV and divides by a process called endodyogeny where two daughter cells emerge from within

the mother (Hu et al., 2002). After several rounds of replication *Toxoplasma* exits the cell in a process called egress that is characterized by rupture of the PVM and host plasma membrane (Blader et al., 2015; Hu et al., 2002). Parasites can then infect a new host cell and continue their replicative cycle (Fig. 1.5).

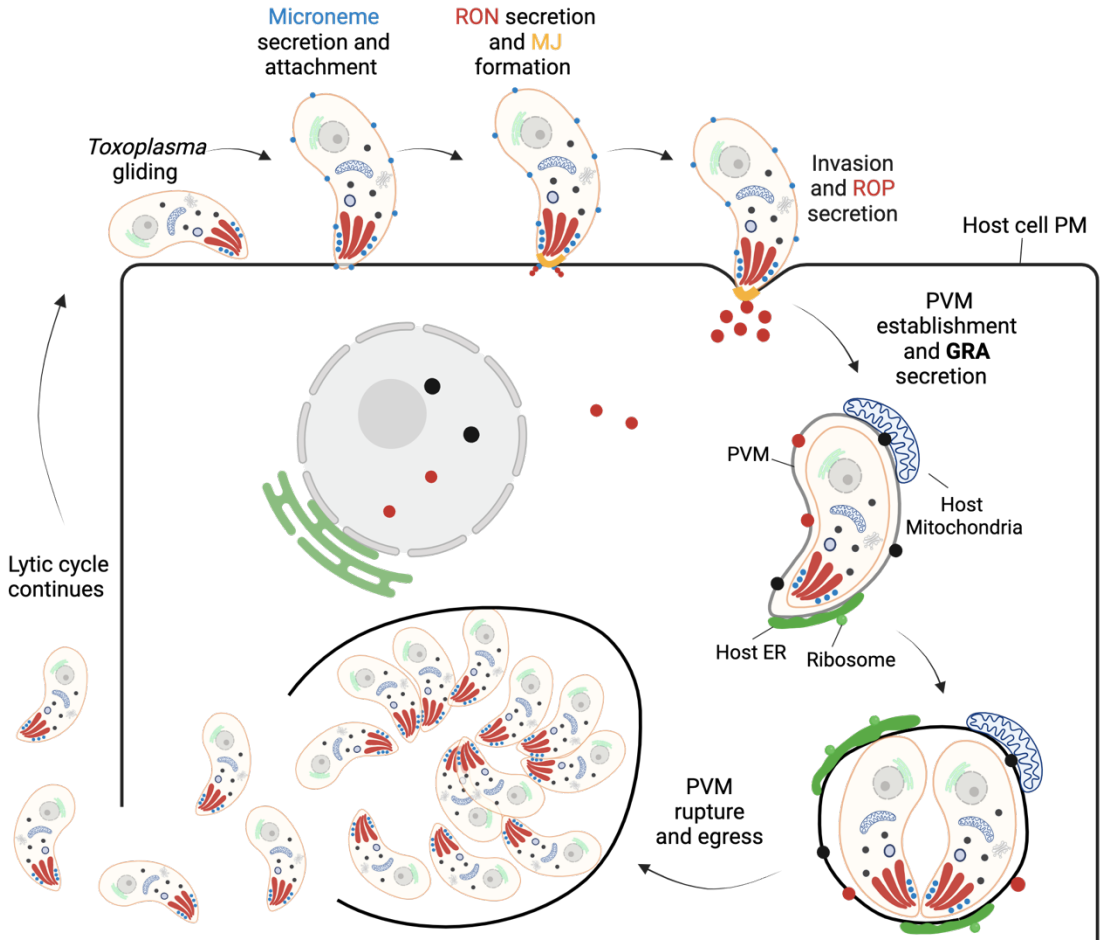

Fig. 1.5: *Toxoplasma* secretory proteins orchestrate its lytic cycle. This figure is inspired from Rastogi et al., 2019. *Toxoplasma* microneme secretion allows attachment to the host cell plasma membrane (PM). Once attached, invasion begins simultaneously with rhoptry secretion. Rhoptry neck proteins (RONs) are secreted first and enable formation of the moving junction (MJ). Then rhoptry bulb proteins ROPs are released at the time of invasion. The parasitophorous vacuole membrane (PVM) forms as the parasite is invading and houses the parasite throughout its intracellular life cycle. Either during or post invasion dense granules (GRAs) are released. Soon after invasion, host organelles mitochondria and endoplasmic reticulum (ER) associate with the PVM. The parasite replicates until egress which is marked by PVM and host cell PM rupture. The parasite continues the lytic cycle.

1.8 Two *Toxoplasma* organelles that affect host functions

During the intracellular life of the parasite *Toxoplasma gondii* rhoptry bulb proteins (TgROPs) and *Toxoplasma gondii* dense granules (TgGRAs) are key to parasite survival as they contain effector proteins that are involved in host cell rewiring and manipulation of host cell functions (Rastogi et al., 2019). Rhoptries are club-shaped organelles located at the apical end of the parasite with each *Toxoplasma* containing 8-12 rhoptry organelles (Dubremetz, 2007). ROPs are secreted at the onset of invasion and can be incorporated in the PVM or travel to various regions of the host cell, thus positioning them at key places enabling interaction with or manipulation of the host cell (Rastogi et al., 2019). More than 50 ROP proteins have been identified till date with several functions ascribed to them (Barylyuk et al., 2020; Bradley et al., 2005; Dubremetz, 2007). Toxofilin, a ROP protein localizes to the host cytosol and interacts with host actin depolymerizing it and this is suggested to facilitate the invasion process (Delorme-Walker et al., 2012; Poupel et al., 2000). Some others localize to the nucleus such as TgROP16 and affect activation of signal transducer and activator of transcription (STAT) signalling pathway (Saeij et al., 2007). TgROP1, a PVM-localized ROP protein was the first identified ROP protein over 30 years ago but only recently was shown to contribute to parasite resistance in response to interferon γ treatment (Butterworth et al., 2022). However, the mechanism by which TgROP1 exerts this function is unknown. An important ROP virulence factor is the serine-threonine kinase TgROP18 that can phosphorylate immunity-related GTPases (IRGs) which are the main defences against intracellular pathogens (Fentress et al., 2010). Furthermore, TgROP18 was reported to form a complex with TgROP17 and TgROP5 and together they were suggested to avoid the recruitment of IRGs to the PVM, thus avoiding damage to the parasite vacuole and mediating evasion of immune clearance by the host (Behnke et al., 2012; Etheridge et al., 2014; Fentress et al., 2010).

Once intracellular, it is believed that the parasite releases many dense granule proteins (Rastogi et al., 2019). GRAs are electron dense structures about 200 nm in diameter and akin to rhoptry proteins localize to various niches such as the *Toxoplasma* PV, PVM or in the host cell (Griffith et al., 2022; Rastogi et al., 2019). TgGRA16, TgGRA24 and inhibitor of STAT1 signalling (TgIST) are exported to the nucleus, and these effector proteins are

important for parasite virulence and influencing host cell transcription (Bougdour et al., 2013, 2014; Braun et al., 2013). There are many key examples of GRAs at the PVM. TgGRA17 and TgGRA23 are PVM proteins that act as molecular sieves allowing the transfer of small molecules from the host cytosol to the PV (Gold et al., 2015). While some mediate import, GRA proteins TgMYR1, TgMYR2 and TgMYR3 are responsible for dense granule protein export beyond the PVM (Franco et al., 2016; Marino et al., 2018). TgGRA45 on the other hand, is responsible for the localization of GRA proteins onto the PVM (Wang et al., 2020). Given the myriad functions coordinated by GRA proteins their importance in supporting the intracellular survival of *Toxoplasma* is evident (Rastogi et al., 2019). Such a PVM-localized GRA protein called *Toxoplasma gondii* mitochondrial association factor 1 (TgMAF1) that can mediate a host function that is pivotal to this project will be discussed in more detail in the next section (Pernas et al., 2014; Rastogi et al., 2019).

1.9 Host mitochondrial association

A hallmark of infection with *Toxoplasma* is the association of host mitochondria and endoplasmic reticulum with the PVM of the parasite (Fig. 1.6). This was first observed in 1954 when EM images revealed that mitochondria associated with the parasite vacuole of intracellular *Toxoplasma* parasites (Gustafson et al., 1954). Further advances into the understanding of this process were not achieved until 40 years later where a remarkable paper described this association biochemically (Sinai et al., 1997). The final breakthrough was when the tether mediating this MCS was identified in the 2010s (Pernas et al., 2014). *Toxoplasma* exhibits strain specificity in mediating host-mitochondrial association (HMA); Type I and III strains can establish contact with mitochondria whereas Type II cannot (Pernas et al., 2014). This strain-specificity allowed the identification of the parasite factor both required and sufficient for mediating these MCS which is known as TgMAF1 (Pernas et al., 2014). Subsequent work identified host OMM protein TOM70 as the interacting partner of TgMAF1 and together they mediate mitochondria-*Toxoplasma* MCS (Blank et al., 2021; X. Li et al., 2022).

Having both the parasite and host mediator of HMA in hand allowed further investigation of the function of this MCS. The prevailing view in the field is that pathogens scavenge nutrients from the host. Indeed, *Toxoplasma* exploits host cell lipophagy to access fatty acids for its development (Nolan et al., 2017; Pernas et al., 2018). However, subsequent work identified a role of host mitochondria in mediating a metabolic defense against *Toxoplasma* (Pernas et al., 2018). Mitochondria were reported to elongate by mitochondrial fusion and enhance their fatty acid (FA) uptake in cells. This in turn limited the fatty acid availability in cells and resulted in reduced parasite replication (Pernas et al., 2018). In line with this, upon loss of mitochondrial fusion proteins mitofusin 1 (MFN1) and 2 (MFN2), the parasite uptake of FA was increased and parasite replication was rescued (Pernas et al., 2018). A parasite counter response was recently identified where *Toxoplasma* was reported to remodel the OMM and trigger the budding of large mitochondria-derived structures that contained proteins of the OMM such as MFN1 and MFN2 (X. Li et al., 2022). Interestingly, these structures bud off at MCS between mitochondria and *Toxoplasma* and in the absence of both TgMAF1 and TOM70 these structures were no longer formed (X. Li et al., 2022). These reports suggest that the mitochondria-*Toxoplasma* MCS are the site of a molecular arms race.

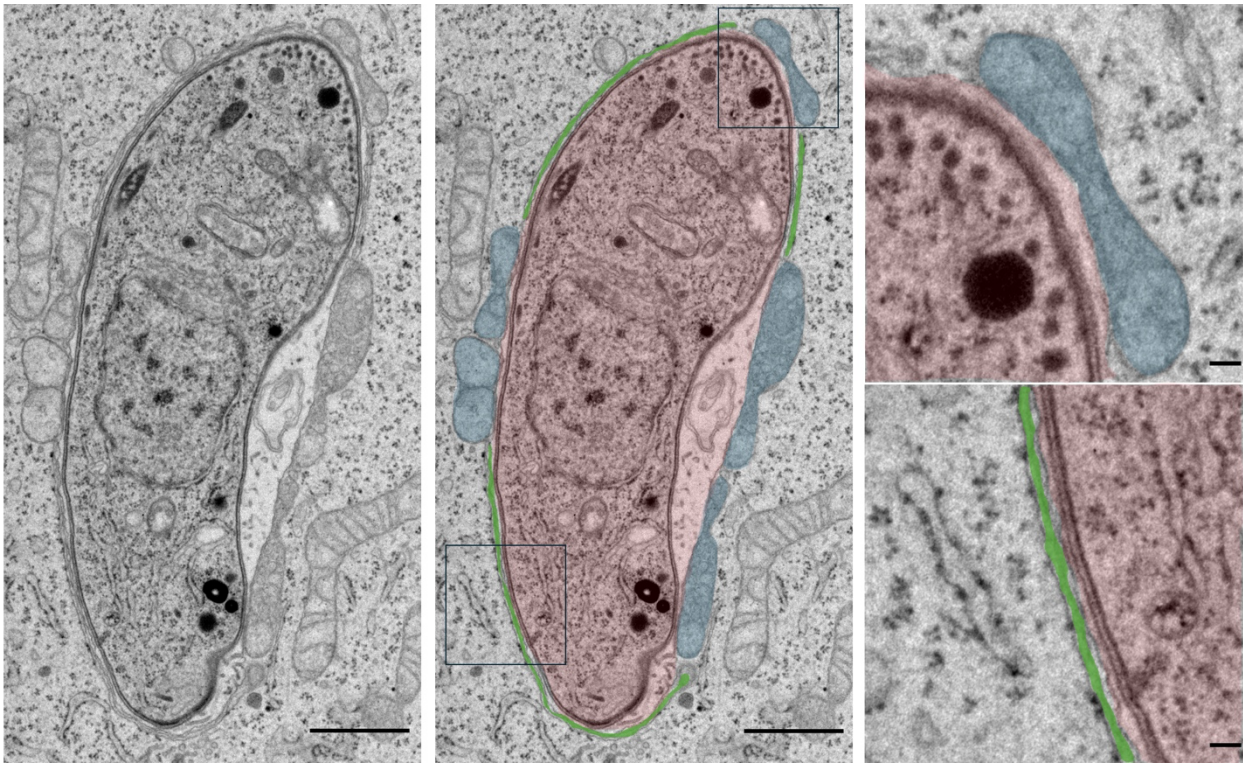

Fig. 1.6: Host ER and host mitochondria associate with the *Toxoplasma* vacuole. Electron micrograph of HeLa cells infected with *Toxoplasma* Type I (RH) parasite strain and imaged at 3 hours post infection. Middle panel- host ER labelled with green, host mitochondria coloured with blue and *Toxoplasma* vacuole is labelled red. Right panel- higher magnification showing the association of host mitochondria (top) and host ER (bottom) with the parasite vacuole. Imaged by Katrin Seidel from the CECAD imaging facility, Cologne, Germany. Scale bars: 1 µm; inset, 100 nm.

HMA has been a long-reported phenomenon in various microbes (Fig. 1.7) (Medeiros et al., 2021). Electron dense structures of <10 nm bridging OMM and the parasite vacuole of *Microsporidia* species *Encephalitozoon hellem* (*E. hellem*) were reported as contacts that are mediated by parasite protein *E. hellem* sporoplasm surface protein 1 (EhSSP1) and host VDAC (Hacker et al., 2014; Han et al., 2019). Interestingly, these parasites are unable to produce ATP and thus interaction with VDAC—an ATP transporting channel—may be a means to acquire ATP from their hosts (Hacker et al., 2014; Rostovtseva & Bezrukov, 1998). Furthermore, direct contact has also been reported between host mitochondria and the flagellum of the parasite *Trypanosoma cruzi* that causes Chagas disease in humans, but the factors that mediate this contact remain unknown (Lentini et al., 2018). Some prokaryotic pathogens such as intracellular bacteria *Legionella pneumophila* (*L. pneumophila*) and *Chlamydia* that are responsible for causing severe pneumonia called Legionnaire's disease and a common sexually transmitted disease,

respectively, also mediate HMA (Cheong et al., 2019; Derré et al., 2007; Horwitz, 1983; Matsumoto et al., 1991; Mondino et al., 2020). A role of *L. pneumophila* effector protein mitochondrial fragmentation factor (MitF) was reported to drive mitochondrial fragmentation and influence the extent of contacts between the *L. pneumophila*-containing vacuole (LCV) and mitochondria (Escoll et al., 2017). Whether MitF is a tether mediating these MCS needs further validation. Interestingly, like *Toxoplasma* the main strains of *Chlamydia* that cause human diseases also exhibit strain-specific differences in mediating HMA. The vacuolar membrane of *Chlamydia psittaci* associates with host mitochondria, but this contact is not observed post-infection with *Chlamydia trachomatis (C. trachomatis)* and *Chlamydia pneumoniae* (Matsumoto et al., 1991). The factors that mediate these MCS also remain unknown. Interestingly, *Chlamydia caviae* (*C. caviae*), a *Chlamydia* species that infects guinea pigs, also associates with host mitochondria. An RNAi screen identified that the loss of host translocase of outer mitochondrial membrane 40 (TOM40) mildly reduced HMA upon infection with *C. caviae* (Derré et al., 2007). However, given the role of TOM40 in mediating protein import into the mitochondria whether TOM40 itself is the tether or if its loss perturbs the import of the tether requires further investigation (Derré et al., 2007; Schmidt et al., 2010).

1.10 Host endoplasmic reticulum association

Other than the mitochondria, the endoplasmic reticulum is the other major host organelle known to associate with many vacuoles of intracellular pathogens here after referred to as host ER association (hERa) (Fig. 1.7) (Jones & Hirsch, 1972; Mehra & Pernas, 2023; Sinai et al., 1997; Vormittag, Ende, et al., 2023a). The most well characterized example of hERa has been reported for intracellular microbe *C. trachomatis* that in cells resides in a membrane-bound vacuole called the inclusion. *C. trachomatis* expresses two effector proteins that interact with the host ER. First *C. trachomatis* Inclusion (Inc) protein IncD binds CERT that in turn interacts with VAP on ER (Derré et al., 2011). A second *C. trachomatis* effector protein IncV contains FFAT motifs that bind the MSP domain of VAP proteins tethering host ER to the bacterial vacuole (Stanhope et al., 2017). Indeed, loss of CERT or VAP proteins decreases bacterial burden (Agaisse & Derré, 2014; Derré et al., 2011; Elwell et al., 2011). Furthermore, a third ER protein STIM1 that as mentioned

previously mediates ER-PM MCS, was also shown to localize to the ER-*Chlamydia* vacuole interface (Agaisse & Derré, 2015; Voeltz et al., 2024). However, the interacting partner of STIM1 and the role of this protein in mediating this MCS is unclear.

Of note, VAPs are present in some capacity in many host-pathogen MCS with the ER underscoring their crucial role in not just organellar but also host-pathogen MCS (Vormittag, Ende, et al., 2023a; H. Wu et al., 2018). Furthermore, the interaction of VAPs with some pathogens are classic examples of molecular mimicry where pathogens have evolved to express eukaryotic motifs, such as the *C. trachomatis* effector IncV that possess a FFAT motif that enables interaction with ER (Murphy & Levine, 2016; Stanhope et al., 2017). Similarly, the Norovirus—the cause of gastroenteritis—nonstructural protein (nsp) called nsp 1/2 contains FFAT motifs that allows interaction with host VAPs (McCune et al., 2017). This was recently also postulated for bacteria *Rickettsia parkeri (R. parkeri)* that forms MCS with host ER. Upon mutating FFAT-binding domains of the VAP proteins, *R. parkeri*-ER MCS were completely abolished (Acevedo-Sánchez et al., 2025).

Coxiella-burnetii (*C. burnetii*) is the causative agent of Q fever in humans (Dragan & Voth, 2020). MCS between *C. burnetii*-containing pathogen vacuole and host ER are mediated by lipid transport protein ORP1L which binds to the pathogen vacuole and host VAP, bringing the two membranes together (Justis et al., 2017). The intracellular pathogen *L. pneumophila* also associates with ER and at this bacterial vacuole-ER interface many host ER proteins are present (Vormittag, Hüsler, et al., 2023). Interestingly, VAPs localize to the ER but also to the *L. pneumophila*-containing vacuole membrane (LCVM) (Vormittag, Hüsler, et al., 2023). Furthermore, proteins PI4P phosphatase Sac1 and OSBP8 were reported preferentially localizing to the ER membrane whereas OSBP11 localizes to the LCVM. While OSBP11, Sac1 and VAP were reported to promote bacterial replication OSBP8 was shown to restrict it (Vormittag, Hüsler, et al., 2023). Given the general role of the host proteins in lipid transfer led the authors to hypothesize that the pathogen-ER MCS of both *C. burnetii* and *Legionella* represent sites of lipid exchange (Justis et al., 2017; Vormittag, Ende, et al., 2023a; Vormittag, Hüsler, et al., 2023).

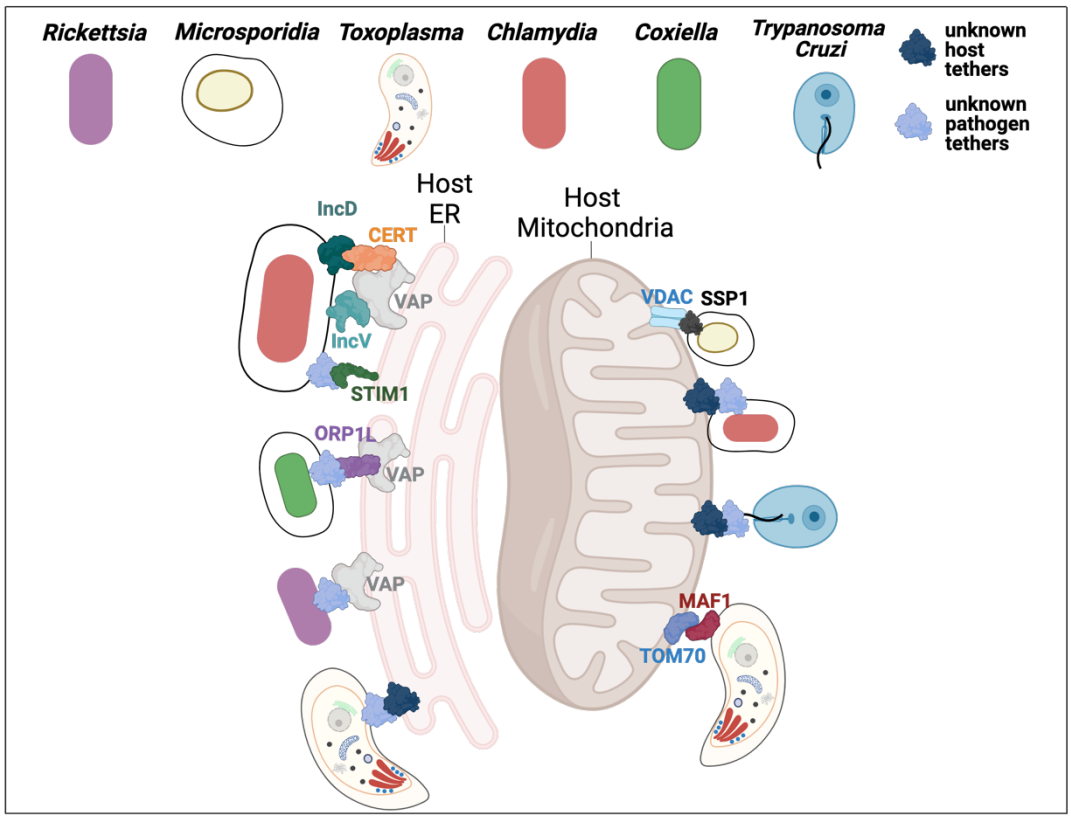

Fig. 1.7: Schematic of host organellar-pathogen association of intracellular pathogens. Pathogens depicted are *Rickettsia parkeri, Microsporidia* species *Encephalitozoon sp., Toxoplasma gondii, Chlamydia, Coxiella, Trypanosoma cruzi*. Host proteins mediating these interactions include VDAC (voltage dependent anion-selective channel), TOM70 (translocase of the outer membrane 70), VAP (Vesicle-associated membrane protein (VAMP)-associated protein), ER Ca^{2+} sensor stromal interaction molecule 1 (STIM1) and ORP1L (oxysterol binding protein-like protein 1 Long). Pathogen effectors mediating these interactions include *Encephalitozoon hellem* SSP1 (sporoplasm surface protein 1), MAF1 (Mitochondrial association factor 1), Inc protein IncD and IncV.

1.10.1 Host ER-*Toxoplasma* membrane contact sites

hERa in *Toxoplasma*-infected cells was described at the same time as HMA yet relatively little is known about it since its discovery (Jones & Hirsch, 1972). The first proper description of host organellar-*Toxoplasma* association was from authors Jones and Hirsch who were trying to understand how *Toxoplasma* evades lysosomal fusion and acidification. They performed EM of intracellular parasites in infected macrophages and compared dead versus alive vacuoles (Jones & Hirsch, 1972). Interestingly, they observed that the *Toxoplasma* vacuoles that were alive were “overcoated” with or “apposed” to host organelles such as the ER (Jones & Hirsch, 1972). They postulated that this

association may be 1) to avoid lysosomal fusion, 2) a way for the parasite to get nutrients (Jones & Hirsch, 1972). Surprisingly, this observation was not studied further for many years. In 1997, a hallmark paper by authors Sinai and Joiner further studied this both biochemically and morphologically. They characterized hERa as a high-affinity interaction mediated by two proteins, reminiscent of what we would today refer to as membrane contact sites (Scorrano et al., 2019; Sinai et al., 1997). First, they observed hERa occurs soon after invasion and required an active invasion process (Sinai et al., 1997). Second, they reported the mean distance between the PVM and ER to be 18 nm (MCS generally range from 10-80 nm) and observed that approximately 56% of the PV perimeter was associated with ER at 4 hours post infection (Scorrano et al., 2019; Sinai et al., 1997). Third, this association was not due to steric constraints imposed by parasite replication and the growing vacuole. Fourth, parasite viability was not required to maintain ER association with the vacuole once it had been established. Last, following cell homogenization hERa remained intact (Sinai et al., 1997).

Since these observations, many studies in the field have tried to identify the molecular tethers that mediate host ER-*Toxoplasma* MCS. However, the studies designed to investigate them have failed to identify the tethers. For example, initial studies hypothesized a role of parasite effector *Toxoplasma* rhoptry protein 2 (TgROP2) in mediating hERa. This was based on experiments that indicated that TgROP2 localizes to host ER upon transfection in cells. However, this study did not further investigate a role of this protein in mediating hERa, for instance via creating a knockout of TgROP2 and then assessing hERa (Sinai & Joiner, 2001). Another study speculated that *Toxoplasma* dense granule proteins TgGRA3 and ER protein calcium modulating ligand (CAMLG) may mediate hERa based on coimmunoprecipitation assays suggesting an interaction between these two proteins. However, the caveat here is that just the presence of the proteins at the right location and an interaction does not indicate a role in mediating MCS (J. Y. Kim et al., 2008). Recently, ER protein motile sperm domain-containing protein 2 (MOSPD2) was suggested as the host counterpart mediating these MCS due to its enrichment at the PVM in certain *Toxoplasma* strains. However, ER-*Toxoplasma* MCS remained intact in MOSPD2 knockout cells suggesting that this is not the tether (Ferrel et

al., 2023). Thus, the molecules that mediate *Toxoplasma*-ER membrane contact sites have remained a mystery for over six decades, with no tethers identified to date.

While considerable progress has been made in recent years for several host-pathogen MCS, in most cases only one of the tethers mediating the interaction is known and needs further investigation (Fig. 1.7). One possible explanation for the delay is that the classical methods used such as cell fractionation, confocal and electron microscopy approaches are low throughput in nature which, allows investigating only a few proteins at a time. While great for targeted approaches, this is akin to finding a needle in a haystack when there are over 100s of potential candidates. Such is the case for *Toxoplasma* effector proteins belonging to dense granule and rhoptry protein families where most effectors have the potential to mediate MCS with host ER. Therefore, a testing tool to study host-pathogen MCS that allows to screen multiple genes at the same time may benefit the field. Despite the discovery of host ER-*Toxoplasma* MCS, the function and proteins mediating this contact remains enigmatic (Fig. 1.8). Identification of the tethers will give invaluable insights into the mechanism and function of this host-pathogen MCS.

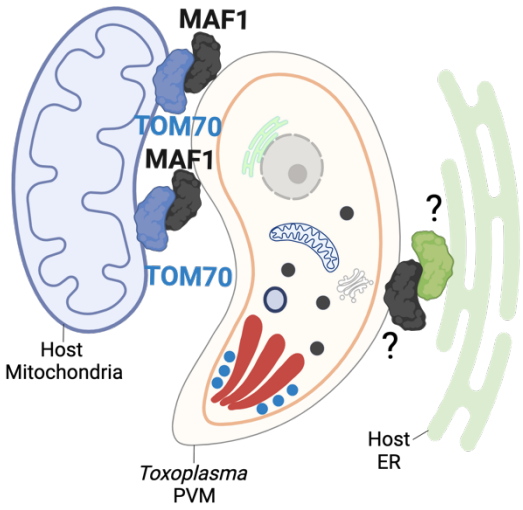

Fig. 1.8: Schematic of host organellar-*Toxoplasma* association. Host mitochondria-*Toxoplasma* MCS are mediated by host OMM protein TOM70 and pathogen effector protein TgMAF1. The proteins mediating host ER-*Toxoplasma* MCS are unknown.

2 Aims of the thesis

The host endoplasmic reticulum-*Toxoplasma* membrane contact sites were discovered decades ago, however the tethers mediating this contact, its function and impact on parasite or host remain open questions. The overall aims of this thesis can be divided into two main parts:

1) Establish a high-throughput method to study host-pathogen MCS. As a foundation, I developed a high-throughput method to study host-pathogen membrane contact sites. I confirmed the use of this system in two CRISPR-Cas9 based screening approaches by applying it to study the mitochondria-*Toxoplasma* MCS for which the tethers are known.

2) Identify the molecular machinery that mediates the host ER-*Toxoplasma* MCS. For this, I performed an unbiased CRISPR screen with our host-microbe split-GFP system to identify the *Toxoplasma* effector protein that mediates the MCS between the ER and *Toxoplasma*. I then validated putative *Toxoplasma* gene candidates for their role in mediating these MCS and subsequently identified the host proteins that mediate these contact sites.

3 Results

3.1 Identification of proteins mediating host ER-*Toxoplasma* MCS.

This section of this thesis represents most of my PhD work and is written in the form of a manuscript. A version of this manuscript has been submitted. This manuscript version is a modified version containing additional data and some modifications to the text and figures.

This manuscript is a collaborative effort. All the experiments were conducted by me except for the following which were performed by co-authors: transfection of sgRNAs against *Toxoplasma* effector proteins was performed by Dr. Francesca Torelli (Lab of Dr. Moritz Treeck); the IP's depicted in Fig. 4a and Fig. 5a were performed with help from Julian Straub; the western blot in Extended Data Fig. 9b was performed by Michelle Tellez Sutterlin; the search for putative FFAT motifs from the CRISPR screen (Supplementary table 4), AlphaFold modelling of all candidates including TgROP1 and TgROP6 with VAPA in Fig. 3d and Extended Data Fig. 8a, respectively, and the sequence alignment of Extended Data Fig. 9a were performed by Dr. Jesús Alvarado Valvarde (Lab of Dr. Katja Luck). Furthermore, the CRISPR, FACS & Imaging, electron microscopy and proteomics core facilities at MPI for Biology of Ageing and CECAD were vital to the success of this project. Last, contributions of cell lines and parasite lines from the scientific community have been mentioned in the materials and methods section. The references cited in the manuscript were combined with the entire thesis at the end.

3.1.1 Abstract

The discovery of membrane contact sites (MCS) between organelles coincided with that of trans-kingdom MCS, which form between host organelles and intracellular pathogens. Although we have reached a considerable understanding of the importance of organelle-organelle MCS in maintaining cellular homeostasis, our comprehension of host organelle-pathogen MCS remains limited. Here, we developed a fluorescent sensor to identify the factors that mediate the MCS between the human parasite *Toxoplasma gondii* and host ER. By coupling the sensor to loss-of-function CRISPR screening, we identified the *Toxoplasma* effector TgROP1 and host VAPA/B as the factors required for *Toxoplasma*-ER MCS. Structural modelling and mutational studies indicate that TgROP1 mimics conserved VAPA/B binding motifs known to mediate MCS between host ER and other organelles. The identification of TgROP1 and VAPA/B as the tethers of *Toxoplasma*-ER MCS paves the way for future studies to define their role in host-pathogen interactions.

3.1.2 Introduction

The view that organelles are independent entities that function autonomously of each other has changed dramatically in the past decades. We now know that organelles directly communicate and coordinate functions at membrane contact sites (MCS), regions of close membrane apposition tethered by proteins (Scorrano et al., 2019). To date, MCS have been demonstrated to enable the bidirectional transport of signalling molecules, coordinate biosynthetic processes, and to regulate the spatial distribution of organelles (Voeltz et al., 2024; H. Wu et al., 2018). For example, the outer mitochondrial membrane (OMM) import receptor TOM70 interacts with the IP3R3 on the ER membrane to promote the transfer of Ca^{2+} from the ER to mitochondria (Filadi et al., 2018). ORP1L and VAPA/ VAPB (VAPs) on the endosomes and ER, respectively, form MCS that regulate late endosomal positioning in response to cellular cholesterol levels (Rocha et al., 2009). The importance of MCS for organismal health is evidenced by human diseases that are linked to altered MCS or mutations in contact site proteins such as Parkinson's disease and amyotrophic lateral sclerosis (ALS) (S. Kim et al., 2021; Moustaqim-barrette et al., 2014).

Not long after the discovery of organelle-organelle MCS, interactions reminiscent of MCS were described to occur between host organelles and several eukaryotic and prokaryotic pathogens (Bernhard & Roullier, 1956; Jones & Hirsch, 1972; Sinai et al., 1997; Vormittag, Ende, et al., 2023b). Although initially attributed to steric constraints imposed by large pathogen vacuoles, recent findings show that host-pathogen MCS are mediated by protein tethers and may represent molecular battlegrounds for host-pathogen arms races. Effector proteins of the bacterial pathogen *Chlamydia* interact with host VAPs and the lipid transfer protein CERT to form MCS between host ER and *Chlamydia* inclusions (Derré et al., 2011; Stanhope et al., 2017). Because the depletion of CERT or VAPs leads to a decrease in inclusion size and infectious progeny production, it is hypothesized that *Chlamydia* exploits ER-MCS for the acquisition of host lipids (Agaisse & Derré, 2014; Derré et al., 2011; Elwell et al., 2011). MCS between the vacuole of the human parasite *Toxoplasma gondii* (*Toxoplasma*) and host mitochondria are mediated by the parasite effector TgMAF1 and host TOM70 (Blank et al., 2021; X. Li et al., 2022; Pernas et al., 2014).

Their formation induces the shedding of large structures positive for outer mitochondrial membrane (SPOTs) (X. Li et al., 2022; Pernas et al., 2014). SPOTs mediate the depletion of OMM proteins such as mitofusin 1 and mitofusin 2 that enable mitochondrial restriction of FAs needed for parasite replication (X. Li et al., 2022; Pernas et al., 2018). Thus, *Toxoplasma*-mitochondria MCS may represent a parasite countermeasure to mitochondrial nutrient competition (Medeiros et al., 2021).

Toxoplasma also forms MCS with host ER and is the only known eukaryotic pathogen reported to do so (Sinai et al., 1997). The significance of host ER-*Toxoplasma* MCS during infection is unknown. This lack of understanding—and in fact our understanding of the role of most host-pathogen MCS—is due to our limited knowledge of the protein tethers that mediate their formation. Biochemical and proteomic techniques that have traditionally been used to define tethers are labour intensive, low throughput, and have failed to reliably identify mediators of host-pathogen MCS (Ferrel et al., 2023; J. Y. Kim et al., 2008; Sinai & Joiner, 2001).

We pioneered a versatile fluorescent sensor of host-pathogen contact sites to study the MCS that form between *Toxoplasma* and host organelles. By coupling our sensor to FACS-based loss-of-function CRISPR-Cas9 screening, we identified both the parasite effector TgROP1, and host ER proteins VAPA/B, as the tethers required for *Toxoplasma*-host ER MCS. Using a combination of live cell-imaging, electron microscopy, and proteomic approaches we found that TgROP1 and VAPA/B interaction occurs at domains known to mediate ER contact sites with other organelles and *Chlamydia* (Stanhope et al., 2017; H. Wu et al., 2018). Last, we show that infection influences the VAP interactome during infection. Our discovery of TgROP1 and VAPA/B as the mediators of host ER-*Toxoplasma* MCS reveals that the targeting of host MCS tethers appears to be a common strategy exploited by pathogens. Furthermore, our work paves the way for future studies exploring the factors underlying MCS between diverse pathogens and host organelles, as well as their significance during infection.

3.1.3 Results

The canonical strains of *Toxoplasma* associate with host ER

The three predominant strains of *Toxoplasma*—Types I, II, and III—differ greatly in their interactions with the host cell (Howe & Sibley, 1995; Saeij et al., 2005). For example, MCS between host mitochondria and *Toxoplasma* occurs in a strain-specific manner, and this has also been reported for the bacteria *Chlamydia* (Matsumoto et al., 1991; Pernas et al., 2014). Previous work exploited these strain-specific differences—Type I tethers mitochondria whereas Type II do not—to identify the *Toxoplasma* mediator of host mitochondria-*Toxoplasma* MCS, termed host mitochondrial association (HMA) (Pernas et al., 2014). We therefore asked whether the canonical *Toxoplasma* strains also differentially associated with host ER. To do so, we examined the interaction between the host ER and the *Toxoplasma* parasite vacuole (PV) in human ovarian cancer (ES-2) cells infected with *Toxoplasma* strains Type I, Type II, and Type III. However, we found that at 3 hours post infection (hpi), the ER membrane protein calnexin was similarly enriched around Type I, II, and III parasites (Fig. 1a). As expected, at 24 hpi HMA was only observed during infection with Type I and III parasites that tether host mitochondria (Fig. 1b) (Pernas et al., 2014).

Organelle-organelle MCS are generally defined as two membranes apposed between 10-30 nm (ranging up to 80 nm) in distance (Scorrano et al., 2019). To therefore determine whether host ER forms MCS with *Toxoplasma*, we performed quantitative electron microscopy (EM) analysis of ES-2 cells infected with strains Type I and Type II, while the Type III *Toxoplasma* strain was assessed only qualitatively (Extended Data Fig. 1). The average distance between the host ER and the PV membrane (PVM) in cells infected with Type I parasites was ~25 nm, consistent with previous reports (Fig. 1c,d) (Sinai et al., 1997). Type II parasites exhibited similar distances of on average ~25.5 nm between host ER and the *Toxoplasma* PVM (Fig. 1d). Similarly, we observed that host ER closely associated to the vacuoles of Type III parasites (Fig. 1c). Furthermore, on average ~64% of the total perimeter of Type II PVs exhibited MCS with host ER in comparison to ~36% for Types I parasites (Fig. 1e). Of note, ribosomes were excluded at the host ER-

Toxoplasma interface, as occurs during mitochondria-ER MCS (Fig. 1c) (H. Wu et al., 2018). Thus, our data suggests that all *Toxoplasma* strains form contact sites with the host ER.

The fact that Types II parasites associated with ER more than Type I parasites which inversely correlates with their ability to form contact sites with host mitochondria, led us to ask whether HMA influenced the extent of host ER-*Toxoplasma* interactions (Pernas et al., 2014). To address this, we assessed their formation during infection with WT Type I and Type I:Δ*maf1* parasites that are deficient for HMA (Pernas et al., 2014). Indeed, Type I:Δ*maf1* parasites vacuoles exhibited a ~30% increase in host ER association relative to WT parasites (Extended Data Fig. 2). Thus, our data suggests that HMA limits the extent of MCS between host ER and *Toxoplasma*.

A reporter of host-pathogen membrane contact sites coupled to loss-of-function CRISPR-Cas9 screening

Our finding that the major strains of *Toxoplasma* associate with the ER precluded the use of genetic crosses between the canonical lineages to determine the genes responsible for mediating these MCS (Pernas et al., 2014). To overcome this, we sought to establish a reporter of host organelle-*Toxoplasma* membrane contact sites that would be amenable to unbiased and high throughput approaches. To this end, we turned to a split-GFP-based reporter previously used to monitor organelle-organelle MCS (Cieri et al., 2018). In brief, the system consists of targeting non-fluorescent moieties of GFP—namely $GFP^{1–10}$ and $GFP^{\beta 11}$—to the membranes of distinct organelles. Following the formation of MCS between the respective membranes, GFP is reconstituted and fluoresces (Cieri et al., 2018).

To adapt this reporter to detect host-pathogen MCS, we first turned to host mitochondria-*Toxoplasma* MCS because both the host and parasite tethers are known (Blank et al., 2021; X. Li et al., 2022; Pernas et al., 2014). To this end, we generated ES-2 cells expressing $GFP^{1–10}$ targeted to the OMM ($OMM^{GFP1–10}$) via the transmembrane domain (TM) of TOM20 (Fig. 2a and Extended Data Fig. 3a) (Cieri et al., 2018). For PVM-targeting, we engineered Type I:mCherry-expressing parasites (*Toxo*^{mCherry}) to express $GFP^{\beta 11}$ fused to

the signal peptide and TM-containing N-terminus of TgMAF1 (PVM$^{\beta11}$) (Fig. 2a and Extended Data Fig. 3b). Because previous work reported that the distance between host mitochondria and the *Toxoplasma* vacuole is on average 12 nm, we also included a spacer of 32 amino acids between the TgMAF1 TM domain and GFP$^{\beta11}$ (Feng et al., 2017; Sinai et al., 1997). First, we analysed WT and OMM$^{GFP1–10}$-expressing ES-2 cells (OMM$^{GFP1–10}$ ES-2) infected with either *Toxo*^{mCherry} or PVM$^{\beta11}$-expressing *Toxo*^{mCherry} parasites (*Toxo*$^{PVM\beta11}$) by immunofluorescence (IF). We found that GFP was only detected at the host mitochondria-PVM interface when both GFP moieties were present (Fig. 2b). In line with this result, live cell microscopy of primary human foreskin fibroblasts (HFFs) expressing OMM$^{GFP1–10}$ and infected with *Toxo*$^{PVM\beta11}$ parasites revealed that GFP was detected at the mitochondria-*Toxoplasma* interface following the formation of MCS (Fig. 2c and Supplementary Video 1). We next asked whether our sensor was amenable to high throughput approaches. To test this, we analysed OMM$^{GFP1–10}$ ES-2s that were uninfected, or infected with either *Toxo*^{mCherry} or *Toxo*$^{PVM\beta11}$ parasites by flow cytometry. Consistent with our IF data, GFP was detected in OMM$^{GFP1–10}$ ES-2s infected with *Toxo*$^{PVM\beta11}$, but not *Toxo*^{mCherry} parasites by flow cytometry analysis (Fig. 2b and Extended Data Fig. 4). Thus, our split-GFP sensor reports on mitochondria-*Toxoplasma* MCS in microscopy and high throughput approaches.

A caveat of split-GFP systems is the irreversible nature of GFP reconstitution, resulting in the forcing of contact sites (Scorrano et al., 2019). To test the extent to which our split-GFP system artificially induced host mitochondria-*Toxoplasma* contact sites, we turned to HeLa cells deficient for TOM70 (*TOM70 KO*), the host factor required for HMA (Extended Data Fig. 5a). (Blank et al., 2021; X. Li et al., 2022). We first confirmed the localization of our OMM$^{GFP1–10}$ construct to the mitochondria of WT HeLa and *TOM70 KO* cells (Extended Data Fig. 5b). Next, we infected these cells with *Toxo*$^{PVM\beta11}$ parasites and assessed by confocal microscopy. We detected GFP mostly at the host mitochondria-PVM interface in WT but not OMM$^{GFP1–10}$ *TOM70 KO* cells (Extended Data Fig. 5c). Flow cytometry analysis further confirmed this, as infected *TOM70 KO* OMM$^{GFP1–10}$ cells were mostly GFP-negative at 8 hpi and 24 hpi (Fig. 2d). Thus, our split-GFP sensor recapitulates mitochondria-*Toxoplasma* contact site biology.

We next asked whether our system may be amenable to loss-of-function CRISPR screening approaches that could be applied to identify the tethers required for host organellar-*Toxoplasma* MCS in an unbiased manner. To this end, we turned to a previously established CRISPR library containing sgRNAs targeting 325 predicted *Toxoplasma* effector proteins that are derived from *Toxoplasma* secretory organelles: rhoptry neck proteins (RONs), rhoptry bulb proteins (ROPs), and dense granule proteins (GRAs) (Supplementary Table 1) (Butterworth et al., 2023; Young et al., 2019). We chose this library because a subset of ROPs and GRAs localize to the PVM, making them ideal candidates for contact site tethers, as in the case of the dense granule effector TgMAF1 (Pernas et al., 2014; Rastogi et al., 2019). To test the validity of our reporter for CRISPR screening, we created a new *Toxoplasma* strain expressing the PVM$^{\beta11}$ construct in the Type I *Toxoplasma* background without a fluorophore and transfected this parasite strain with a *Toxoplasma* effector sgRNA library (containing mCherry) (Fig. 2e). The resulting pool of mCherry-expressing KO parasites were then used to infect the OMM$^{GFP1–10}$ ES-2s at a low multiplicity of infection (MOI) of 0.5 to ensure a single parasite per cell and thereby assess the role of individual *Toxoplasma* effectors in mediating HMA (Fig. 2e).

At 24 hpi, mCherry-positive infected cells were FACS-sorted into GFP-negative (GFP^{neg}) and GFP-high (GFP^{hi}) populations (Fig. 2e). We reasoned that sgRNAs enriched in the GFP^{neg} population but depleted in the GFP^{hi} population would include genes that encode for candidate mediators of host mitochondria-*Toxoplasma* MCS (Fig. 2e). To identify these genes, we extracted *Toxoplasma* genomic DNA (gDNA) and amplified *Toxoplasma* sgRNAs from the GFP^{neg} and GFP^{hi} populations for next generation sequencing (NGS) (Fig. 2e). Using the model-based analysis of genome-wide CRISPR-Cas9 knockout (MAGeCK) method, we quantified the median $\log_2$ fold change (Log_2FC) in the sgRNA abundance between the GFP^{hi} and GFP^{neg} populations and ranked genes using robust rank aggregation (RRA) (Fig. 2f) (W. Li et al., 2014). Our analysis identified TgMAF1, dense granule protein 45 (TgGRA45) and TgME49_323110 as the top candidate promoters of HMA (Fig. 2f and Supplementary Table 2). These results were expected because TgMAF1 binds TOM70 to mediate HMA (Blank et al., 2021; X. Li et al., 2022; Pernas et al., 2014). Indeed, OMM$^{GFP1–10}$ ES-2s infected with Δ*maf1* parasites engineered to express PVM$^{\beta11}$ were mostly GFP-negative at 8 hpi and 24 hpi (Fig. 2g,h). TgGRA45 is a chaperone-like

protein required for the PVM localization of GRAs such as TgMAF1 (Y. Wang et al., 2020). Last, the TgMAF1 locus comprises of multiple *TgMAF1* gene copies that belong to two distinct TgMAF1 paralogs: TgMAF1a variants including TgME49_323110, and TgMAF1b variants (Adomako-Ankomah et al., 2016). Although TgMAF1b, but not TgMAF1a tethers mitochondria, the targeting of TgME49_323110 likely disrupted the *MAF1* locus and thus TgMAF1b (Adomako-Ankomah et al., 2016; Blank et al., 2021). Thus, our host-pathogen MCS sensor is compatible with unbiased and high throughput loss-of-function approaches.

Unbiased approach to determine ER-*Toxoplasma* contact sites tethers

Having validated our split-GFP sensor using host mitochondria-*Toxoplasma* MCS, we adapted it to the study of host ER-*Toxoplasma* MCS, for which the host and parasite tethers are unknown. To do so, we used the TM domains of the ER phosphatase SAC1 to target GFP^{1-10} to the host ER membrane ($ERM^{GFP1-10}$) (Extended Data Fig. 6a,b) (Cieri et al., 2018). As with our host mitochondria-*Toxoplasma* MCS sensor, GFP was detected at the host ER-*Toxoplasma* interface (Extended Data Fig. 6c). Furthermore, at 24 hpi upto 50% of $ERM^{GFP1-10}$ ES-2s infected with $Toxo^{PVM\beta11}$ but not $Toxo^{mCherry}$ were GFP-positive (Extended Data Fig. 6d). Thus, our split-GFP sensor can be adapted to study diverse host organelle-pathogen MCS.

To identify the *Toxoplasma* factor(s) that mediates host ER-*Toxoplasma* MCS, we applied the same experimental pipeline as for our host mitochondria-*Toxoplasma* MCS screen (Fig. 3a). To this end, we infected $ERM^{GFP1-10}$ ES-2s with the same $PVM^{\beta11}$-expressing *Toxoplasma* that were transfected with the *Toxoplasma* effector sgRNA library. At 24 hpi, we sorted mCherry-positive infected cells into GFP^{hi} and GFP^{neg} populations (Fig. 3a). We expected that sgRNAs enriched in the GFP^{neg} population but depleted in the GFP^{hi} population would represent candidate mediators of host ER-*Toxoplasma* MCS, as was the case for TgMAF1 (Fig. 2f). We subsequently extracted *Toxoplasma* gDNA from these populations and amplified *Toxoplasma* sgRNAs for NGS. We then calculated the Log_2FC of *Toxoplasma* sgRNA abundances in the sorted GFP^{hi} and GFP^{neg} populations and RRA scores using MAGeCK (W. Li et al., 2014). Interestingly, TgGRA45 emerged as the top candidate promoter of host ER-*Toxoplasma* MCS (Fig. 3b and Supplementary Table 3).

We speculated that this is likely due to its role in the PVM insertion of our reporter, as it does for TgMAF1 (Fig. 2f, and Extended Data Fig. 7a) (Y. Wang et al., 2020). To test this, we infected ES-2 cells with WT and Δ*gra45* parasites and analysed by EM at 3 hpi (Y. Wang et al., 2020). As expected, Δ*gra45* still mediated host ER-*Toxoplasma* MCS but had reduced host mitochondria-*Toxoplasma* MCS (Extended Data Fig. 7b,c). Thus, the MCS between host ER and *Toxoplasma* form independently of TgGRA45 (Extended Data Fig. 7b,c).

The *Toxoplasma* effector rhoptry protein 1 (TgROP1) is required for host ER-*Toxoplasma* MCS

This finding that the loss of TgGRA45 did not perturb host ER-*Toxoplasma* association allowed us to exclude other GRAs from our list of candidates and indicated a possible role for rhoptry proteins. As aforementioned, other than GRAs our CRISPR library consisted of rhoptry neck (RONs) and rhoptry bulb (ROPs) proteins. RONs are required for host cell attachment and invasion and remain localized at the host plasma membrane (Rastogi et al., 2019). Thus, they are unlikely mediators of host ER-*Toxoplasma* MCS as we would expect PVM localization of our tether. ROPs on the other hand are secreted during invasion, a subset of which localize to the PVM (Rastogi et al., 2019). We therefore focused on ROP effectors with a $Log_2FC < -0.05$ (>= 2 guides/ gene) of which there were 12 candidates (Fig. 3b,c). We next asked which of our ROP candidates had potential features of a host ER-*Toxoplasma* tether. We reasoned that a parasite tether must localize to the PVM. Second, because to form MCS with mitochondria TgMAF1 binds TOM70, a known mitochondria-organelle tether, we hypothesized that *Toxoplasma* might also exploit a known ER-organelle tether (Blank et al., 2021; Eisenberg-Bord et al., 2021; Filadi et al., 2018; X. Li et al., 2022; Pernas et al., 2014). Indeed, the *Chlamydia* effector protein IncV interacts with the homologous major sperm protein (MSP) domains of host VAPA/B, which tether the ER to several organelles including endosome, Golgi and plasma membrane (Murphy & Levine, 2016; Stanhope et al., 2017; H. Wu et al., 2018).

TM domains or PVM localization were predicted for 7 of our 12 ROP candidates (Fig. 3c) (Barylyuk et al., 2020; Butterworth et al., 2023). We next screened these 7 ROPs for the presence of a VAP-interacting motif. For this, we used the canonical VAP-interacting FFAT motif (EFFDAxE) taken from the eukaryotic linear motif (ELM) database (M. Kumar et al.,

2024). The FFAT motif contains an aromatic residue at position 2, and an alanine or cysteine at position 5. Because the flanking acidic residues can vary in position, we also modified the canonical FFAT motif to ExFxDAxE allowing for variation in distance from the core motif. We found that 5 of the 7 ROP candidates had putative FFAT motif matches (Fig. 3c and Supplementary Table 4). We then used AlphaFold multimer to generate structural models of the MSP domain of VAPA together with the different protein fragments containing the motif matches in our candidates; using protein fragments has been shown to boost AlphaFold specificity in comparison with using full-length proteins and generates models of higher confidence (C. Y. Lee et al., 2024). We extracted model confidence (iptm+ptm) for each domain-motif pair, evaluated the pLDDT (predicted local distance difference test), and inspected the PAE (predicted aligned error) scores of the residues at the interacting interface. We then ranked the matches: a model score ≥ 0.7 and average pLDDT of ≥ 70 was considered a high confidence model, whereas a model score < 0.7 and pLDDT values below 70 were considered as low confidence (Fig. 3c and Supplementary Table 4) (C. Y. Lee et al., 2024). Our analysis yielded only two ROPs with putative FFAT motifs that had high-confidence interactions with VAPA: TgROP6 and TgROP1.

TgROP6 had both a canonical EFFDAxE motif at residues 88-89, and a modified ExFxDAxE motif at residues 323-332, which had AlphaFold model scores of 0.82 and 0.74, and motif pLDDT values of 79.4 and 86.89, respectively (Extended Data Fig. 8a and Supplementary Table 4). To address the role of TgROP6 in host ER-*Toxoplasma* MCS, we first generated Type I parasites deficient for TgROP6 (Δ*rop6*) (Extended Data Fig. 8b-d). Then, we compared the association between host ER and the PVM of WT and Δ*rop6* Type I *Toxoplasma* parasites by EM at 3 hpi. However, we observed no significant differences in host ER-*Toxoplasma* MCS between WT and Δ*rop6* parasites (Extended Data Fig. 8e,f). Thus, loss of TgROP6 does not impair host ER-*Toxoplasma* MCS.

We next focused on TgROP1. TgROP1 had three predicted modified motifs although only one had a high-confidence VAP-interacting score which is the third predicted ExFxDAxE motif at residues 134-143 (in Type II parasites), with an AlphaFold model score of 0.83 and a motif pLDDT value of 91.45 (Fig. 3d). Asp 139 of TgROP1 was predicted to form

hydrogen bridges with Lys 50 and Lys 52 of the MSP domain of VAPA, with Phe 137 and Ala 140 positioned in its two hydrophobic pockets (Fig. 3d). Of interest, the TgROP1 putative VAP interacting motif DDTFHDALQE was conserved across the canonical *Toxoplasma* strains that are all positive for host ER-*Toxoplasma* association (Fig. 1; Extended Data Fig. 9a). We confirmed that TgROP1 localized to the PVM, which is consistent with previous reports (Fig. 3e) (Butterworth et al., 2023). Next, we examined ES-2 cells infected with *Toxoplasma* Type I WT and TgROP1 KO parasites (Δ*rop1*) by EM (Butterworth et al., 2022). Δ*rop1* parasites exhibited a ~80% decrease in ER association, and corresponding increase in HMA relative to WT parasites at 3 hpi (Fig. 3f,g). Importantly, the expression of Tg*ROP1-HA* in Δ*rop1* parasites (Δ*rop1*:*ROP1-HA*) rescued host ER-*Toxoplasma* MCS formation (Fig. 3f,g) (Butterworth et al., 2022). Similar results were observed for Type II WT, Δ*rop1*, and Δ*rop1*:*ROP1-HA* parasites (Extended Data Fig. 9b-d) (Butterworth et al., 2022). Thus, TgROP1 is the major parasite factor required for host ER-*Toxoplasma* MCS.

Host VAPA/B are required for ER-*Toxoplasma* membrane contact sites

To test whether TgROP1 interacted with VAPA/B as predicted by our *in silico* analysis, we immunopurified TgROP1 from cells infected with Δ*rop1*:*ROP1-HA* parasites. To control for TgROP1 interactors that resulted from the nonspecific enrichment of PVM proteins, we also immunopurified TgMAF1 from cells infected with Δ*maf1:HA-MAF1* parasites. Although we did not observe an HA signal in the input, as expected, TOM70 but not VAPA or VAPB, was enriched in HA-TgMAF1 IPs (Fig. 4a) (X. Li et al., 2022). Interestingly, VAPA and VAPB were enriched in TgROP1-HA IPs. TgGAP45 which is a marker for *Toxoplasma* infection indicated that our Δ*rop1*:*ROP1-HA* parasites had a significantly higher percentage of infection in cells, which could explain the increased interaction (Fig. 4a). However, our immunoblot analysis revealed that the ER membrane protein calnexin was not enriched in TgROP1-HA IPs (Fig. 4a). Thus, our data indicates that TgROP1 interacts with VAPA/B.

Having established a potential interaction between TgROP1 and VAPA/B, we next asked whether VAPA/B are the host factors that mediate host ER-*Toxoplasma* MCS. As protein tethers are often present at MCS, we examined the distribution of VAPA/B during infection

(Scorrano et al., 2019). To do so, we performed live-cell imaging of HFFs stably expressing GFP-VAPA, and infected with Type I *Toxoplasma* parasites. Soon after infection, VAPA was strongly enriched around the parasite vacuole (Fig. 4b and Supplementary Video 2). To determine whether the enrichment of VAPA/B was dependent on TgROP1 we infected HeLas deficient for VAPA and VAPB (VAP DKO) cells re-expressing either GFP-VAPA^{WT} or GFP-VAPB^{WT}, with *Toxoplasma* Type I and II: WT, Δ*rop1*, and Δ*rop1*:*ROP1-HA* parasites (Fig. 4c,d and Extended Data Fig. 10 and Fig. 11) (Dong et al., 2016). Indeed, VAPA/B enrichment was dependent on TgROP1 because neither VAPA nor VAPB was enriched at the parasite vacuoles of most Δ*rop1* parasites (Fig. 4c,d and Extended Data Fig.10 and Fig. 11). Thus, both VAPA and VAPB are enriched at the *Toxoplasma* vacuole in a TgROP1-dependent manner.

To determine whether VAPA/B are required for host ER-*Toxoplasma* MCS, we compared the association of host ER around *Toxoplasma* in WT HeLas and VAP DKO HeLas (Dong et al., 2016). Using calnexin as a marker for host ER, we found that in most VAP DKO cells, host ER failed to associate with the parasite vacuole (Extended Data Fig. 12). To more closely assess the effect of VAP ablation on host ER-*Toxoplasma* MCS, we examined WT and VAP DKO cells infected with Type I WT parasites by EM (Dong et al., 2016). The loss of VAPA/B led to a great reduction in host ER association with the *Toxoplasma* vacuole at 3 hpi (Fig. 4e,f). Conversely, HMA was increased in VAP DKO cells, suggesting that host ER-*Toxoplasma* MCS limit the extent of contact sites between the mitochondria and *Toxoplasma* (Fig. 4e,f). Thus, VAPA and VAPB are the host factors required for ER-*Toxoplasma* MCS.

Toxoplasma exploits the MSP domain of host VAPs

To determine whether TgROP1 interacted with the MSP domain of VAPA/B, we used proteomics to compare interacting partners of VAP DKO cells re-expressing either GFP-VAPA^{WT}, or the GFP-VAPA$^{K94D/M96D}$ MSP mutant that is deficient for binding FFAT containing-proteins in uninfected or *Toxo*^{mCherry}-infected cells (Extended Data Fig. 13 and Supplementary Table 5) (Kaiser et al., 2005; Murphy & Levine, 2016). TgROP1 was the most abundant *Toxoplasma* protein found in GFP-VAPA^{WT} IPs (Fig. 5a). However, TgROP1 was de-enriched ~16-fold in GFP-VAPA$^{K94D/M96D}$ IPs relative to GFP-VAPA^{WT} (Fig. 5b). We next

tested the role of the VAP MSP domain in host ER-*Toxoplasma* contact sites. We found that in the majority of cells neither GFP-VAPA$^{K94D/M96D}$ nor calnexin were enriched at the *Toxoplasma* vacuole as assessed by confocal microscopy (Fig. 5c,d). In line with this, GFP-VAPA$^{K94D/M96D}$ cells had reduced host ER-*Toxoplasma* contact sites compared to GFP-VAPA^{WT} cells as analysed by EM (Fig. 5e,f). Similar results were obtained for the MSP mutant of GFP-VAPB$^{K87D/M89D}$ via both confocal and EM analysis (Extended Data Fig. 14) (Kaiser et al., 2005). Thus, *Toxoplasma* exploits the conserved MSP binding domain of VAPA/B to form host ER-*Toxoplasma* MCS.

To address the role of host ER-*Toxoplasma* MCS, we compared abundances of interacting partners of VAPA between uninfected and *Toxo*^{mCherry}-infected GFP-VAPA^{WT}-expressing DKO cells. To do so, we curated a list of 245 putative VAPA-interactors as identified from previous reports, OpenCell and BioPlex databases (Supplementary Table 6) (Cho et al., 2022; Huttlin et al., 2015; James & Kehlenbach, 2021). Our preliminary analysis of these proteins revealed that several lipid transfer proteins, including C2CD2L, VPS13A and members of the family of oxysterol-binding proteins (OSBP) and OSBP-related (ORP/OSBPL) protein, were more abundant in VAPA-IPs during infection (Fig. 5g) (N. Kumar et al., 2018; Olkkonen & Ikonen, 2024; Raychaudhuri & Prinz, 2010). The result that infection leads to the enrichment of VAPs at the PVM, and in increased interaction between VAPA and lipid-transfer proteins lead us to hypothesize that host ER-*Toxoplasma* MCS may be a potential avenue for parasites to scavenge lipids from their hosts.

3.1.4 Discussion

Here, we developed a sensor to study the MCS that form between *Toxoplasma* and host ER or mitochondria. Thus, our sensor can be adapted for the study of host-pathogen MCS between any genetically tractable pathogen and host organelle. Furthermore, it is amenable to high throughput approaches and genetic screening. Coupling this sensor to loss-of-function CRISPR screening in *Toxoplasma*, we discovered that TgROP1 and VAPA/VAPB are the tethers that mediate host ER-*Toxoplasma* MCS.

Our finding raises several questions, beginning with what is the role of host ER-*Toxoplasma* MCS? VAPA and VAPB interact with key lipid-transfer proteins facilitating non-vesicular, direct trafficking of lipids at membrane contact sites (Voeltz et al., 2024). *Toxoplasma* require lipids, bioenergetically costly molecules, to sustain the biogenesis of both its parasite vacuole membrane and parasite plasma membrane during proliferation. MCS therefore may promote parasite acquisition of host lipids (Voeltz et al., 2024; H. Wu et al., 2018). In line with this possibility, our proteomics dataset suggests that *Toxoplasma* infection promoted the interaction between VAPA and lipid transfer proteins.

Our data show that *Toxoplasma* uses effectors from distinct secretory organelles to tether host ER and host mitochondria; TgROP1 from rhoptries and TgMAF1 from dense granules, respectively (Pernas et al., 2014). Rhoptries are released concomitant with *Toxoplasma* invasion. Meanwhile, dense granules are released following invasion and throughout the intracellular life cycle of the parasite (Rastogi et al., 2019). Thus, host organelle-*Toxoplasma* MCS are temporally regulated. Furthermore, our data indicates competition between host ER and host mitochondria for binding to the *Toxoplasma* vacuole. One possibility for this potential competition is that the ER/mitochondria-*Toxoplasma* MCS are linked to the needs of the parasite. For example, early access to ER-derived host lipids may support a growing vacuole, while tethering mitochondria activates a *Toxoplasma* defence at later stages. In line with this, TgMAF1 drives the shedding of OMM proteins, effectively eliminating mitochondrial nutrient competition (X. Li et al., 2022).

Why are VAPA/B and TOM70 frequently targeted by diverse pathogens such as *Toxoplasma, Chlamydia* and SARS-CoV-2 (Blank et al., 2021; Jiang et al., 2020; X. Li et al., 2022; Vormittag, Ende, et al., 2023a). One commonality between VAPA/B and TOM70 is that these proteins are key mediators of organelle-organelle MCS (Filadi et al., 2018; H. Wu et al., 2018). Thus, by interacting with MCS mediators, pathogens may benefit from the various functions of MCS such as lipid transfer or disrupt organelle-organelle communication that facilitates immune signalling (Cook et al., 2022; Vormittag, Ende, et al., 2023a). Our data suggests that *Toxoplasma* infection promotes the interaction

between VAPs and lipid transfer proteins OSBPs and OSBP-related (ORP/OSBPL) proteins. *Chlamydia* effectors interact with host VAPs and the lipid transfer protein CERT to form MCS between host ER and *Chlamydia* inclusions (Agaisse & Derré, 2014; Derré et al., 2011; Stanhope et al., 2017). The depletion of CERT or VAP restricts *Chlamydia* inclusion size and infectious progeny production (Agaisse & Derré, 2014; Derré et al., 2011; Elwell et al., 2011). Conversely, human cytomegalovirus infection leads to a decrease in ER-mitochondria MCS, thereby facilitating evasion of STING-dependent immune signalling (Cook et al., 2022).

Our development of a sensor for host-pathogen MCS enabled our identification of the only tethers known to mediate MCS between a eukaryotic pathogen and host ER. Our discovery shows that the targeting of host contact-site tethers appears to be a common strategy exploited by pathogens during infection. This paves the way for future studies exploring non-canonical pathogen effector strategies and the role of host-pathogen contact sites during infection.

Acknowledgments and funding: We thank the MPI-Proteomics facility; the MPI-AGE FACS and Imaging Core for flow cytometry and microscopy support-in particular Kat-Folz Donahue, Lena Schumacher and Maximilian Germer; the CECAD electron microscopy facility, in particular Katrin Seidel and Frederic Wolf. We thank all members of the Pernas laboratory for helpful discussions and in particular Dr. Johannes Felix Stortz, Dr. Tânia Catarina Medeiros, Dr. Sebastian Kreimendahl, Silvia Reato and Michelle Téllez Sutterlin, and Ana Matias from the Treeck lab for technical support. We also thank Dr. Pietro De Camilli for sharing VAP DKO cells, Dr. Tito Calì for split-GFP construct information and plasmids, Dr. Jeroen P. J. Saeij for the Δ*gra45* parasites and Dr. Martin Blume for Type III parasites. This work was supported by Cologne Graduate School of Ageing research (C.M.); the European Research Council ERC-StG-2019 852457 (L.F.P.); Deutsche Forschungsgemeinschaft SFB 1218 Project ID 269925409 (L.F.P.); and the Howard Hughes Medical Institute (L.F.P.). M.T is supported by the Wellcome Trust (223192/Z/21/Z) & The Francis Crick Institute, which receives its core funding from Cancer Research UK (CC2132 & CR2023/030/2132), the UK Medical Research Council (CC2132& CR2023/030/2132), and the Wellcome Trust (CC2132& CR2023/030/2132). MT is also

supported by the FCT - Fundação para a Ciência e Tecnologia, I.P. through project reference 2023.06167.CEECIND. F.T. is supported by the Deutsche Forschungsgemeinschaft (TO 1349/1-1). Funding for transmission election microscope instrumentation: JEOL JEM-2100 Plus: INST 216/793-1 FUGG. Certain figures were created using BioRender.com.

Author contributions: Conceptualization: C.M and L.F.P. Methodology: C.M., F.T., J.A.V., J.S., S.L., M.T. and L.F.P. Investigation: All authors. Resources: All authors. Funding acquisition: C.M. and L.F.P. Project administration: L.F.P. Writing, original draft: C.M. and L.F.P. Review and editing: All authors. Supervision: L.F.P.

Competing interests: Authors declare that they have no competing interests.

Data and materials availability: All data are available in the main text or the supplementary materials.

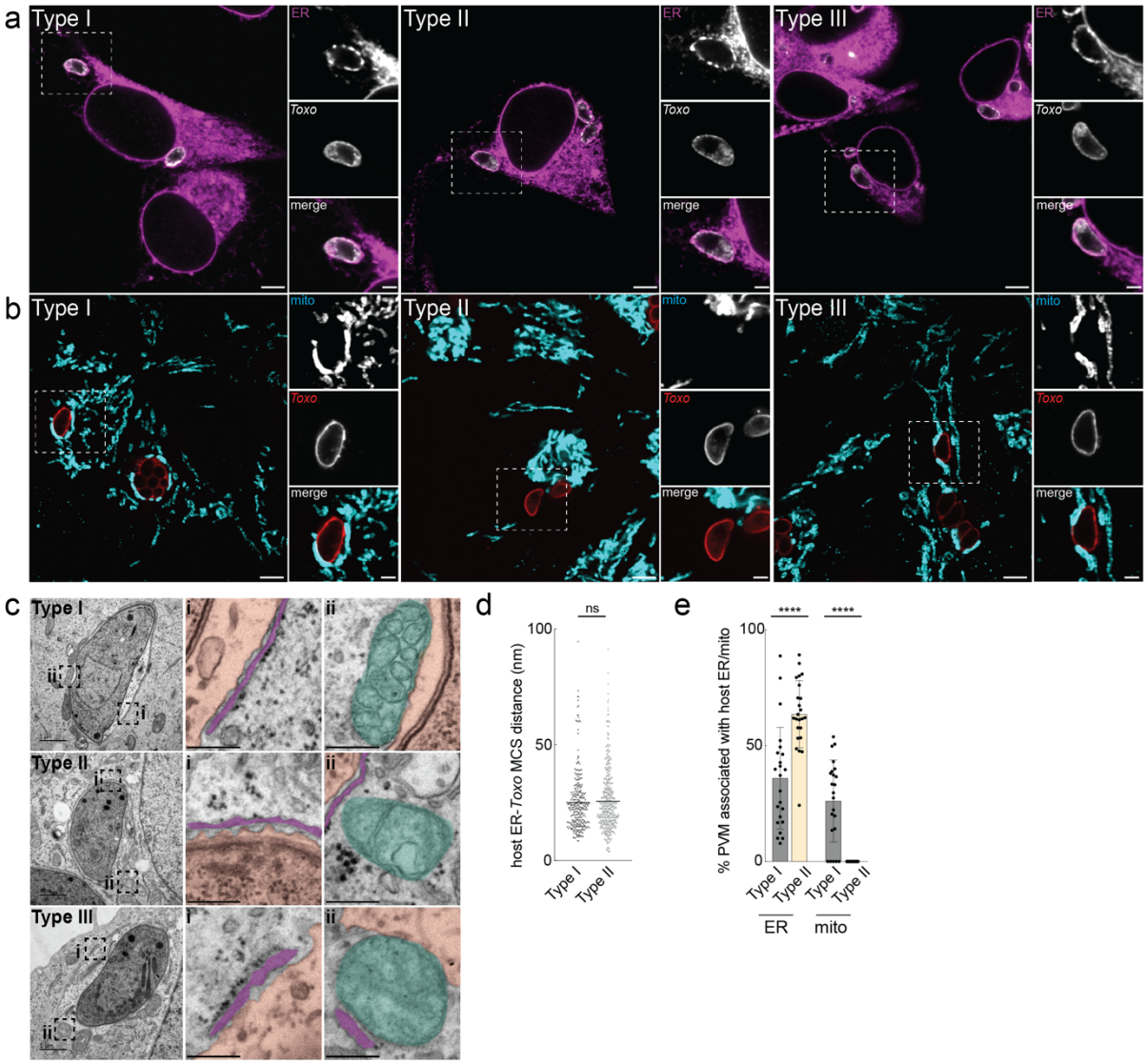

Fig. 1: *Toxoplasma* Type I and Type II form membrane contact sites with host ER
a,b, Immunofluorescence images of ES-2 cells infected with *Toxoplasma* strains Type I (RH), Type II (ME49) and Type III (VEG). *Toxo* (surface antigen 1; TgSAG1); ER (calnexin); mito (TOM70). Scale bars: 5 µm; inset, 2 µm. Data is representative of one biological replicate. **c,** Representative electron micrograph (EM) images of ES-2 cells infected with indicated *Toxoplasma* strains. Membrane contact sites (MCS) between the *Toxoplasma* parasite vacuole membrane (PVM) and (**i**) host ER and (**ii**) host mito. Scale bars: 1 µm; inset, 250 nm. Red, parasite vacuole; purple, ER; turquoise, mito. **d,** Quantification of the MCS distance between host ER and *Toxoplasma* PVM from images as in (**c**) from Type I and Type II parasites of one-pack parasite stage at 3 and 24 hours post infection. Data are mean of >20 *Toxoplasma* vacuoles from n=1 biological replicate. **e,** Percentage of *Toxoplasma* PVM associated with host ER and mitochondria from infected cells as in (**c**). **** $p<0.0001$ by means of unpaired t-test. Data are mean ± SD of >20 *Toxoplasma* vacuoles from n=1 biological replicate.

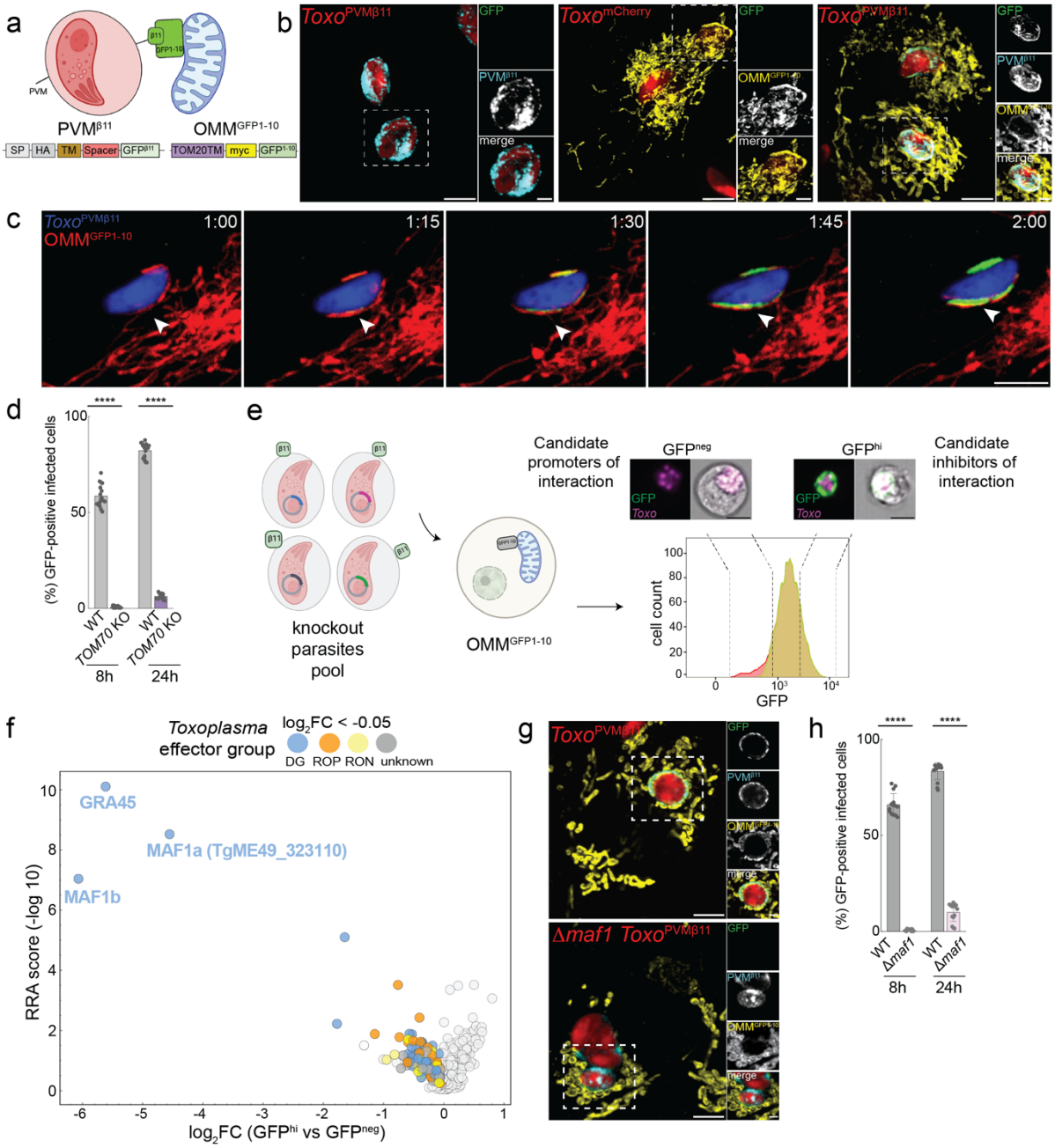

Fig. 2: A sensor to identify host organelle-*Toxoplasma* membrane contact sites

a, Schematic of the PVM^{β11} and OMM$^{GFP1-10}$ constructs generated for the host mitochondria-*Toxoplasma* split-GFP system. PVM, parasite vacuole membrane; SP, signal peptide; TM, transmembrane domain; OMM, outer mitochondrial membrane; TOM20; translocase of the outer membrane 20. **b,** Immunofluorescence (IF) images of: (left) WT ES-2 cells infected with parasites expressing PVM^{β11} (*Toxo*^{PVMβ11}); (center) OMM$^{GFP1–10}$-expressing ES-2 cells (OMM$^{GFP1–10}$ ES-2) infected with mCherry-expressing *Toxoplasma* (*Toxo*^{mCherry}); and (right) *Toxo*^{PVMβ11}-infected OMM$^{GFP1-10}$ ES-2 cells. PVM^{β11} (HA); OMM$^{GFP1-10}$ (myc). Scale bars: 5 µm; inset, 2 µm. Data is representative of two biological replicates **c,** Live cell images of a MitoTracker Deep Red labelled human foreskin fibroblast cell expressing OMM$^{GFP1-10}$ and infected with *Toxo*^{PVMβ11} parasite. Represented are 5 time points at 15-minute intervals where arrowheads indicate GFP at the mitochondria-*Toxoplasma* interface. Scale bar: 5 µm. (Supplementary Video 1). **d,** WT

and *TOM70 KO* HeLa cells expressing OMM$^{GFP1-10}$ were infected with *Toxo*$^{PVM\beta11}$ and analysed at 8 and 24 hours post infection (hpi) by means of flow cytometry for GFP expression. Data are mean ± SD of n=5 biological replicates. Each dot represents a technical replicate. ****p<0.0001 for WT versus *TOM70 KO* HeLa cells by two-way ANOVA. **e,** Schematic of CRISPR screen to identify parasite mediators of host mitochondria-*Toxoplasma* MCS. Type I *Toxoplasma* expressing PVM$^{\beta11}$ were transfected with a sgRNA library targeting *Toxoplasma* effector proteins. The resulting pool of KO parasites were used to infect OMM$^{GFP1-10}$ ES-2 cells. Approximately 24 hpi, mCherry-positive infected cells were sorted based on GFP expression. Images were obtained during test sorts. Arbitrary dashed lines were drawn to represent GFP^{neg} and GFP^{hi} populations. Scale bar: 10 µm. **f,** Volcano plot showing the log_2fold change (Log_2FC, x-axis) and robust rank aggregation score (RRA, y-axis) of genes from GFP^{hi} versus GFP^{neg} MAGeCK analysis. Genes with log_2FC change < -0.05 (>=2 guides/ gene) are coloured as indicated. **g,** Immunofluorescence images of OMM$^{GFP1-10}$ ES-2 cells infected with *Toxo*$^{PVM\beta11}$ or Δ*maf1* parasites engineered to express PVM$^{\beta11}$ (Δ*maf1 Toxo*$^{PVM\beta11}$). PVM$^{\beta11}$ (HA); OMM$^{GFP1-10}$ (myc). Scale bars: 5 µm; inset, 2 µm. Data is representative of two biological replicates. **h**, Cells infected as in (**g**) were harvested at 8 hpi and 24 hpi and analysed by flow cytometry for GFP expression. WT (*Toxo*$^{PVM\beta11}$); Δ*maf1* (Δ*maf1 Toxo*$^{PVM\beta11}$). Data represent mean ± SD of n=3 biological replicates. Each dot represents a technical replicate. ****p<0.0001 for *Toxo*$^{PVM\beta11}$ versus Δ*maf1 Toxo*$^{PVM\beta11}$ by two-way ANOVA.

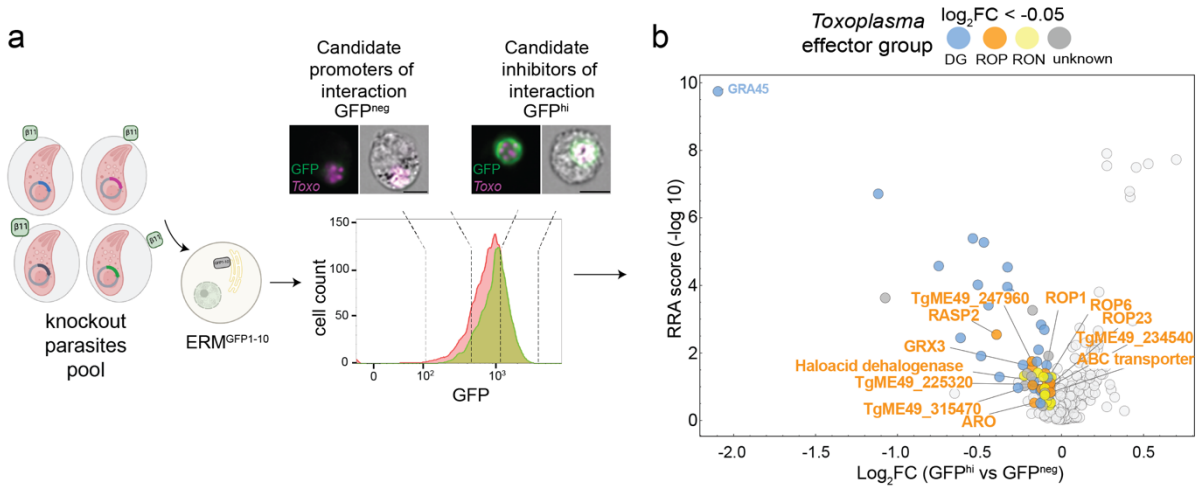

c

Toxoplasma ID	Hyperlopit/ *Toxoplasma* database description	TM/ PVM localization	FFAT motif (s)	VAPA interaction assessment
TGME49_315160	RASP2	No	-	-
TGME49_247960	Hypothetical protein	Yes	No	-
TGME49_247580	GRX3	No	-	-
TGME49_315470	Hypothetical protein	Yes	Yes (1)	Low
TGME49_261440	Armadillo_ Repeats-Only (ARO)	No	-	-
TGME49_258660	**ROP6**	**Yes**	**Yes (2)**	**High**
TGME49_309590	**ROP1**	**Yes**	**Yes (3)**	**High**
TGME49_225320	Hypothetical protein	No	-	-
TGME49_239600	ROP23	No	-	-
TGME49_234540	Hypothetical protein	Yes	No	-
TGME49_236860	Haloacid dehalogenase*	Yes	Yes (1)	Low
TGME49_305590	ABC transporter*	Yes	Yes (1)	Low

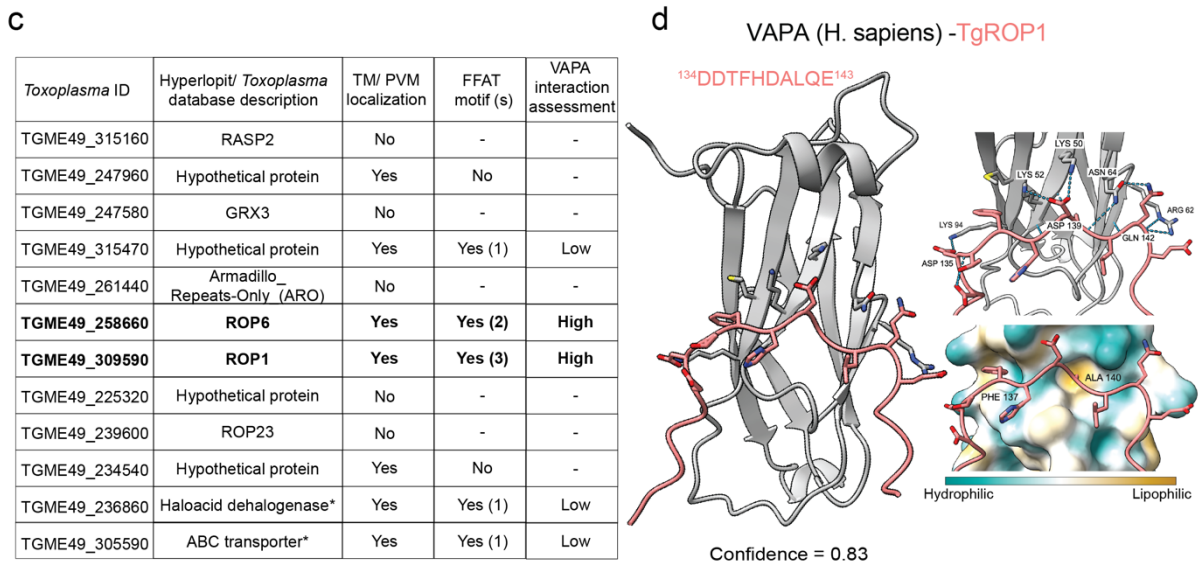

Fig. 3: TgROP1 tethers host ER to the parasite vacuole

a, Schematic of CRISPR screen. Type I *Toxoplasma* expressing GFP$^{\beta 11}$ were transfected with an sgRNA library targeting *Toxoplasma* effectors. The resulting pool of KO parasites was used to infect ERM$^{GFP1\text{-}10}$ ES-2 cells (ERM: endoplasmic reticulum membrane). Approximately 24 hours post infection (hpi), mCherry-positive infected cells were sorted based on GFP. Images were obtained during test sorts. Arbitrary dashed lines were drawn to represent GFP^{neg} and GFP^{hi} populations. Scale bar: 10 µm. **b,** Volcano plot showing the

log_2fold change (Log_2FC, x-axis) and robust rank aggregation score (RRA, y-axis) of genes from GFP^{hi} versus GFP^{neg} MAGeCK analysis. Genes with Log_2FC change < -0.05 (>=2 guides/ gene) are colored according to: blue, dense granule (DG); orange, rhoptry bulb protein (ROP); yellow, rhoptry neck protein (RON); dark grey, unknown effectors. **c,** Table of top *Toxoplasma* ROP candidates. *Represents genes for which the names were shortened for representation. They include TGME49_236860- haloacid dehalogenase family hydrolase domain-containing protein; TGME49_305590- ABC transporter transmembrane region domain-containing protein. TM: transmembrane domain; FFAT motif (EFFDAxE or ExFxDAxE) with the numbers in brackets representing the number of motifs predicted for each gene; and VAPA-interaction prediction (see materials and methods). **d,** AlphaFold multimer model of the MSP domain of VAPA with the TgROP1 ExFxDAxE motif. **e,** Immunofluorescence images of ES-2 cells infected with WT (*Toxo*^{mCherry}), Δ*rop1:ROP1-HA* and Δ*rop1* parasites at 3 hours post infection (hpi). PVM: parasite vacuole membrane (MAF1). Scale bar: 2 µm. Data is representative of one biological replicate. **f,** Representative electron micrograph images of ES-2 cells infected with WT (*Toxo*^{mCherry}), Δ*rop1:ROP1-HA* and Δ*rop1* parasites at 3 hpi. Membrane contact sites between the *Toxoplasma* parasite vacuole membrane (PVM) and (**i**) host ER and (**ii**) host mito. Scale bars: 1 µm; inset, 250 nm. Red, parasite vacuole; purple, ER; turquoise, mito. **g,** Percentage of *Toxoplasma* PVM associated with host ER and mitochondria in images as in (**f**). EM data are mean ± SD from >60 *Toxoplasma* vacuoles from n=2 biological replicates. ****p<0.0001 by means of one-way ANOVA.

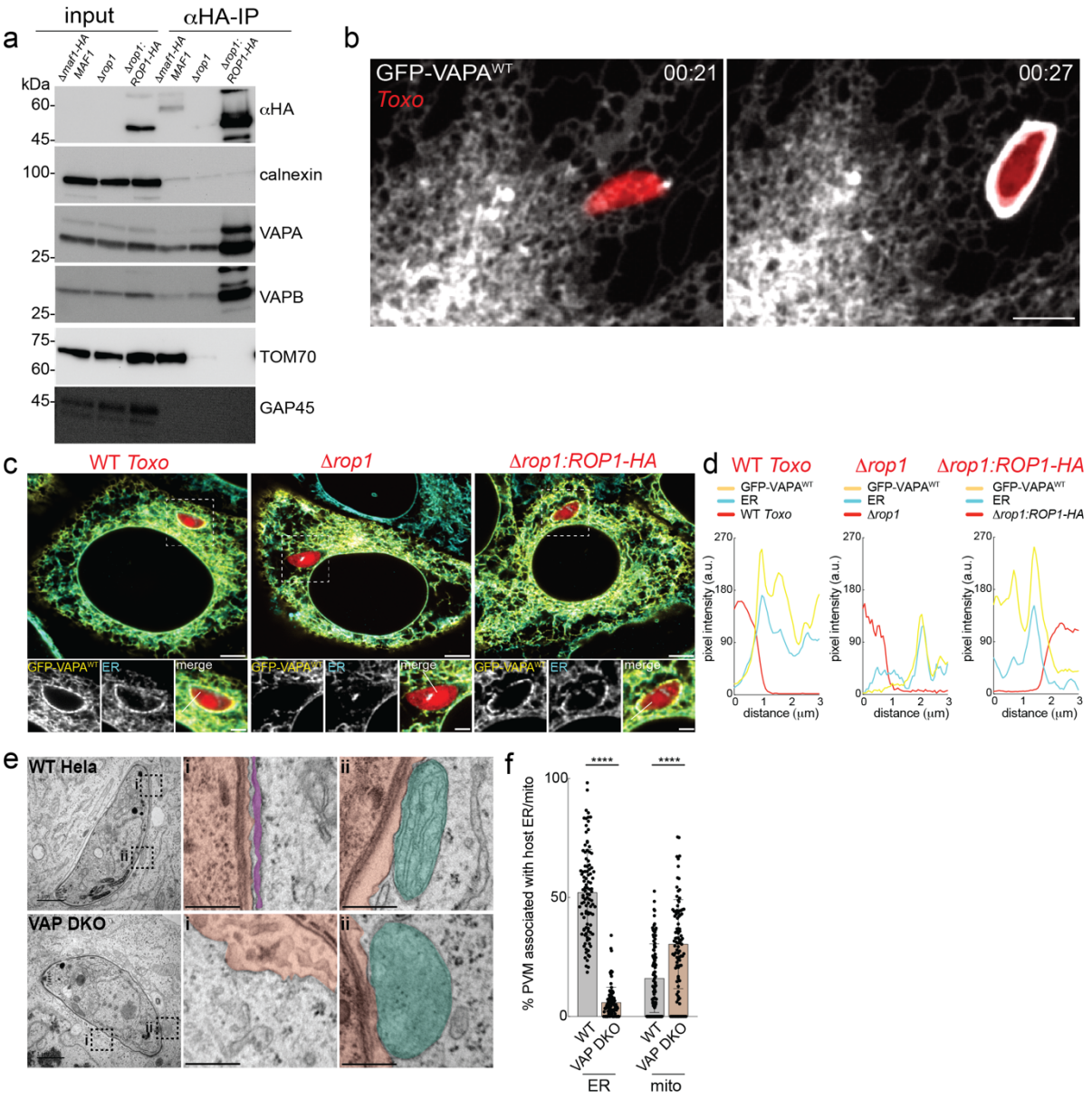

Fig. 4: VAPA and VAPB are the host factors that mediate host ER-*Toxoplasma* MCS
a, Anti-HA immunoprecipitates from ES-2 cells infected with Δ*rop1*, Δ*rop1:ROP1-HA* and Δ*maf1*:HA-MAF1 parasites that were analysed by means of immunoblotting and the same membrane was probed for different antibodies as indicated. Data is from of one biological replicate. **b,** Live-cell images of human foreskin fibroblasts expressing GFP-VAPA^{WT} and infected with Type I *Toxoplasma* parasite. Scale bar: 5 μm. (Supplementary Video 2). **c,** Immunofluorescence (IF) images of VAP DKO HeLa cells expressing GFP-VAPA^{WT} and infected with the Type I WT (*Toxo*^{mCherry}), Δ*rop1*, and Δ*rop1*:*ROP1-HA* parasites at 3 hours post infection (hpi). ER (calnexin). Scale bars: 5 μm; inset, 2 μm. Data is representative of two biological replicates. **d,** Corresponding pixel intensity plots for white line in the (**c**) inset. **e,** Representative electron microscopy images of WT and VAP DKO HeLa cells infected with Type I *Toxoplasma* parasites at 3 hpi. Membrane contact sites between the *Toxoplasma* parasite vacuole membrane (PVM) and (**i**) host ER and (**ii**) host mito. Scale bars: 1 μm; inset, 250 nm. Red, parasite vacuole; purple, ER; turquoise, mito. **f,** Percentage of *Toxoplasma* PVM associated with host ER and mitochondria in

images as in (**e**). EM data are mean ± SD from >95 *Toxoplasma* vacuoles from n=3 biological replicates ****p<0.0001 by means of unpaired t-test.

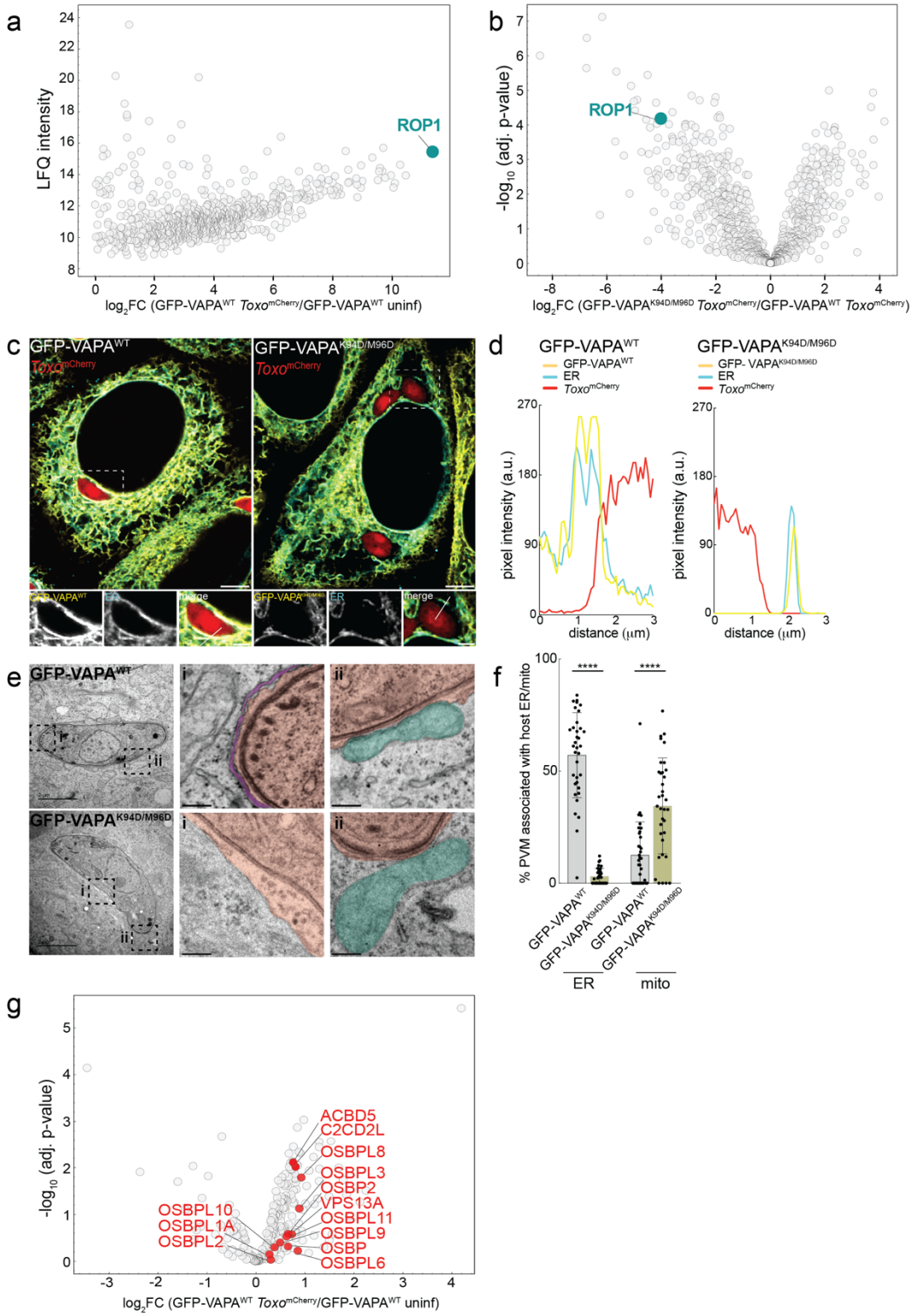

Fig. 5: *Toxoplasma* exploits the MSP domain of VAPA to form host *Toxoplasma*-ER MCS

a, Anti-GFP immunoprecipitates (IPs) from VAP DKO cells expressing GFP-VAPA^{WT} (GFP-VAPA^{WT}) that were uninfected (uninf) or infected with *Toxo*^{mCherry} and analysed by means of mass spectrometry (MS); data represent only *Toxoplasma gondii* proteins that had a positive Log_2FC. LFQ, label-free quantification. **b,** Volcano plot of *Toxoplasma* proteins representing anti-GFP IPs from GFP-VAPA^{WT} or VAP DKO cells expressing GFP-

VAPA$^{K94D/M96D}$ infected with *Toxo*^{mCherry} and analysed by MS. **c,** Immunofluorescence images of GFP-VAPA^{WT} and GFP-VAPA$^{K94D/M96D}$ cells infected with *Toxo*^{mCherry}. ER (calnexin). Scale bars: 5 µm; inset, 2 µm. Data is representative of two biological replicates. **d,** Corresponding pixel intensity plots for white line in (**c**) inset. **e,** Representative electron micrograph images of GFP-VAPA^{WT} and GFP-VAPA$^{K94D/M96D}$ HeLa cells 3 hours post infection (hpi) with *Toxo*^{mCherry}. Membrane contact sites between the *Toxoplasma* parasite vacuole membrane (PVM) and (**i**) host ER and (**ii**) host mito. Scale bars: 2 µm; inset, 250 nm. Red, parasite vacuole; purple, ER; turquoise, mito. **f,** Percentage of *Toxoplasma* PVM associated with host ER and mitochondria in images as in (**e**). EM data are mean ± SD from >25 *Toxoplasma* vacuoles from n=1 biological replicate. ****p<0.0001 by means of unpaired t-test. **g,** Volcano plot of (**a**) depicting changes in VAPA-interacting proteins upon infection. OSBP: oxysterol binding proteins; OSBPL: OSBP-related proteins.

3.1.5 Materials and Methods

Mammalian Cell Culture

HeLa adenocarcinoma cells, ES-2 ovary clear cell carcinoma and human foreskin fibroblasts (HFFs) cells were obtained from ATCC (CCL-2, CRL-1978, and SCRC-1041, respectively); VAP A/B double knockout (VAP DKO) cells were a kind gift from Dr. Pietro Di Camelli (Dong et al., 2016). HeLa WT and *TOM 70* KO cells were generated as previously described in the lab (X. Li et al., 2022). All cells were cultured at 37°C and 5% CO_2 in Dulbecco's Modified Eagle's GlutaMAX™ medium and supplemented with 10% heat-inactivated FBS (Gibco: A3840402) and 100 U/ml Penicillin-Streptomycin (Thermo Fisher Scientific: 15070063) (referred to as cDMEM). Cells were routinely tested for *Mycoplasma* infection by polymerase chain reaction (PCR).

Cloning

For stable expression of plasmids, the triple hemagglutinin tag (3XHA-) enhanced green fluorescent protein (eGFP) and outer mitochondria membrane protein OMP25 targeting sequence pMXs-3XHA-eGFP-OMP25 (Addgene #83356) was always used and modified as discussed. For split-GFP constructs, a cDNA containing myc-GFP1-10 gene strand was synthesized by Eurofins Genomics GmbH (Ebersberg, Germany). This was digested with restriction enzymes (RE) BamHI and NotI and inserted into pMXs-3XHA-eGFP vector (pMXs-myc-GFP1-10). For creation of OMM-targeted GFP1-10, the TOM20 N-terminal targeting sequence was added to primers 1 and 2 and a PCR was performed with the pMXs-myc-GFP1-10 plasmid (Cieri et al., 2018). The PCR product was treated with the KLD enzyme (NEB: M0554S) according to manufacturer's protocol. To create ERM-targeted GFP1-10, the Sac1 ER targeting sequence was amplified from a plasmid and sequence information provided by Dr. Cali using primers 3 and 4 with the forward primer containing a myc tag and subsequently inserted into pMXs-myc-GFP1-10 with RE XhoI and NotI (pMXs_myc_ER) (Cieri et al., 2018). pMXs_myc_ER was further modified by inserting GFP (amplified from pMXs-3XHA-eGFP-OMP25) or GFP1-10 (amplified from pMXs-myc-GFP1-10) with primers 5 and 6, and 7 and 8, respectively using RE BamHI and XhoI with HiFi DNA assembly cloning (NEB: E2621L).

Human VAPA and VAPB cDNA was amplified from ES-2 cells with primers 9 and 10, and 11 and 12, respectively, and inserted into the pMXs-3XHA-eGFP plasmid backbone with RE SacII and NotI to create pMXs-3xHA-GFP-VAPA (GFP-VAPA^{WT}) and pMXs-3xHA-GFP-VAPB (GFP-VAPB^{WT}). To create VAPA K94D/M96D mutant (GFP-VAPA$^{K94D/M96D}$) and VAPB K87D/M89D mutant (GFP-VAPB$^{K87D/M89D}$), the plasmids pMXs-3xHA-GFP-VAPA and pMXs-3xHA-GFP-VAPB were modified using primers 13 and 14 and 15 and 16, respectively. The PCR products were treated with the KLD enzyme.

For creation of *Toxoplasma* split-GFP constructs, the previously described N-terminally tagged MAF1 expression construct containing only the HA tag and N-terminus of the

MAF1 sequence until the MAF1 transmembrane domain was modified by primers 17 and 18 to introduce a 32 amino acid spacer and β_{11} with RE XhoI and NotI (PVM$^{\beta 11}$) (Cieri et al., 2018; Feng et al., 2017; Pernas et al., 2014). PVM$^{\beta 11}$ plasmid was further modified with primers 19 and 20 to insert chloramphenicol (CAT) selection cassette via ClaI and BclI enzymes (X. Li et al., 2022). All primer sequences are listed in Supplementary Table 7.

Lentiviral production and creation of cell lines

For production of lentivirus, human embryonic kidney (HEK) 293T cells were transfected using the X-tremeGENE 9 DNA Transfection Reagent (Sigma: 6365787001) with the following plasmid combination: 1 µg UMVC (Gagpol) packaging vector, 0.3 µg pCMV-VSVG envelope vector (Addgene #8454) and 1 µg of the relevant plasmid of interest. The next day, the medium of each well was exchanged and two days post transfection, the virus-containing supernatant was filtered through a 0.45 µm filter and supplemented with polybrene (Sigma: TR-1003) to a final concentration of 5 µg/ml. The virus-containing filtrate was added to 50,000 target cells and exchanged for cDMEM the next day. ES-2, HeLa and HFF cells were subsequently selected with 10-18 µg/ml blasticidin as required. The cells GFP-ER in HeLa WT or VAP DKOs expressing GFP-ER, GFP-VAPA^{WT}, GFP-VAPB^{WT}, GFP-VAPA$^{K94D/M96D}$ and GFP-VAPB$^{K87D/M89D}$, WT OMM$^{GFP1\text{-}10}$ HeLa and *TOM70 KO* OMM$^{GFP1\text{-}10}$ HeLas, all express the indicated constructs at the population level. The cells OMM$^{GFP1–10}$ ES-2 and ERM$^{GFP1–10}$ ES-2 were cloned out in 96 well plates to obtain a single cell population. The clones were tested by flow cytometry to choose cells with maximal GFP reconstitution. Experiment in Fig. 2a and Extended Data 3 were conducted with OMM$^{GFP1–10}$ ES-2 cells expressing the construct at the population level. All the other split-gfp experiments and CRISPR screens are done with clonal cell lines in this chapter and in the result section 3.2.

Parasite culture and generation of parasite strains

All parasite strains were maintained by serial passage on HFF monolayers in cDMEM. *Toxoplasma* strains used in this study include: Type I RHΔ*hxgprt*, Type II ME49Δ*hxgprt*:mScarlet, and Type III VEGΔ*hxgprt* strains [deleted for the *hypoxanthine–xanthine–guanine phosphoribosyl transferase* (*HXGPRT*) gene], Type I RH*ΔKU80Δhxgprt*; Type I Δ*gra45* (Δ*gra45*); Type I RH*Δhxgprt*:mCherry+ (*Toxo*^{mCherry}); Type I RHΔ*maf1:mCherry*+ (Δ*maf1*)*;* Type I RHΔ*maf1:mCherry*+ (Δ*maf1:HA*)*;* RHΔ*maf1-HA-MAF1:mCherry*+ (Δ*maf1*:HA-MAF1) (X. Li et al., 2022; Pernas et al., 2014; Y. Wang et al., 2020). For TgROP1 characterization, the following parasites were used- Type I *Toxoplasma*- RH Δ*rop1* and RH Δ*rop1:ROP1-HA,* Type II *Toxoplasma*- PruΔKU80Δ*hxgprt* (Type II WT), PruΔ*rop1,* PruΔ*rop1:ROP1-HA* (Butterworth et al., 2022). All strains were routinely tested for *Mycoplasma* infection by polymerase chain reaction (PCR).

To create transgenic parasites, RHΔ*hxgprt* (for CRISPR screen), RHΔ*hxgprt*:mCherry+ (*Toxo*$^{PVM\beta 11}$) and RHΔ*maf1:mCherry*+ (Δ*maf1 Toxo*$^{PVM\beta 11}$) were transfected with the PVM$^{\beta 11}$

plasmid following BglIII-linearization and then selected with 20 µM chloramphenicol (Sigma: R4408). 2-3 weeks post-selection, the populations were cloned out via serial dilution. Single clones were confirmed with HA staining in immunofluorescence assays. Throughout the thesis *Toxo*^{mCherry} and *Toxo*^{PVMβ11} parasites were used as WT controls interchangeably, and this has been indicated in the figure legends.

To create ROP6 knockout parasites, a protospacer targeting the coding region of ROP6 was introduced into the pCas9-GFP:sgRNA CRISPR plasmid (generated using primers 21 and 22) via KLD cloning. For ROP6, Pro^{GRA1}-mCherry-T2A-HXGPRT-Ter^{GRA2} construct was amplified from a template plasmid using primers 23 and 24 to introduce a 40 base pair homology to the 5' and 3' UTRs of ROP6 (Young et al., 2019). Approximately 5 µg of the PCR product and 30 µg of plasmid were co-transfected into Type I *Toxoplasma* strain RHΔ*KU80*Δ*hxgprt* and selected with 25 µg/mL mycophenolic acid (Sigma: 475913) and 50 µg/mL xanthine (Alfa Aesar: A11077) for one week. The populations were tested for ROP6 expression with IF and then cloned out and further verified via western blot and integration of repair cassette by PCR using primers 25-30.

Live cell imaging

Cells were seeded on 24-well CELL view glass bottom cell culture plates (Greiner Bio-One) and imaged using an Olympus IXplore SpinSR 50 mm spinning disk confocal microscope. Live cell imaging was performed with incubation at 37°C and 5% CO2. Images were taken with cellSens software using a 100X/1.35 silicon oil objective using z-stacks and excitation with either 488, 561, or 640 laser lines.

Immunofluorescence assays and antibodies

ES-2 or HeLa cells were plated in a 24 well glass-bottom (Greiner Bio-One) and infected with *Toxoplasma* strains for 3 hpi, 8hpi or 24 hpi as indicated in text. Plates were fixed in 4% paraformaldehyde in prewarmed cDMEM for 15 min at 37°C, permeabilized for 10 min at RT with 0.2% triton, blocked in 3% BSA for 30 min and mostly incubated in primary antibody (abs) overnight at 4°C. After 3x 5 min washes with 1x PBS, cells were incubated in secondary antibody for 40 min to 1 h at room temperature. Plates were rinsed 3x 5 min in 1x PBS and maintained in 1x PBS until imaging. Primary Abs: Calnexin (GeneTex: GTX109669 [C3], C-term) or Calnexin (Proteintech: 10427-2-AP); TOMM70 (Sigma: HPA048020); Myc-tag (CST: 2276, 9B11) or Myc-tag (Proteintech: 16286-1-AP); Antisera of TgMAF1(Pernas et al., 2014); HA (CST:3724) or HA (Roche (3F10): 11867423001); GFP (Takara Bio: 632380); TgROP1 (Abnova: MAB17504); TgROP6 (Dr. P. Bradley; UCLA) and TgSAG1 (mouse DG52) were used at 1:300-1:1000 or 1:2000 (only for TgMAF1). Secondary Abs used were: Alexa Fluor Plus 405, Alexa Fluor Plus 488, Alexa Fluor Plus 594, Alexa Fluo Plus 647 (Thermo Fisher Scientific). Images were taken with a 60X/1.35 or 100X/1.35 silicon oil objective and excitation with either 405, 488, 561, or 640 confocal or Olympus

super resolution laser lines with an Olympus IXplore SpinSR spinning disk confocal microscope.

Electron microscopy sample preparation and analysis
ES-2 and HeLa cells were grown on small discs of aclar foil (Science Services, #E50425-10) in either 24-well or 12-well plates and infected with *Toxoplasma* strains for the times as indicated in text. Following that the discs were fixed for 1 h in 2% Glutaraldehyde (Sigma: G5882-100ML) with 2.5 % Sucrose (Roth: 4621.1) and 3mM $CaCL_2$ (Sigma: C7902-500G) in 0.1M HEPES buffer (Sigma: C7902-500G) pH 7,4. Samples were washed three times with 0.1M HEPES buffer and incubated with 1% Osmiumtetroxid (Science Services: E19190) and 1% Potassium hexacyanoferrat (Sigma: P8131) for 1 h at 4°C. After 3 x 5 min wash with 0.1M Cacodylate buffer (Applichem: A2140,0100), samples were dehydrated at 4°C using ascending ethanol series (50%, 70%, 90%, 3x100%) for 7 min each. Infiltration was performed with a mixture of 50% Epon/ethanol for 1h, 70% Epon/ethanol for 2h and with pure Epon (Sigma: 45359-1EA-F) overnight at 4°C. Samples were embedded into TAAB capsules (Agar Scientific: G3744) and cured for 48 h at 60°C. Ultrathin sections of 70 nm were cut using an ultramicrotome (Leica Microsystems, UC6) and a diamond knife (Diatome, Biel, Switzerland) and stained with 1.5 % uranyl acetate (Agar Scientific: R1260A) for 15 min at 37°C and 3 % Reynolds lead citrate solution made from Lead (II) nitrate (Roth: HN32.1) and tri-Sodium citrate dehydrate (Roth: 4088.3) for 4 min. Images were acquired using a JEM-2100 Plus Transmission Electron Microscope (JEOL) operating at 80kV equipped with a OneView 4K camera (Gatan).

For quantification of host-ER *Toxoplasma* MCS, images of *Toxoplasma* parasite vacuoles in infected ES-2 or HeLa cells were analysed using the Fiji software by hand. Contact distance was measured approximately every 200 nm if the host ER-*Toxoplasma* PVM continuity was shorter than 1 µm distance, and for lengths > 1 µm, the distance was measured approximately every 500 nm. For small patches of ER (mostly under 200 nm) the distance was measured at the beginning and at the end of the contact. To measure the percentage of the PVM associated with host organelles, the total length of contacts between the organelles was added and divided by the perimeter of the PVM (PVM associated with host ER or mitochondria /total PVM perimeter ×100). In Fig. 1, one packs from 3 hpi and 24 hpi were analysed. In all other figures parasite vacuoles only from the indicated times were assessed.

Flow cytometry analysis
For split GFP assays, monolayers of infected-ES2 or HeLa cells were rinsed with PBS, trypsinzed and fixed in 2% paraformaldehyde in 3% FBS in 1x PBS (FACS buffer) for 5 min. After a spin at 1000 rpm for 5 min, cells were resuspended in FACS buffer and a minimum of 10,000 events were analysed on a FACSFortessa using BD FACSDiva software. The data was then analysed in BD FlowJo software as outlined in Extended Data Fig. 4.

Creation of the CRISPR parasite pool

A pool of ssDNA oligonucleotides encoding the protospacer sequences targeting the *T. gondii* secretome was selected from an arrayed library using an Echo 550 Acoustic Liquid Handler (Labcyte) in three independent events and then pooled to minimize loss of guides. The pooled oligonucleotides were integrated in the pCas9-mCherry-HXGPRT:sgRNA CRISPR vector by Gibson cloning after digestion with PacI/NcoI (NEB), resulting in a library of 1644 sgRNAs targeting 325 genes, with an average of 5 sgRNAs/gene (Butterworth et al., 2023; Young et al., 2019). A total of 180E6 PVM$^{\beta 11}$-expressing parasites were transfected in triplicate with 150 µg of KpnI-linearised (NEB) and phenol-chloroform purified library with the P3 Primary Cell 4D-Nucleofector kit (Lonza V4XP-3032) in a Amaxa 4D Nucleofector (Lonza AAF-1003X, program EO-115). Stable integration of the pCas9-mCherry-HXGPRT:sgRNA library was induced upon treatment with 25 µg/ml Mycophenolic acid and 50 µg/ml Xanthine (Sigma-Aldrich) the following day. An average transfection efficiency of 1.2% corresponding to a coverage of 1000 parasites/sgRNA was estimated from the parasite survival rate at day 7 post transfection in a plaque assay. Three days post transfection, the selected pool of knockout parasites was syringe-lysed and added to fresh HFF monolayers with 100 U/ml Benzonase (Merck) overnight to remove traces of input DNA. Seven days post transfection, parasites from individual transfections were pulled and stored in the -80°C in 50E6 parasite aliquots until use.

CRISPR screen

To perform the screen with technical duplicates, two vials of the split-GFP screen parasites (each considered as a technical duplicate) were thawed onto two T175 flasks of HFF monolayers. The next day the media of the flasks were changed to 25 µg/ml Mycophenolic acid and 50 µg/ml Xanthine. Two days following treatment with selection media, the parasites were expanded by passing 2E6 parasites onto one T175 flask of HFF monolayer. Two days later, 2E6 parasites (to ensure a 1000x representation of guides) were expanded to 6 T175 flasks of HFF monolayers. The next day, 300E6 OMM GFP$^{1-10}$ ES-2 cells and ERM GFP$^{1-10}$ ES-2 cells were plated in 15-cm dishes (8-10E6 cells/ dish). The following morning, split GFP-parasites from each technical replicate were used to infect 150E6 cells of each cell type at a low multiplicity of infection of 0.5. The plates were rinsed after infection and then the next day approximately 24 hours after infection, cells from each technical replicate were trypsinized with accutase (to avoid clumping) and pooled together into 50 ml falcons. The cells were fixed in 2% PFA for 5 minutes in FACS buffer containing 5% accutase and then spun down at 300 x g for 5 minutes to get rid of fixative. The cells were then distributed into FACS tubes (Corning: 352063) for sorting. The host mitochondria-*Toxoplasma* MCS screenncells were sorted using a BD FACSAria III sorter and the host ER-*Toxoplasma* MCS screen cells were sorted using a BD FACSFusion sorter. Gates were drawn to first delineate the infected cells (mCherry fluorescence) and

then the infected cells were gated to represent all cells negative for GFP expression (GFP^{neg}) and the top 20% of the GFP positive [GFP-high (GFP^{hi})] populations. Cells were sorted for both screens at 4°C using a 100 µm nozzle and sheath pressure was set at 20 psi. 0.9 % NaCl was used as sheath fluid. Cell pellets were stored at -80°C. Images representative of screen populations obtained during test sorts were acquired on an ImageStream^X MkII imaging cytometer, X60 magnification. Single, focused cells were recorded based on their area and aspect ratio values in Channel 1 (brightfield) as well as gradient RMS values >50. Image analysis was performed using IDEAS software (Cytek Biosciences).

Cell pellets were then de-crosslinked in a solution of 10 mM Tris pH 7.5 (Thermo: 15567027) and 10 mg/mL Proteinase K (Sigma-Aldrich: 3115887001) at 55 °C for 24 h. Next, cells were lysed with buffer AL (QIAamp DNA Blood Mini Kit: 51104) for two hours and genomic DNA was isolated as per manufacturer's protocol. Library samples and genome-integrated *Toxoplasma* sgRNA sequences were amplified by PCR (22 cycles with 2.5 µg of gDNA as input in 100µl reaction volume) using NEBNext Ultra™ II Q5 Master Mix (New England BioLabs Inc.: M0554L) with a mix of five different forward primers (primers 31-35) to introduce sequence variability and a reverse primer (primer 36). Afterwards, amplicons were pooled, bead-purified and quantified followed by the introduction of Illumina Nextera adaptors and indices by eight cycles in a second round of PCR. Samples were analysed on an Illumina NovaSeq platform by paired end (2 × 100 bp) sequencing with >3 × 10^7 reads per sample.

CRISPR screen data analysis

To analyse the screen data, following demultiplexing, raw NGS libraries were quality-checked using FastQC version 0.11.8 (Andrews & others, 2019). Upstream sequences and sgRNA length were used to trim reads with cutadapt (version 4.5). MAGeCK (version 0.5.9.5) count was used to quantify the number of reads per sgRNA (W. Li et al., 2014). Raw sgRNA counts were median-normalized and MAGeCK test was used to rank sgRNAs and genes sgRNAs with fewer than 50 read counts in treatment or control samples were excluded from the analysis. The log2-fold change (Log_2FC) on a gene level was calculated as follows: Log_2FC = median [log2(sgRNA read counts in '$GFP^{neg'}$ gate + 1) - (sgRNA read counts in 'GFP^{hi}' gate + 1)]. For gene significance, an a-RRA score was calculated by MaGeCK (W. Li et al., 2014). Double-sided volcano plots of gene-level Log_2FCs and RRA scores were created using Instant Clue software (Nolte et al., 2018).

Immunoblotting and antibodies

Uninfected or *Toxoplasma*-infected cells were similarly harvested in chilled lysis buffer - 50 mM Hepes-KOH pH 7.4, 40m M NaCl, 2 mM EDTA, 1% Triton X-100 and protease and phosphatase inhibitors (Thermo Scientific: A32961 and Sigma: 4906837001) for 30 min on ice. Lysates were then centrifuged for 10 min at 14,000 g at 4°C and the clarified

supernatant was transferred to a fresh tube with 5x SDS for a final volume of 1x SDS. Protein lysates were resolved in SDS-PAGE and following gel transfer, the membranes were blocked with TBS-0.05% Tween 20 (TBS-T) and 5% milk and the primary antibodies were incubated overnight. Following incubation, blots were washed three times in TBS-T for 15 minutes and then incubated with horseradish peroxidase (HRP)-conjugated anti-rabbit IgG (CST :7074) or anti-mouse IgG (CST :7076) at a 1:4000 dilution for 45 minutes and developed using a chemiluminescence system (Pierce™ ECL Western Blotting Substrate or Pierce SuperSignal™ West Atto Ultimate Sensitivity Substrate; ThermoFisher Scientific). The following primary antibodies were used: TOMM70 (Sigma: HPA048020); HA-HRP (Roche: 12013819001); VAPA (Proteintech: 15275-1-AP); VAPB (Proteintech: 14477-1-AP); Calnexin (Proteintech: 10427-2-AP); TgROP1 (Abnova: MAB17504); GFP (Takara Bio: 632380); TgGra45 (Dr. D. Soldati; U. of Geneva); Myc-tag (CST: 2276, 9B11); TgROP1 (Dr. P. Bradley; UCLA) and Actin (Proteintech: 66009).

Immunoprecipitation

HeLa VAP DKOs expressing GFP-VAPA^{WT} or GFP-VAPA$^{K94D/M96D}$ were infected with *Toxo*^{mCherry}. ES-2 cells were infected with RH Δ*rop1*, RH Δ*rop1:ROP1-HA* and RH Δ*maf1:HA-MAF1*. At 3 hpi, cells were rinsed twice in chilled 1x PBS, scraped down in chilled 1x PBS + phosphatase inhibitors (Sigma: 4906845001) (1xPBS+inh), centrifuged at 1500 g for 5 min, and resuspended in lysis buffer for 15 min at 4°C. Cleared lysates were incubated with either 25 µl magnetic anti-HA-beads (Thermo Scientific: 88837) or 25 µl magnetic anti-GFP-nanobodies (Chromotek: GTD-20) overnight. The beads were washed 3x with 1x PBS+inh. Afterwards, the samples were eluted from the magnetic beads with 2x SDS buffer by incubating them at 40°C for 10 min. Samples were processed for gel electrophoresis and probed with indicated antibodies.

Proteomics sample preparation

For preparing samples from immunoprecipitation, on-beads digestion was performed to elute the proteins off the beads. Before adding the elution buffer, the beads were washed with detergent free buffer (50mM Tris-HCl pH7.5) four times to remove any detergents used previously. Then 100 µl of the elution buffer (5ng/µl trypsin, 50mM Tris-HCl pH7.5, 1mM Tris (2- carboxyethyl)phosphine), 5mM chloroacetamide) was added to the beads and incubated at room temperature by vortexing from time to time or rotating on a rotator. After 30 min, the supernatant was transferred to a 0.5 ml tube and incubated at 37°C overnight to ensure a complete trypsin digest. The digestion was stopped in the next morning by adding formic acid to the final concentration of 1%. The resulted peptides were cleaned with home-made StageTips. Peptides were separated on a 25 cm, 75 µm internal diameter packed emitter column (Coann emitter from MS Wil, Poroshell EC C18 2.7 micron medium from Agilent) using an EASY-nLC 1200 (Thermo Fisher Scientific). The column was maintained at 50°C. Buffer A and B were 0.1% formic acid in water and 0.1% formic acid in 80% acetonitrile, respectively. Peptides were separated on a gradient from

4% to 30% buffer B for 19 min at 400 nl / min, followed by a higher organic wash. Eluting peptides were analyzed on a QExactive HF mass spectrometer (Thermo Fisher Scientific) in DIA mode. Peptide precursor m/z measurements were carried out at 120000 resolution in the 400 to 800 m/z range followed by 29 DIA scans with an isolation width of 14 Th and a resolution of 15000. MS1 and DIA MS2 scans were recorded in centroid mode.

Proteomics LC-MS/MS analysis

The raw data were analyzed with Spectronaut 16.2 (Biognosys) using default parameters against the reference proteome for human, UP000005640, downloaded September 2018. Methionine oxidation and protein N-terminal acetylation were set as variable modifications; cysteine carbamidomethylation was set as fixed modification. The digestion parameters were set to "specific" and "Trypsin/P," with two missed cleavages permitted. Protein groups were filtered for at least two valid values in at least one comparison group and missing values were imputed from a normal distribution with a down-shift of 1.8 and standard deviation of 0.3. Differential expression analysis was performed using limma, version 3.34.9 in R version 3.4.3 (R Core Computing Team, 2017; Ritchie et al., 2015).

For VAPA-interacting proteins, we curated a list of 245 putative VAPA-interactors based on previously published interactors and proteins from BioPlex (https://bioplex.hms.harvard.edu/), and OpenCell (https://opencell.czbiohub.org/) and assessed changes in the binding of these proteins to VAPA upon infection with *Toxoplasma* (Cho et al., 2022; Huttlin et al., 2015; James & Kehlenbach, 2021). Volcano plots of proteomics data were generated using Instant Clue software (Nolte et al., 2018).

FFAT motif search and AlphaFold multimer predictions

All *Toxoplasma gondii* sequences were retrieved from *Toxoplasma* database (Amos et al., 2022). The canonical FFAT motif (EFFDAxE) FFAT motif using the Regular Expression (REGEX) model was retrieved from the ELM database with the entry name TRG_ER_FFAT_1 (M. Kumar et al., 2024). The FFAT relaxed REGEX was defined as [EDST].{1,2}[FY].[DEST][ALCFS].{1,2}[EDST] based on other FFAT motif sequences at the ELM database. We mainly changed the distance of the acidic residue in position 1 of the core motif, allowing for any residue at position 3 and adding more hydrophobic residues at position 5. We screened our candidates for either the canonical or modified FFAT motif and found 8 matches in 5 rhoptry candidates. We then made 8 AlphaFold multimer predictions for the 5 rhoptry candidates following the fragmentation approach previously published (C. Y. Lee et al., 2024). To generate the models, we obtained the MSP domain of VAPA and the extended sequence of the motif matches. The human VAPA sequence was retrieved from UniProt with the accession Q9P0L0-1 (Bateman et al., 2023). The VAPA MSP domain was first defined based on the InterPro boundaries and then manually extended on both flanks to include residues with high pLDDT values, based on the

AlphaFold database reference model (Evans et al., 2022). The motif matches were extended on both flanks by 5 residues. We used a local installation of AlphaFold Multimer version 2.3.2 for all domain-motif pairs using the following parameters to produce five models per pair (Evans et al., 2022):

--model_preset=multimer
--db_preset=full_dbs
--max_template_date=2020-05-14
--num_multimer_predictions_per_model=1
--use_gpu_relax=True
--data_dir=/mnt/storage/alphafold/v232
--
bfd_database_path=/mnt/storage/alphafold/v232/bfd/bfd_metaclust_clu_complete_id30_c90_final_seq.sorted_opt
--
mgnify_database_path=/mnt/storage/alphafold/v232/mgnify/mgy_clusters_2022_05.fa
--obsolete_pdbs_path=/mnt/storage/alphafold/v232/pdb_mmcif/obsolete.dat
--pdb_seqres_database_path=/mnt/storage/alphafold/v232/pdb_seqres/pdb_seqres.txt
--template_mmcif_dir=/mnt/storage/alphafold/v232/pdb_mmcif/mmcif_files
--uniprot_database_path=/mnt/storage/alphafold/v232/uniprot/uniprot.fasta
--uniref90_database_path=/mnt/storage/alphafold/v232/uniref90/uniref90.fasta
--uniref30_database_path=/mnt/storage/alphafold/v232/uniref30/UniRef30_2021_03
--use_precomputed_msas=True

Model scoring

Using the ranking_debug json file, the confidence of the highest scored model per pair was extracted. The model confidence is a weighted metric calculated from the pTM and ipTM as follows: confidence = 0.8ipTM +0.2pTM. Using the 0.7 threshold, values above 0.7 were considered as high confidence and the ones below as low confidence (C. Y. Lee et al., 2024). The average pLDDT value of the core motifs (excluding the 5 residues flank expansions) was further calculated. Using again the pLDDT value threshold of 70 were considered as high confidence and the ones below 70 were accordingly considered low confidence (C. Y. Lee et al., 2024).

Line scan analyses

Line-scan analysis of relative fluorescence intensity was performed by measuring pixel intensity across one line as indicated using Fiji software.

Statistical analyses

All statistical analyses were performed using one-way analysis of variance (ANOVA), two-way ANOVA, or an unpaired t test in GraphPad Prism 8 software and has been indicated accordingly.

a

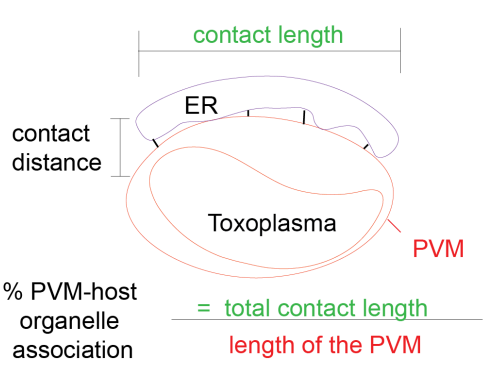

Extended Data Fig. 1: Schematic of host ER-*Toxoplasma* MCS analysis

a, Schematic of the analysis of membrane contact sites (MCS) between host ER and *Toxoplasma* parasite vacuole membrane (PVM).

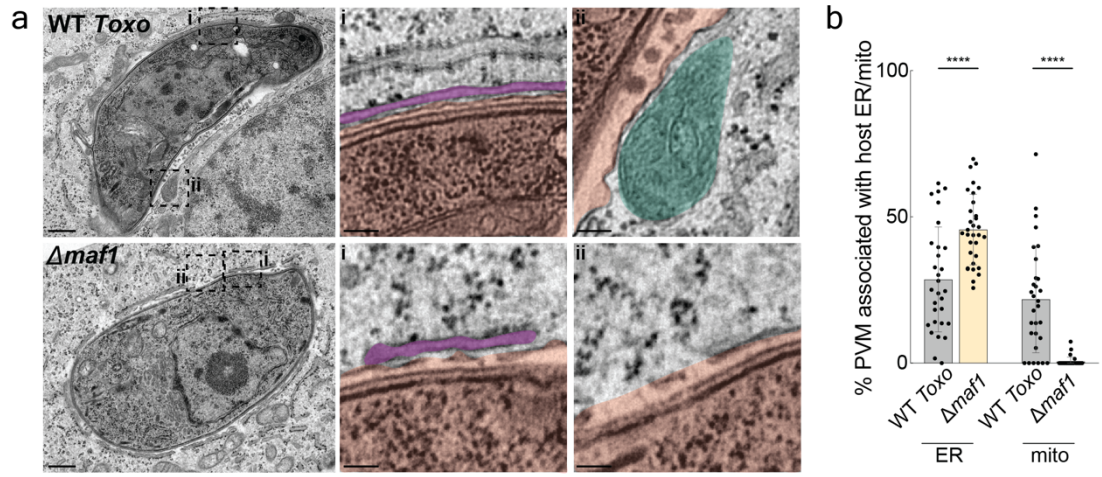

Extended Data Fig. 2: Δ*maf1* parasites have increased MCS with host ER

a, Representative electron micrograph images of ES-2 cells infected with WT (*Toxo*$^{PVM\beta11}$) and Δ*maf1 (*Δ*maf1*:HA) *Toxoplasma* at 4 hours post infection. Membrane contact sites between the *Toxoplasma* parasite vacuole membrane (PVM) and (**i**) host ER and (**ii**) host mito. Scale bars: 500 nm; inset, 100 nm. Red, parasite vacuole; purple, ER; turquoise, mito. **b,** Percentage of *Toxoplasma* PVM associated with host ER and mitochondria in images as in (**a**). EM data are mean ± SD from > 29 *Toxoplasma* vacuoles of n=1 biological replicate. ****p< 0.0001 by means of unpaired t-test.

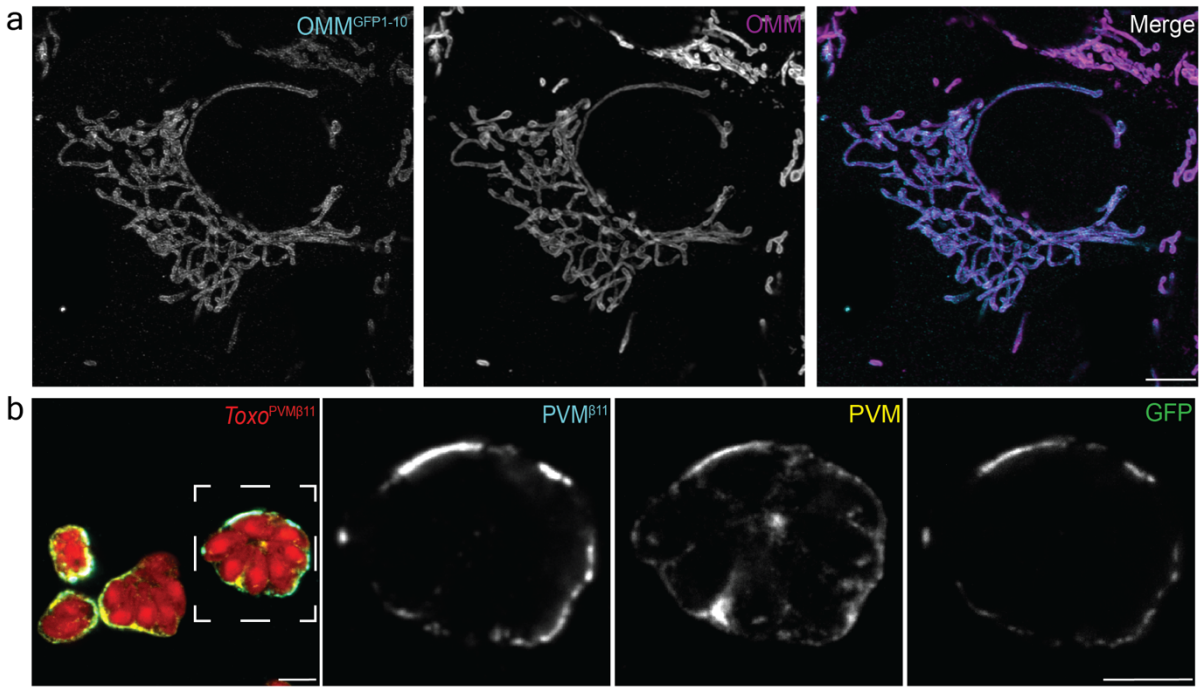

Extended Data Fig. 3: Characterization of the host mitochondria-*Toxoplasma* MCS sensor

a, Immunofluorescence (IF) images of OMM$^{GFP1–10}$-expressing ES-2 cells (OMM$^{GFP1–10}$ ES-2s). OMM$^{GFP1-10}$ (myc); OMM (TOM20). Scale bar: 5 µm. OMM: outer mitochondrial membrane. **b,** IF images of OMM$^{GFP1-10}$ ES-2s infected with parasites expressing PVM^{β11} (*Toxo*^{PVMβ11}). PVM^{β11} (HA); PVM (MAF1). PVM: parasite vacuole membrane; MCS: membrane contact sites. Scale bar, including inset, 5 µm. Data is representative of one biological replicate for both experiments.

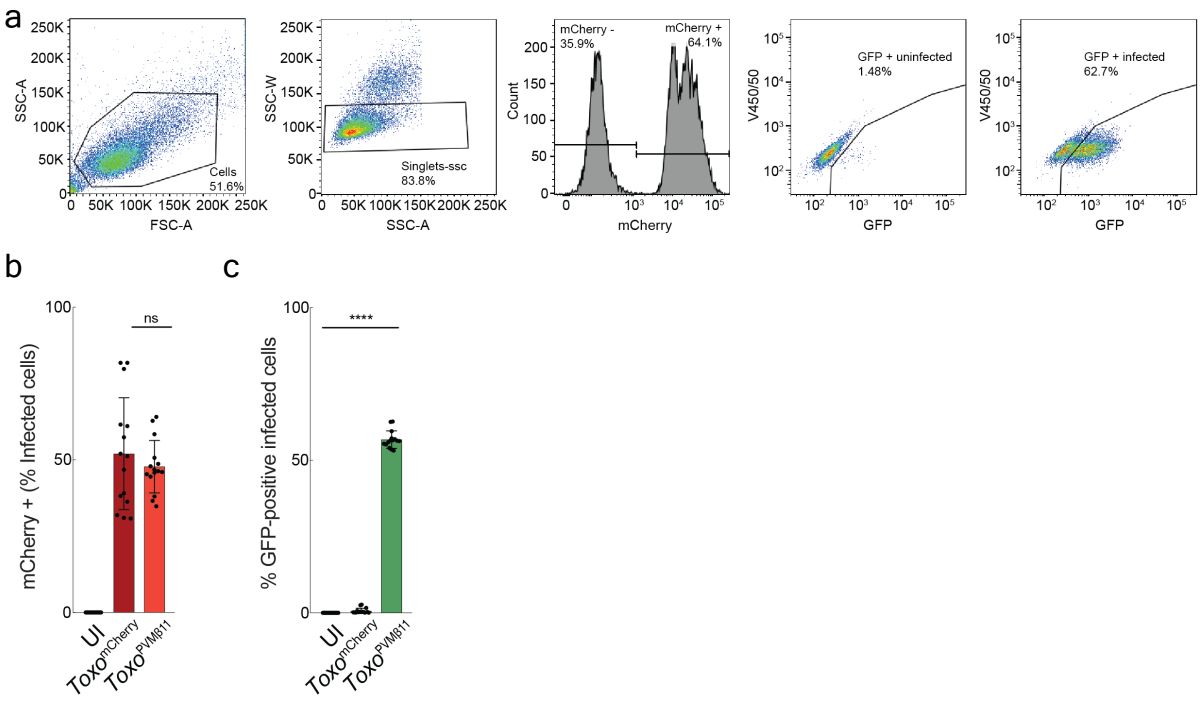

Extended Data Fig. 4: Flow-cytometry based analysis of host organelle-*Toxoplasma* MCS

a, Example of the gating strategy used to quantify GFP reconstitution with the split-GFP assay. Cells were initially gated using forward scatter (FSC) versus side scatter (SSC) to define the population of interest. Then they were gated with SSC- width (W) and SSC- area (A) to gate for single cells. The resulting population was analysed based on mCherry intensity to distinguish between uninfected (mCherry-) and infected (mCherry+) cells. Subsequently, both the uninfected (UI) and infected populations were assessed for their GFP expression levels. **b,c,** The population of OMM$^{GFP1–10}$-expressing ES-2 cells were either UI, infected with parasites expressing mCherry (*Toxo*^{mCherry}), or infected with parasites expressing PVM^{β11} (*Toxo*^{PVMβ11}) and analysed by flow cytometry for (**b**) infection (mCherry) and (**c**) GFP expression. PVM: parasite vacuole membrane; OMM: outer mitochondrial membrane. Data are mean ± SD of n=5 biological replicates. Each dot represents a technical replicate. ****p < 0.0001 by means of one-way ANOVA analysis.

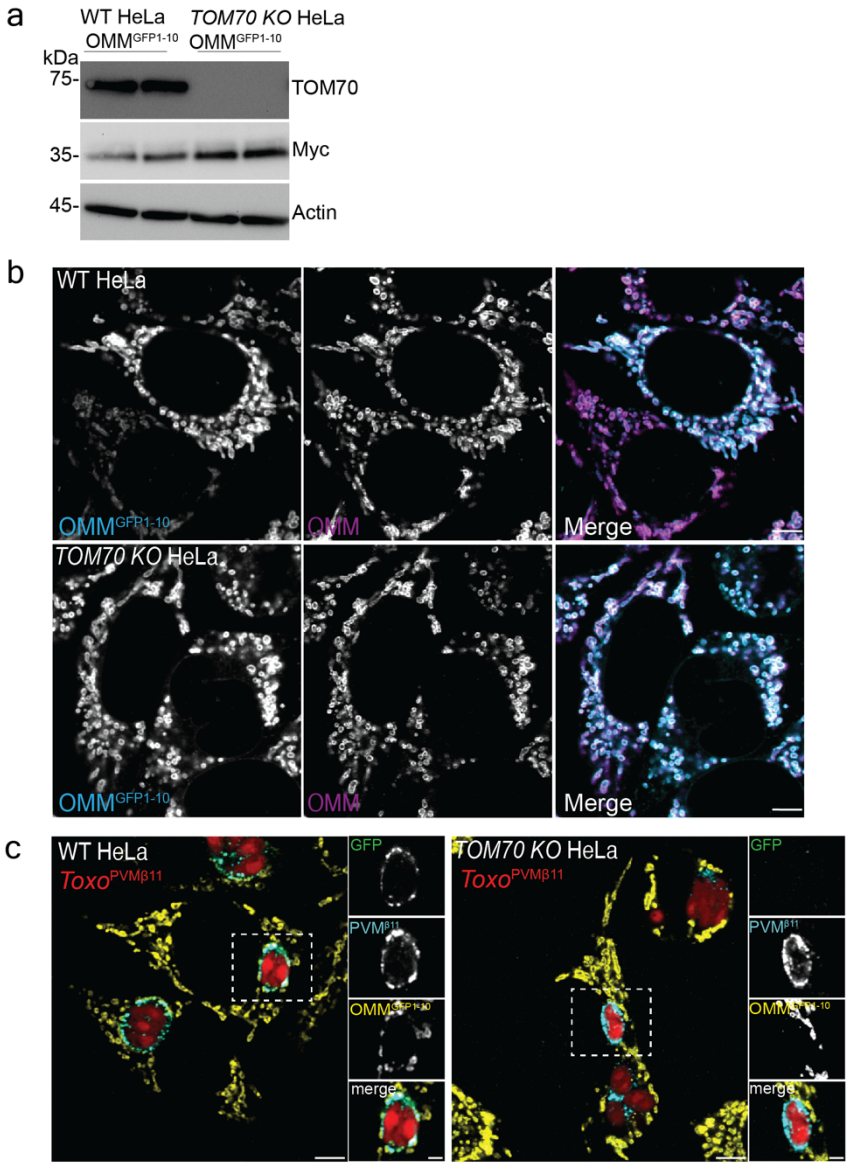

Extended Data Fig. 5: Host mitochondria-*Toxoplasma* MCS require TOM70

a, OMM$^{GFP1-10}$ expressing- WT (WT OMM$^{GFP1-10}$) and *TOM70*-deleted (*TOM70 KO* OMM$^{GFP1-10}$) HeLas were analysed by means of immunoblotting for indicated antibodies. **b,** Immunofluorescence (IF) images of OMM$^{GFP1-10}$ and *TOM70 KO* OMM$^{GFP1-10}$ HeLa cells. OMM$^{GFP1-10}$ (myc); OMM (TOM20). **c,** IF images of WT OMM$^{GFP1-10}$ and *TOM70 KO* OMM$^{GFP1-10}$ HeLas that were infected with parasites expressing PVM^{β11} (*Toxo*^{PVMβ11}). PVM^{β11} (HA); OMM$^{GFP1-10}$ (myc). PVM: parasite vacuole membrane; OMM: outer mitochondrial membrane. Scale bar: 5 µm; inset, 2 µm. All experiments are representative of one biological replicate.

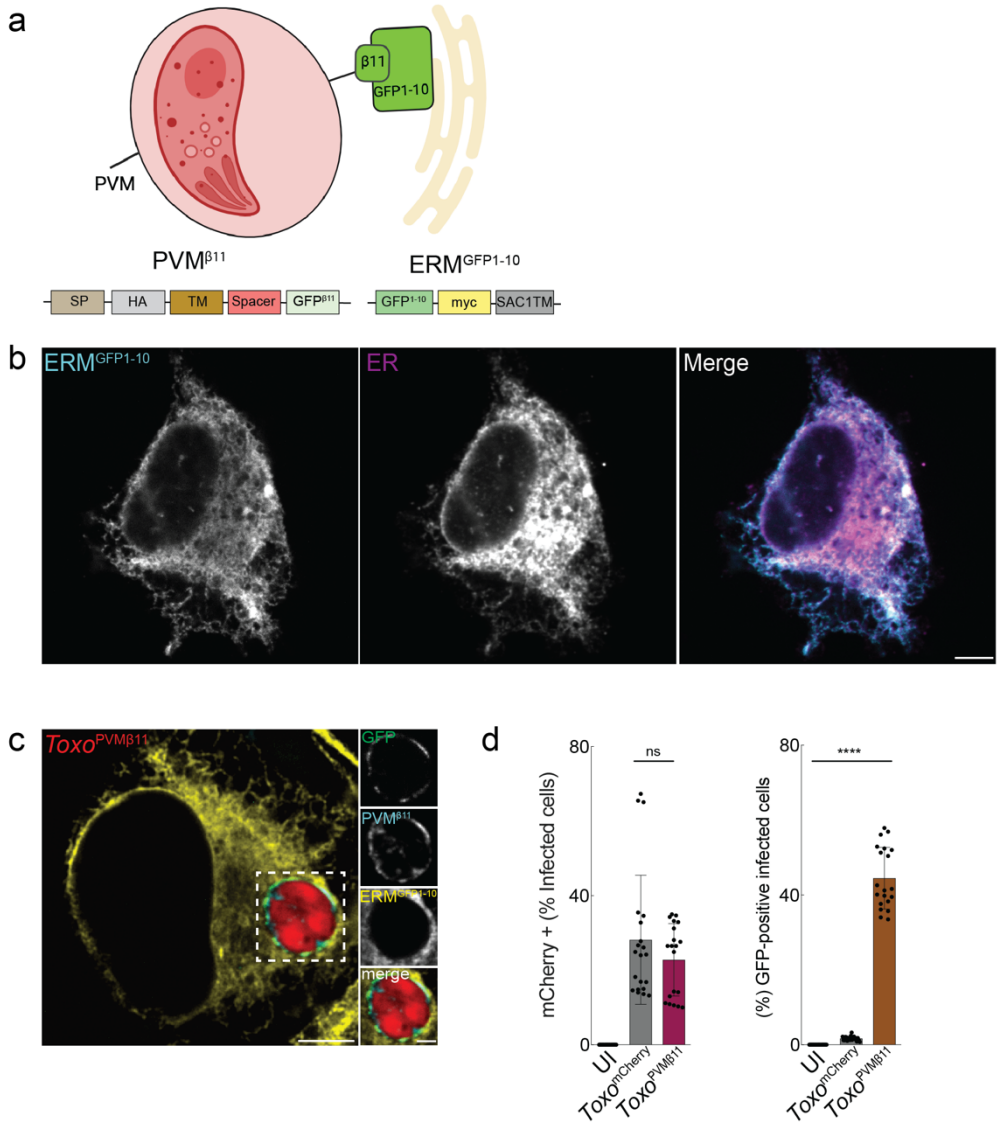

Extended Data Fig. 6: Characterization of the host ER-*Toxoplasma* MCS reporter
a, Schematic of the PVM^{β11} and ERM$^{GFP1-10}$ constructs generated for the host ER-*Toxoplasma* split-GFP system. PVM, parasite vacuole membrane; SP, signal peptide; TM, transmembrane domain; ERM, ER membrane; SAC1, Phosphoinositide phosphatase. **b,** Immunofluorescence (IF) images of ERM$^{GFP1-10}$ -expressing ES-2 cells (ERM$^{GFP1–10}$ ES-2s). ERM$^{GFP1-10}$ (GFP); ER (calnexin). Scale bar: 5 µm. **c,** IF image of ERM$^{GFP1-10}$ ES-2s infected with parasites expressing PVM^{β11} (*Toxo*^{PVMβ11}) at 24 hours post infection (hpi). PVM^{β11} (HA); ERM$^{GFP1-10}$ (GFP). Scale bars: 5 µm; inset, 2 µm. **d,** ERM$^{GFP1-10}$ ES-2 cells were uninfected (UI), infected with parasites expressing mCherry (*Toxo*^{mCherry}) or *Toxo*^{PVMβ11} and analysed by flow cytometry for GFP expression at 24 hpi. FACS data are mean ± SD of n=4 biological replicates. Each dot represents a technical replicate. ****p<0.0001 for by means of one-way ANOVA.

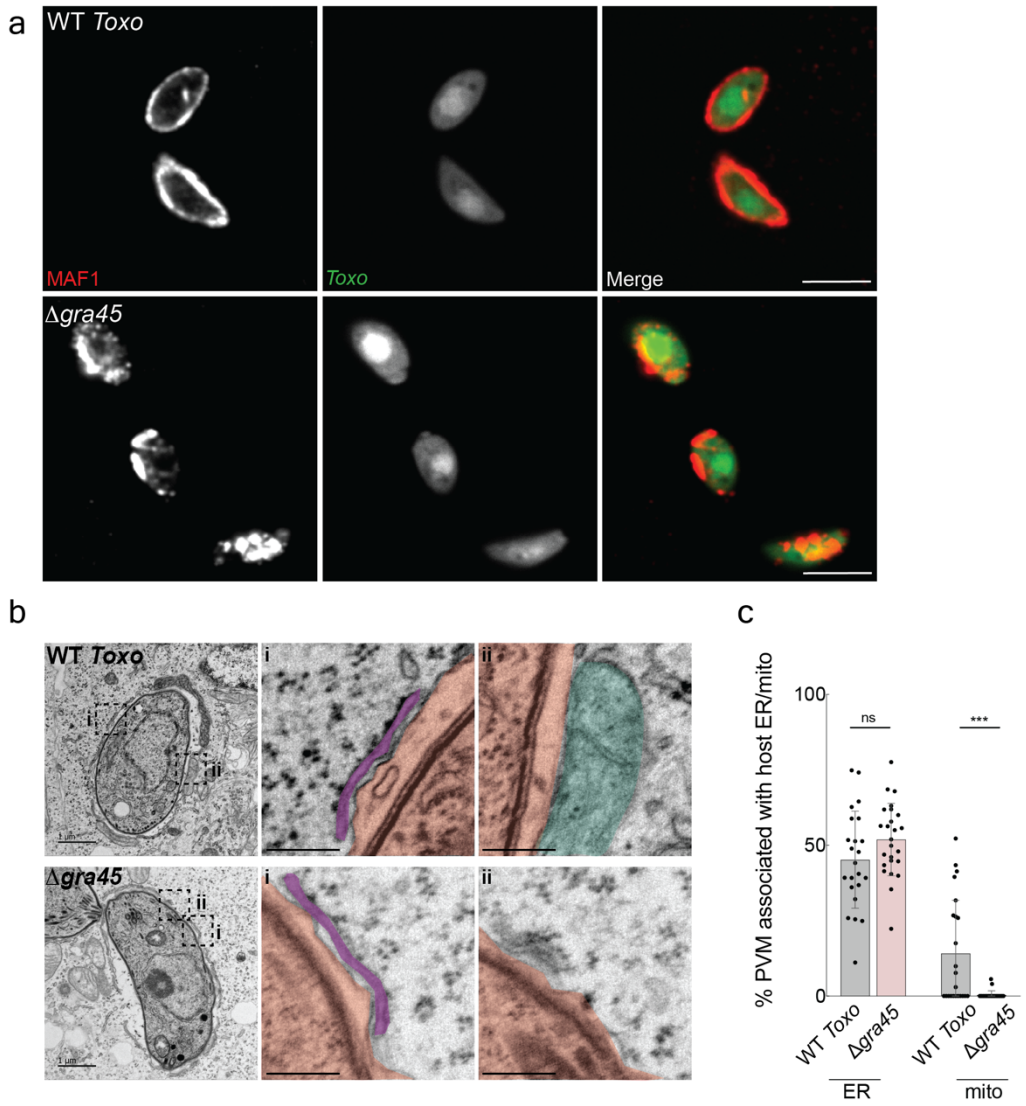

Extended Data Fig. 7: Host ER-*Toxoplasma* MCS form independently of *Toxoplasma* dense granule effector proteins

a, Immunofluorescence images of ES-2 cells infected with WT (*Toxo*^{mCherry}) or Δ*gra45* parasites at 3 hours post infection. Scale bar: 5 µm. **b,** Representative electron microscopy images of ES-2s infected with WT (*Toxo*^{mCherry}) or Δ*gra45* parasites at 3 hpi. Membrane contact sites between the *Toxoplasma* parasite vacuole membrane (PVM) and (**i**) host ER and (**ii**) host mito. Scale bars: 1 µm; inset, 250 nm. Red, parasite vacuole; purple, ER; turquoise, mito. **c,** Percentage of PVM associated with host ER and mitochondria in images as in (**b**). PVM: parasite vacuole membrane. EM data are mean ± SD from >20 *Toxoplasma* vacuoles. ***p=0,0003 by means of unpaired t-test. Both experiments are representative of one biological replicate.

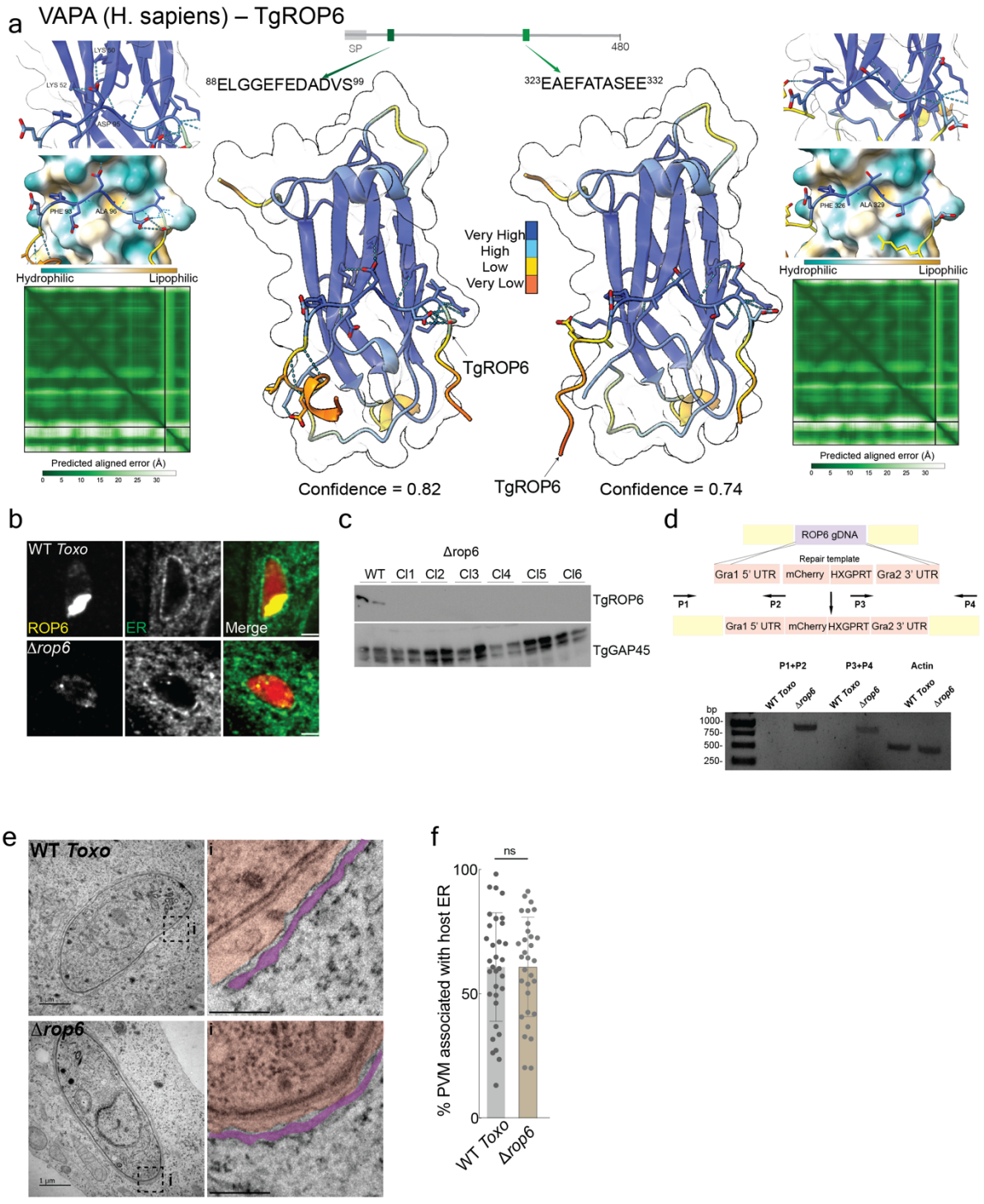

Extended Data Fig. 8: Loss of TgROP6 does not affect host ER-*Toxoplasma* MCS

a, AlphaFold multimer models of the MSP domain of VAPA with the predicted canonical (Left; EFFDAxE) and modified (Right; ExFxDAxE) FFAT motifs of TgROP6. **b,** Immunofluorescence images of HFFs infected with WT (*Toxo*^{PVMβ11}) or the pool of Δ*rop6* parasites at 3 hours post infection (hpi). ER (calnexin). Scale bar: 2 µm. **c,** WT *Toxo* (Type I RHΔ*KU80*Δ*hxgprt*) and clones of Δ*rop6* parasites were analysed by means of immunoblotting for TgROP6 and TgGAP45. **d,** Schematic diagram depicting the genomic loci of TgROP6 (top) and the repair template. Primer pairs P1 - P4 were used to check insertion of the repair template into the TgROP6 locus between WT *Toxo* (Type I

RHΔ*KU80*Δ*hxgprt*) and Δ*rop6* clone 6. Expected products of primer pair- 1+2 = 951 base pairs (bp); primer pair 3+4 = 939 bp; primer actin (loading control) = 598 bp. **e,** Representative electron microscopy images of HeLas infected with WT or Δ*rop6* parasites at 3 hpi. Membrane contact sites between the *Toxoplasma* parasite vacuole membrane (PVM) and (**i**) host ER. Scale bars, 1 µm; inset, 250 nm. **f,** Percentage of PVM associated with host ER in images as in (**e**). Red, parasite vacuole; purple, ER. EM data are mean ± SD from >30 *Toxoplasma* vacuoles. All experiments were conducted n = 1 biological replicate.

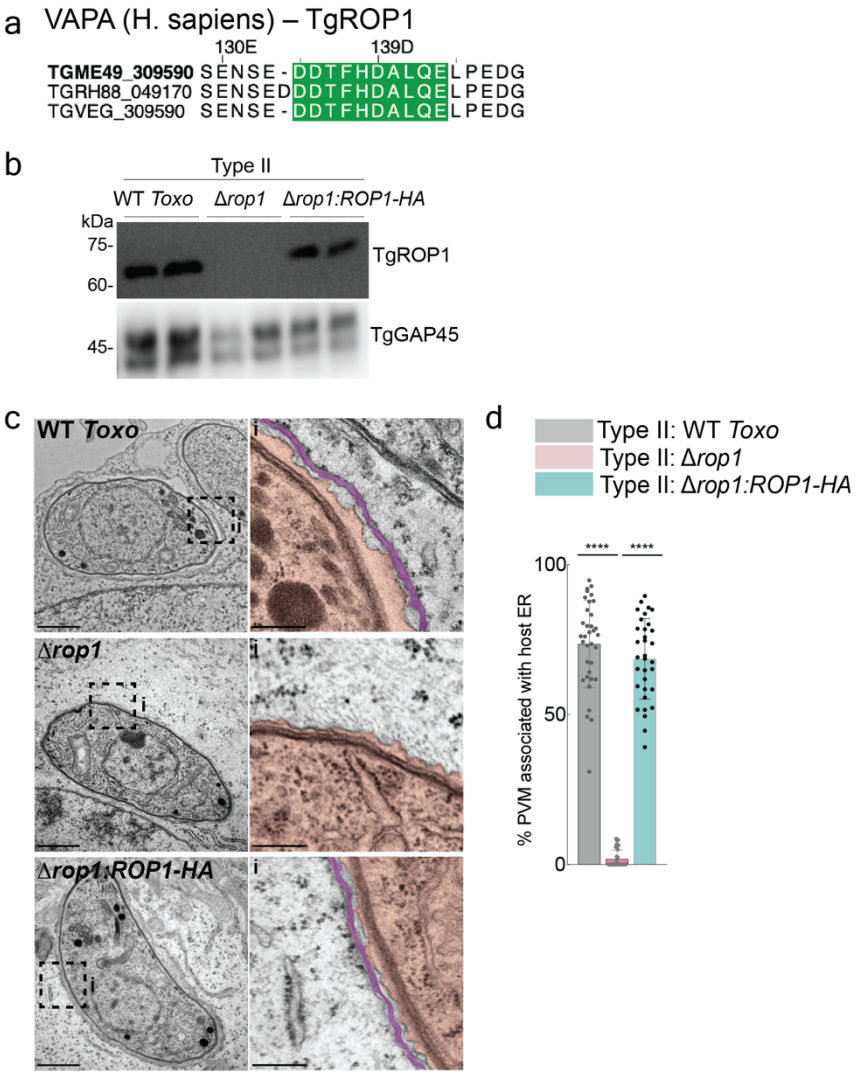

Extended Data Fig. 9: Type II TgROP1 mediates host ER-*Toxoplasma* MCS

a, Sequence alignment of TgROP1 orthologous sequences from the canonical *Toxoplasma* strains- Type I (TGRH88_049170), Type II (TGME49_309590) and Type III (TGVEG_309590) showing the presence of TgROP1 modified FFAT motif matches in green. amino acid numbers correspond to the motif position in Type II parasites. **b,** Type II: WT *Toxo* (PruΔKU80 Δ*hxgprt*), Δ*rop1* and Δ*rop1:ROP1-HA* parasites, were analysed by means of immunoblotting for TgROP1 and TgGAP45. **c,** Representative electron micrograph images of ES-2s infected with indicated *Toxoplasma* strains at 3 hours post infection. Membrane contact sites between the *Toxoplasma* parasite vacuole membrane (PVM) and (**i**) host ER. Scale bars: 1 µm; inset, 250 nm. Red, parasite vacuole; purple, ER. **d,** Percentage of *Toxoplasma* PVM associated with host ER in images as in (**c**). EM data are mean ± SD from >29 *Toxoplasma* vacuoles from n =1 biological replicate. ****p< 0.0001 by means of one-way ANOVA.

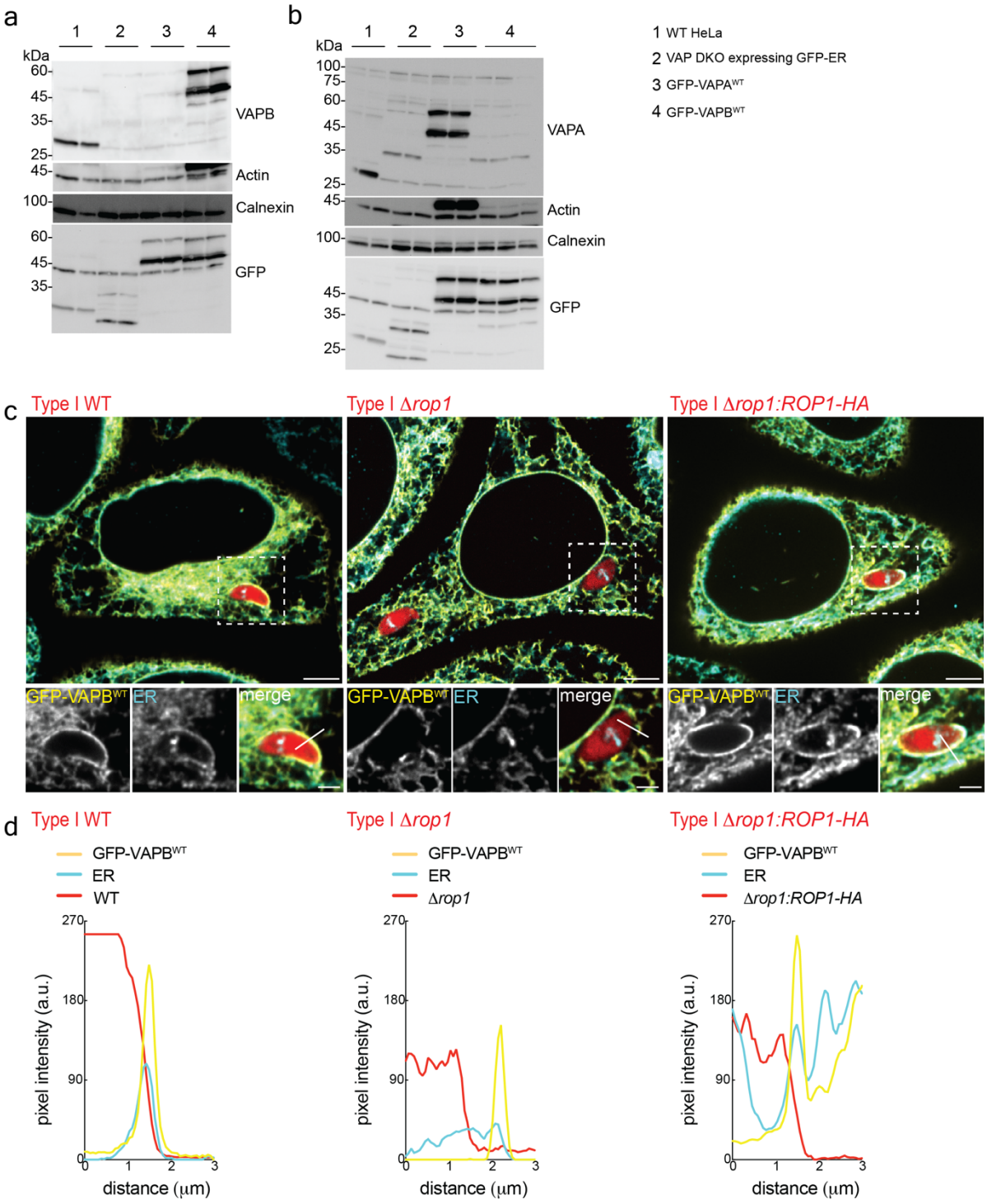

Extended Data Fig. 10: VAPB enrichment around the parasite vacuole requires TgROP1

a,b, (1) WT HeLas (2) *VAPA/VAPB*-deleted (VAP DKO) HeLas expressing GFP on their ER (3) VAP DKO cells expressing GFP-VAPA^{WT} and (4) VAP DKO cells expressing GFP VAPB^{WT} were analysed by means of immunoblotting and the same membrane was probed with different antibodies as indicated. Expected molecular weights: VAPA^{WT}, ~27 kDa; GFP-VAPA^{WT}, ~55 kDa; VAPB^{WT}, ~27 kDa; GFP-VAPB^{WT} ~55 kDa. Each sample was loaded twice except GFP-VAPB^{WT} in (**b**) was loaded thrice. **c,** Immunofluorescence images of VAP DKO HeLa cells expressing GFP-VAPB^{WT} infected with *Toxoplasma* Type I WT (*Toxo*^{mCherry}),

Δ*rop1*, Δ*rop1:ROP1-HA* parasites at 3 hours after infection. ER (calnexin). Scale bars, 5 μm; inset, 2 μm. **d,** Corresponding pixel intensity plots for white line in the (**c**) inset. Data is representative of one biological replicate.

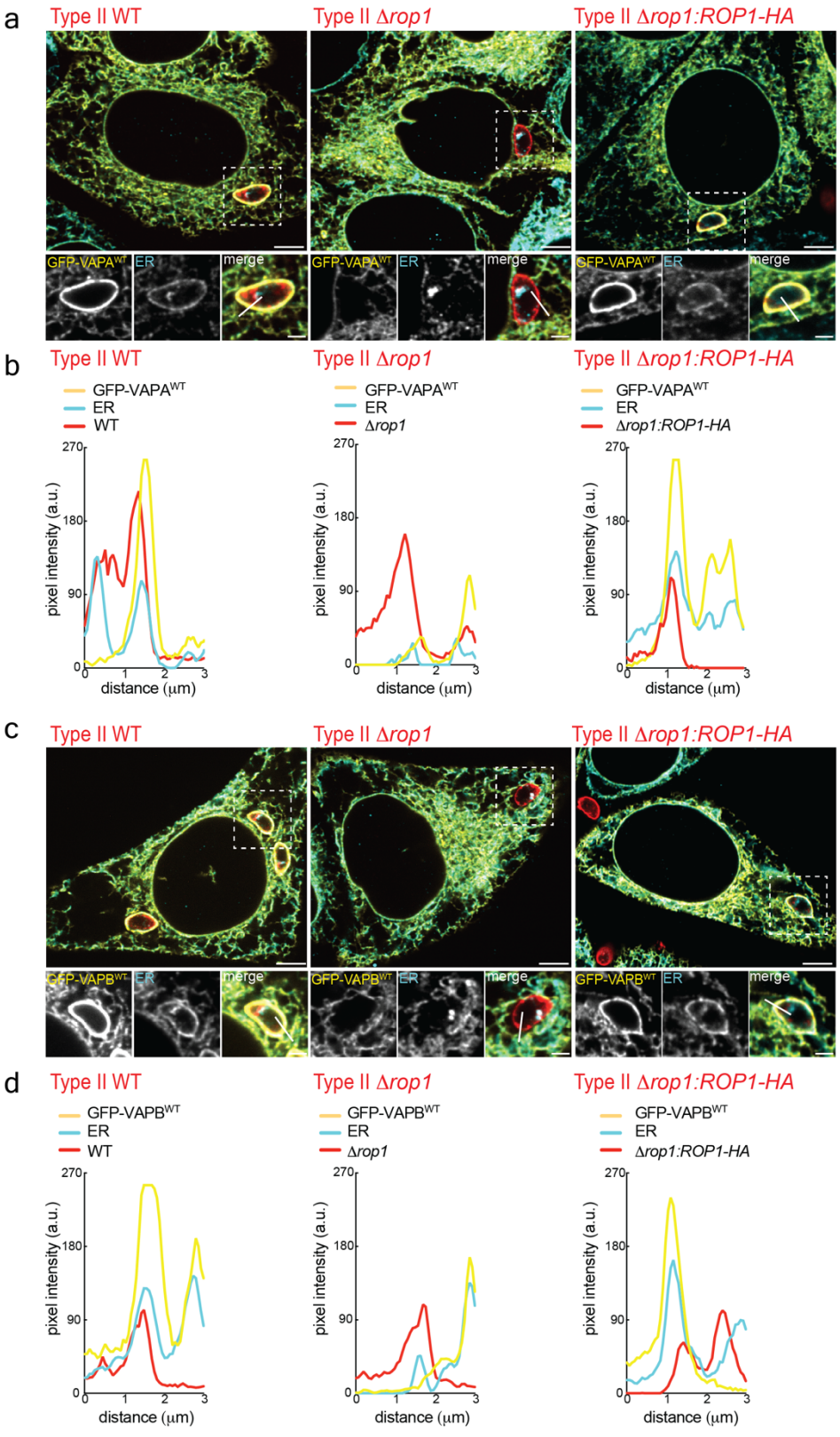

Extended Data Fig. 11: VAPA and VAPB enrichment around Type II parasites requires TgROP1

a, Immunofluorescence (IF) images of *VAP DKO* HeLa cells expressing GFP-VAPA^{WT} and infected with *Toxoplasma* Type II WT (PruΔKU80 Δ*hxgprt*), Δ*rop1*, Δ*rop1:ROP1-HA*

parasites at 3 hours post infection (hpi). *Toxoplasma* strains were labelled with the TgSAG1 (surface antigen 1) antibody; ER (calnexin). **b,** Corresponding pixel intensity plots for white line in (**a**) inset. **c,** IF images of VAP DKO HeLa cells expressing GFP-VAPB^{WT} and infected with indicated parasites at 3 hpi. *Toxoplasma* strains (surface antigen 1; TgSAG1); ER (calnexin). **d**, Corresponding pixel intensity plots for white line in (**c**) inset. Scale bars: 5 µm; inset 2 µm. Data is representative of one biological replicate.

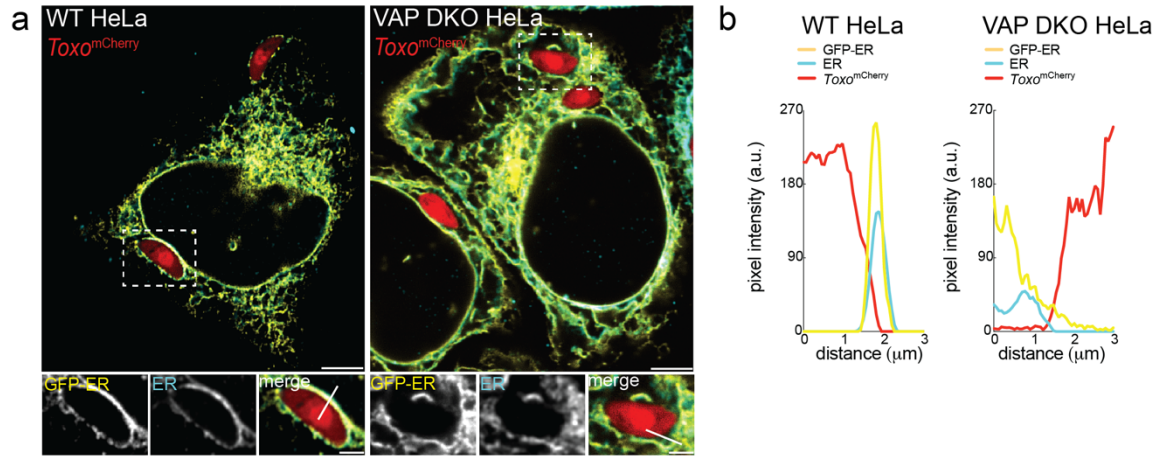

Extended Data Fig. 12: Host ER association around *Toxoplasma* is VAP-dependent
a, Immunofluorescence images of WT and *VAP DKO* HeLa cells expressing GFP-ER and infected with *Toxo*^{mCherry} at 3 hours post infection. ER (calnexin). Scale bars: 5 μm; inset, 2 μm. **b,** Corresponding pixel intensity plots for white line in the (**a**) inset. Data is representative of one biological replicate.

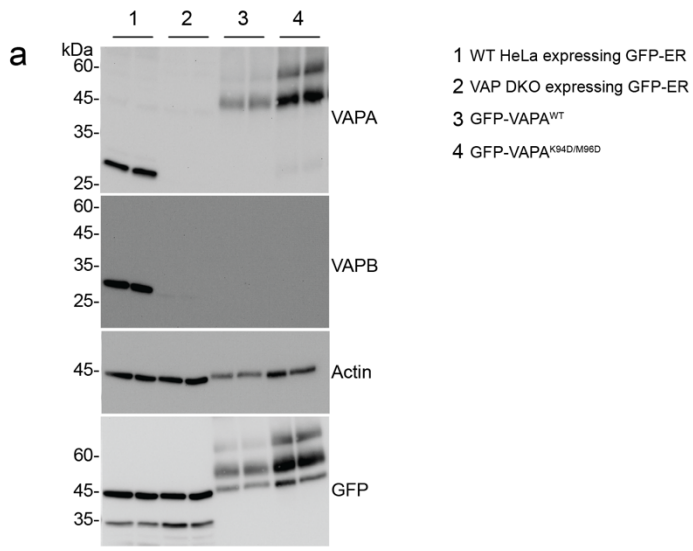

Extended Data Fig. 13: Immunoblot verification of GFP-VAPA$^{K94D/M96D}$ cells

a, (1) WT HeLas expressing GFP on the ER (GFP-ER), (2) GFP-ER expressing- *VAPA/VAPB*-deleted (VAP DKO) HeLas (3) VAP DKO cells expressing GFP-VAPA^{WT} and (4) VAP DKO cells expressing GFP-VAPA$^{K94D/M96D}$ cells were analysed by means of immunoblotting and probed with indicated antibodies. Expected molecular weights: VAPA^{WT}, ~27 kDa; GFP-VAPA^{WT}, ~55 kDa. Each sample was loaded twice.

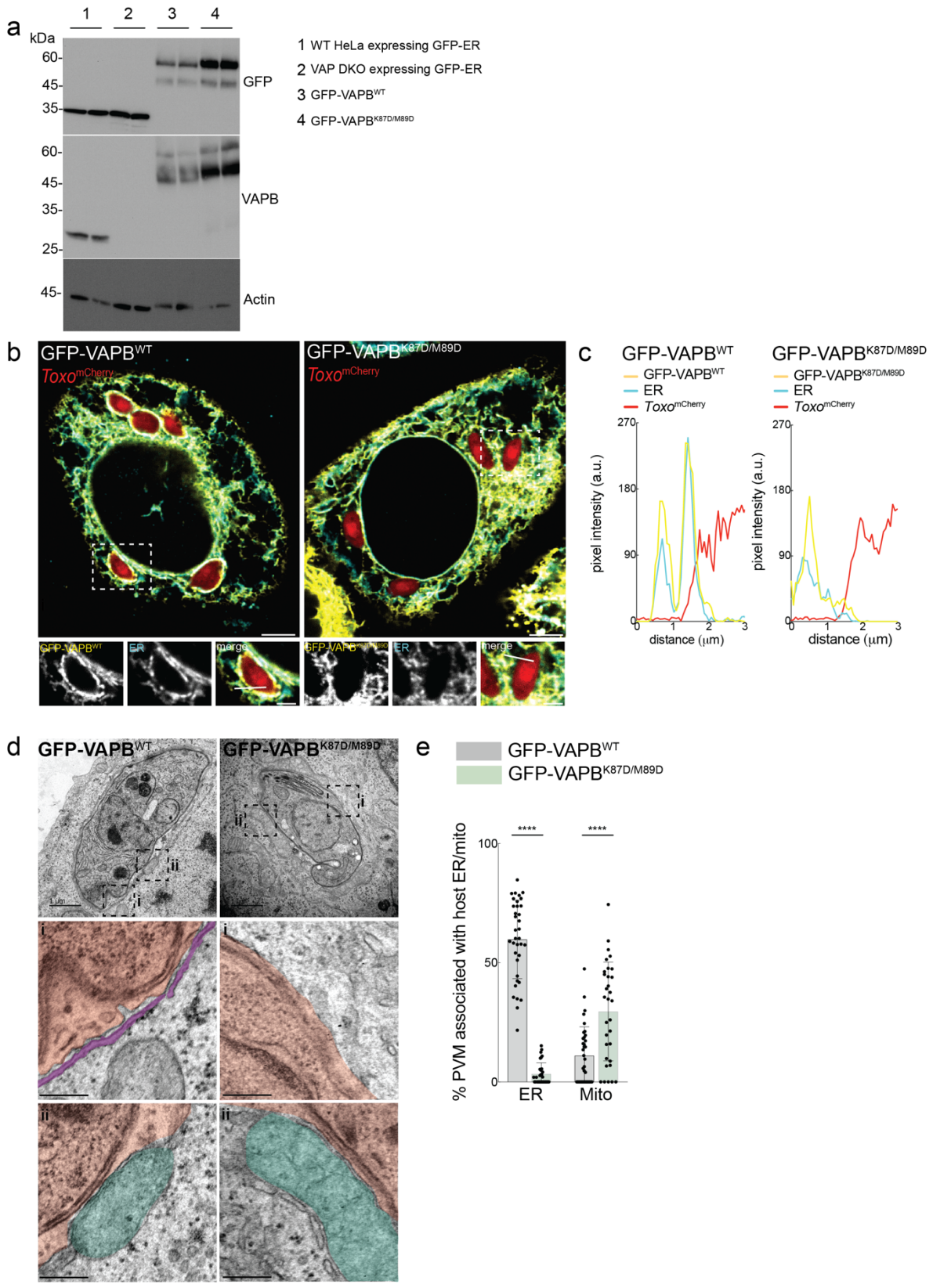

Extended Data Fig. 14: Host ER-*Toxoplasma* MCS depend on the VAPB MSP domain

a, (1) WT HeLas expressing GFP on the ER (GFP-ER), (2) GFP-ER expressing- *VAPA/VAPB*-deleted (VAP DKO) HeLas (3) VAP DKO cells expressing GFP-VAPB^{WT} and (4) VAP DKO cells expressing GFP-VAPB$^{K87D/M89D}$ cells were analysed by means of immunoblotting and probed with indicated antibodies. Expected molecular weight: VAPB^{WT}, ~27 kDa; GFP-

VAPB^{WT} ~55 kDa. Each sample was loaded twice. The HeLa WT and VAP DKO lysates are the same as Extended Data Fig. 13. **b**, Immunofluorescence images of VAP DKO HeLa cells expressing WT GFP-VAPB (GFP-VAPB^{WT}) and FFAT-binding mutant (GFP-VAPB$^{K87D/M89D}$) cells infected with *Toxo*^{mCherry} at 3 hours post infection (hpi). ER (calnexin). Scale bars: 5 µm; inset, 2 µm. Data is representative of two biological replicates. **c,** Corresponding pixel intensity plots for white line in (**b**) inset. **d,** Representative electron microscopy images of GFP-VAPB^{WT} and GFP-VAPB$^{K87D/M89D}$ cells infected with *Toxo*^{mCherry} at 3 hpi. Scale bars: 1 µm; inset, 250 nm. Membrane contact sites between the *Toxoplasma* parasite vacuole membrane (PVM) and (**i**) host ER and (**ii**) host mito. Red, parasite vacuole; purple, ER; turquoise, mito. **e,** Percentage of *Toxoplasma* PVM associated with host ER and mitochondria in images as in (**d**) from >30 *Toxoplasma* vacuoles n = 1 biological replicate. ****p<0.0001 by means of unpaired t-test.

Supplementary Tables 1
List of gene targets and protospacer sequences used in the CRISPR screens.

Supplementary Table 2
List of *Toxoplasma* genes from the host mitochondria-*Toxoplasma* effector CRISPR screen showing the median Log_2 fold change (Log_2FC) in the sgRNA abundances between the GFP^{hi} and GFP^{neg} populations and robust ranking aggregation (RRA) scores.

Supplementary Table 3
List of *Toxoplasma* genes from the host ER-*Toxoplasma* effector CRISPR screen showing the median Log_2 fold change (Log_2FC) in the sgRNA abundance between the GFP^{hi} and GFP^{neg} populations and robust ranking aggregation (RRA) scores.

Supplementary Table 4
Analysis of transmembrane domain containing *Toxoplasma* rhoptry genes from the ER-*Toxoplasma* CRISPR screen for putative canonical or modified FFAT motifs, AlphaFold model scores and motif pLDDT values.

Supplementary Table 5
Proteomic analysis of GFP-IPs from uninfected and *Toxoplasma*-infected GFP-$VAPA^{WT}$ expressing VAP DKO HeLa cells. Also, proteomic analysis of GFP-IPs from GFP-$VAPA^{WT}$ and VAP DKO HeLa cells expressing GFP-$VAPA^{K94D/M96D}$.

Supplementary Table 6
VAPA-interacting proteins from GFP-IPs from *Toxoplasma*-infected GFP-VAPA HeLa cells relative to uninfected cells.

Supplementary Table 7
Primer sequences used in this study.

Supplementary Video 1
Time-lapse images of a live human foreskin fibroblast cell labelled with MitoTracker Deep Red and expressing $OMM^{GFP\text{-}10}$ was infected with a parasite expressing $PVM^{\beta 11}$ (*Toxo*$^{PVM\beta 11}$). GFP is detected at the host mitochondria-*Toxoplasma* interface. Images were acquired every 3 minutes using a spinning-disk confocal microscope. PVM: parasite vacuole membrane; OMM: outer mitochondrial membrane. Scale bar, 5 µm.

Supplementary Video 2
Time-lapse images of a live human foreskin fibroblast cell expressing GFP-$VAPA^{WT}$ on the ER membrane and infected with WT Type I *Toxoplasma* parasite. Images were acquired every 6 min using a spinning-disk confocal microscope. Scale bar, 5 µm.

3.2 Further characterization of the host-microbe split-GFP system

In the previous section we applied the system for loss-of-function *Toxoplasma*-targeted CRISPR screen approaches. To determine whether this system can be used in a host-screen approach we utilized our host-microbe mitochondria split-GFP system and performed a genome wide loss-of-function CRISPR screen. Briefly, $OMM^{GFP1–10}$-expressing ES-2 cells ($OMM^{GFP1–10}$ ES-2) were transduced with a genome-wide Brunello CRISPRko sgRNA library (Doench et al., 2016). This library contains 76,441 sgRNAs targeting the entire human genome as well as *S. pyogenes* Cas9(Doench et al., 2016). We reasoned that a genome-wide rather than a targeted library will allow for the approach to be completely unbiased and ensure the discovery of host tethers. After transduction of this library into $OMM^{GFP1–10}$ ES-2 cells, they were selected with puromycin and then infected with $PVM^{\beta11}$-expressing $Toxo^{mCherry}$ parasites ($Toxo^{PVM\beta11}$) at a low multiplicity of infection of 1.5. The parasites were left to grow for 8-10 hours post infection (hpi). Like our *Toxoplasma* screen approaches, the mCherry-positive infected cells were FACS-sorted into two main populations- GFP-negative (GFP^{neg}) and GFP-high (GFP^{hi}) (Fig. 3.2a). We hypothesized that sgRNAs enriched in the GFP^{neg} population but depleted in the GFP^{hi} population would encode for genes that promote host mitochondria-*Toxoplasma* MCS. Once we obtained the populations, we extracted host genomic DNA (gDNA) and PCR-amplified host sgRNAs from both the GFP^{neg} and GFP^{hi} populations for next generation sequencing. Subsequently, using the model-based analysis of genome-wide CRISPR-Cas9 knockout (MAGeCK) method, we quantified the median $\log_2$ fold change (Log_2FC) in the sgRNA abundance per gene between the two populations and ranked the host genes using robust rank aggregation (RRA) (W. Li et al., 2014). As expected, the top promoter of contact site formation was TOM70 (Fig. 3.2b). In previous work I confirmed with flow cytometry and immunofluorescence that TOM70 cells are negative for HMA, in line with published literature (Blank et al., 2021; X. Li et al., 2022). To further consolidate these findings, I infected HeLa WT and *TOM70 KO* cells expressing $OMM^{GFP1–10}$ with either Type I:mCherry-expressing parasites ($Toxo^{mCherry}$) or $Toxo^{PVM\beta11}$ parasites and assessed the samples by electron microscopy and in parallel repeated flow cytometry analysis at 8 hpi.

Consistent with previous results we observed that the OMM$^{GFP1–10}$ *TOM70 KO* cells were GFP- at 8 hpi by flow cytometry (Fig. 3.2c,d). Furthermore, electron microscopy confirmed this data as we observed no significant difference in the percentage of mitochondria associated with the parasite vacuole in *TOM70 KO* HeLa cells upon infection with either parasite strain (Fig. 3.2e,f). This confirmed the screening approach as TOM70 is the mammalian counterpart for mitochondria-*Toxoplasma* contact sites (Blank et al., 2021; X. Li et al., 2022). Our data supports the versatile use of the mitochondria-microbe system for both host and pathogen high throughput FACS and CRISPR-Cas9 screening approaches.

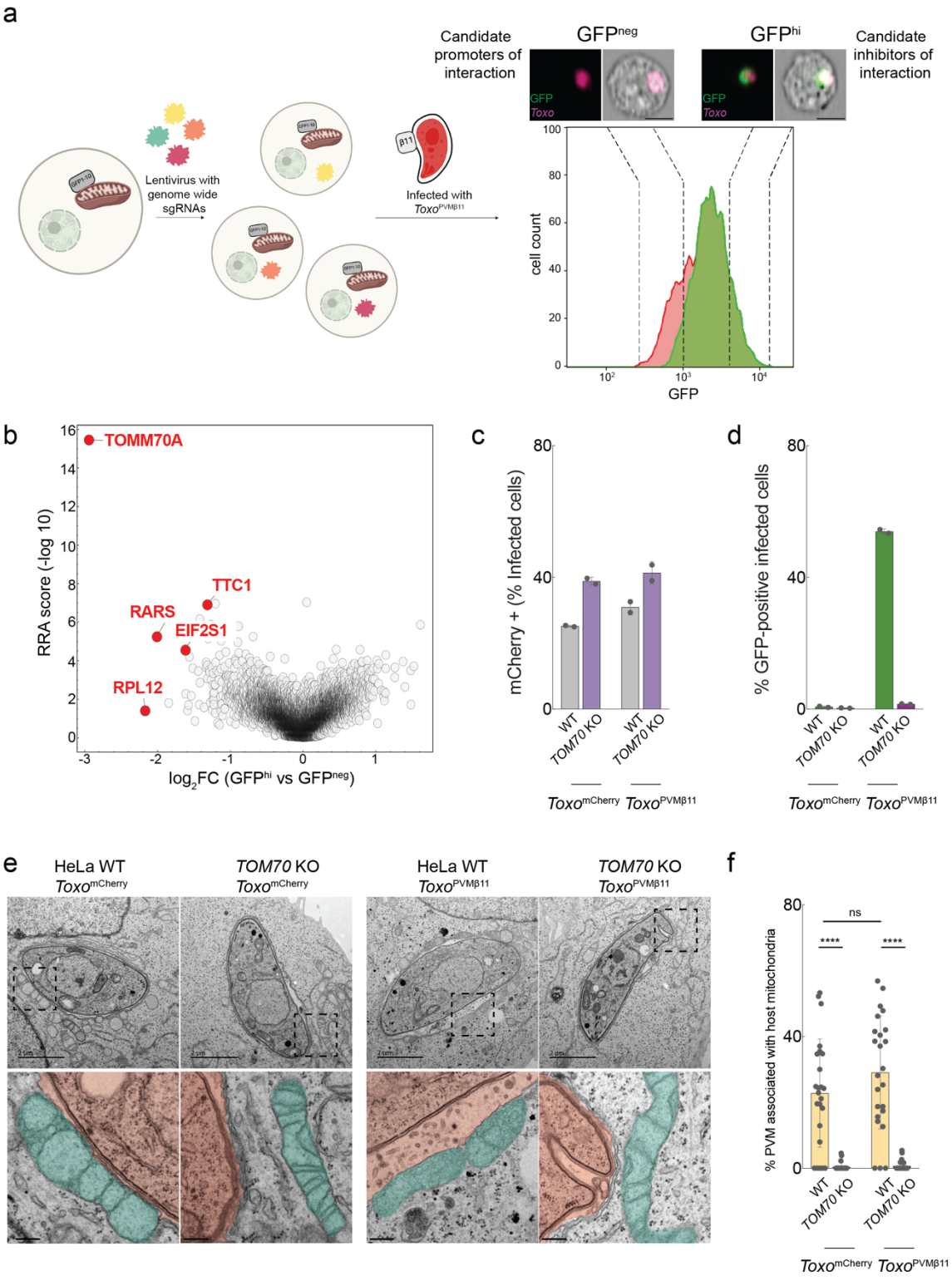

Fig. 3.2: Reporter screen reliably captures host mitochondria-*Toxoplasma* interactions. a, Schematic of CRISPR screen. OMM$^{GFP1-10}$ ES-2 cells were transfected with lentivirus against the human genome. Post-selection, these cells were infected with Type I:mCherry *Toxoplasma* expressing GFP^{β11} (*Toxo*^{PVMβ11}). 8-10 hours post infection, infected mCherry positive cells were sorted based on GFP expression to identify candidate promoters of mitochondria-*Toxoplasma* MCS. Representative images are from

sorted populations obtained during test sorts. Arbitrary dashed lines represent GFP^{neg} and GFP^{hi} populations. Scale bar: 10 µm. **b,** Volcano plot showing the log_2fold change (Log_2FC, x-axis) and robust rank aggregation score (RRA, y-axis) of genes from GFP^{hi} versus GFP^{neg} MAGeCK analysis. **c,d**, WT and *TOM70 KO* HeLa cells expressing $OMM^{GFP1-10}$ were infected with Type I mCherry- *Toxoplasma* (*Toxo*^{mCherry}) and *Toxo*^{PVMβ11} and analysed by flow cytometry at 8 hpi. Data is from one biological replicate. Each dot represents a technical replicate. **e,** Representative electron microscopy images of WT $OMM^{GFP1-10}$ and *TOM70 KO* $OMM^{GFP1-10}$ HeLa cells infected with *Toxo*^{mCherry} or *Toxo*^{PVMβ11}at 8 hpi. Scale bars: 2 µm; inset, 250 nm. Membrane contact sites between the *Toxoplasma* parasite vacuole membrane (PVM) and host mito. Red, parasite vacuole; turquoise, mito. **f,** Percentage of *Toxoplasma* PVM associated with host mitochondria in images as in (**e**) from >20 *Toxoplasma* vacuoles from n= 1 biological replicate. ****p<0.0001 for WT $OMM^{GFP1-10}$ versus *TOM70 KO* $OMM^{GFP1-10}$ HeLa cells by two-way ANOVA.

3.2.1 Material and Methods

The FACS and EM experiments were conducted as previously described in the results section 3.1.

Viral titration

The human genome-wide Brunello CRISPR knock-out library containing 76,441 sgRNAs (4 sgRNAs/gene including 1,000 non-targeting control sgRNAs) as well as Cas9 was a gift from David Root and John Doench (Addgene #73179). The library plasmid together with lentiviral packaging plasmids pCMV-dR8.2 dvpr and pCMV-VSV-G was transfected into HEK293T cells. Plasmids pCMV-dR8.2 dvpr and pCMV-VSV-G were gifts from Bob Weinberg (Addgene plasmid #8455 and #8454). Lentiviral particles were harvested 48h later, filtered with a 0.45µm filter (Merck Millipore, Millex-HP #SLHPR33RS) and stored in aliquots at -80°C. The optimal volume of lentiviral particles for screening was optimised by spinfecting 5x10^6 OMM GFP$^{1-10}$ ES-2 cells in 6-wells plates for 2h at 2000 rpm at 37°C with an increasing range of virus volumes and including a no transduction control, in the presence of 8µg/ml Polybrene (Santa Cruz, sc-134420). Afterwards, the plates were placed in the incubator overnight. The next morning, cells were transferred from the 6 well to 15 cm dishes. After 48 hours the medium was changed to with 3 µg/ml Puromycin (GIBCO- 2318951) and one plate was left untreated. Selection was complete when non-transduced cells in presence of puromycin were completely dead. The optimal virus volume was chosen based on ~50% cells surviving selection (MOI of ~0.3- ~0.5) compared to non-selected conditions.

CRISPR screen

For the screen 50 x10^6 OMM GFP$^{1-10}$ ES-2 cells were transduced with the Brunello library lentivirus at an MOI between ~0.3-0.5, via spinfection in 6-well plates as described above. The next day cells were expanded to 15 cm dishes and 48 h later they were treated with 3 µg/ml puromycin. After two days, cells were expanded from 1x 15 cm plate to 3 x 15 cm plates and left to grow for one day. Then, 10 million cells per 15 cm dish were plated. The next day, PVM$^{\beta 11}$-expressing *Toxo*^{mCherry} parasites (*Toxo*$^{PVM\beta 11}$) were infected at an MOI of 1.5 for 8-10 hours post infection. Then, cells were trypsinzed and pooled together into 50 ml falcons and spun down at 300 x g for 5 minutes. Next, the cells were fixed in 2% PFA for 5 minutes in 3% FBS in 1x PBS buffer and then spun down at 300 x g for 5 minutes to get rid of fixative. The cells were then distributed into FACS tubes for sorting. The cells were sorted via both the BD FACSAria III sorter and the BD FACSFusion sorter. mCherry positive- infected cells were sorted into all cells negative (15% of the population) for GFP expression (GFP^{neg}) and the top 20% of the GFP positive [GFP-high (GFP^{hi})] cells. Sorted cell populations obtained were 6 million cells for GFP^{neg} and 7 million cells for GFP^{hi} (a screen coverage of ~100x.) Cell pellets were stored at -80°C. Images of screen

populations obtained during test sorts were acquired on an ImageStream^X MkII with a X40 magnification. Image analysis was performed using IDEAS software (Cytek Biosciences).

Cell pellets were then de-crosslinked in a solution of 10 mM Tris pH 7.5 (Thermo: 15567027) and 10 mg/mL Proteinase K (Sigma-Aldrich: 3115887001) at 55 °C for 24 h. Cells were then lysed with buffer AL (QIAamp DNA Blood Mini Kit: 51104) for two hours and genomic DNA was isolated as per manufacturer's protocol. Library samples were amplified by PCR (22 cycles with 5 µg of gDNA as input in 100 µl reaction volume) using NEBNext Ultra™ II Q5 Master Mix (New England BioLabs Inc.) with a mix of six different forward primers (primers 37-42; supplementary table 7) to introduce sequence diversity and reverse primer (primer 43). Afterwards, amplicons per sample were pooled, bead-purified and quantified, followed by the introduction of Illumina Nextera adaptors and indices by eight cycles in a second round of PCR, again bead-purified and quantified. Samples were pooled and analysed on an Illumina NovaSeq platform by paired end (2x100 bp) sequencing with >36x10^6 reads per sample.

CRISPR KO screen data analysis

Following demultiplexing, raw NGS libraries were quality-checked using FastQC version 0.11.8 (Andrews & others, 2019) Upstream sequences and sgRNA length were used to trim reads with cutadapt (version 4.5). MAGeCK (version 0.5.9.5) count was used to quantify the number of reads per sgRNA (W. Li et al., 2014). Raw sgRNA counts were median-normalised and MAGeCK test was used to test and rank sgRNAs and genes (sgRNA read count filter of 10 was applied for treatment or control samples). The log2-fold change (Log_2FC) on a gene level was calculated as follows: Log_2FC = median [log2((sgRNA read counts in 'Not GFP positive' gate + 1) - (sgRNA read counts in 'GFP high' gate + 1))]. For gene significance, an α-RRA score was calculated by MaGeCK (W. Li et al., 2014). Double-sided volcano plot of gene-level Log_2FCs and RRA scores was created using Instant Clue software (Nolte et al., 2018).

Supplementary Table 8

List of genes from the host mitochondria-*Toxoplasma* host genome-wide CRISPR screen showing the median Log_2 fold change (Log_2FC) in the sgRNA abundances between the GFP^{hi} and GFP^{neg} populations and robust ranking aggregation (RRA) scores.

4 Discussion

In this study I have developed a sensor to study trans-kingdom membrane contact sites (MCS) formation between the human parasite *Toxoplasma* and two key host organelles- ER and mitochondria, providing a tool for studying host-microbe interactions. I first verified this tool for high-throughput CRISPR-Cas9 screening approaches by performing both a host genome-wide and targeted *Toxoplasma*-effector screen with the mitochondrial-*Toxoplasma* split-GFP system. My top hit in the host screen was TOM70 and in the *Toxoplasma* screen was TgMAF1, which confirmed the robustness of this approach because TOM70 and TgMAF1 are required for mitochondria-parasite vacuole association (Blank et al., 2021; X. Li et al., 2022; Pernas et al., 2014). I then adapted the system to study *Toxoplasma*-ER MCS and performed a similar *Toxoplasma* effector protein targeted CRISPR screen to identify the unknown proteins mediating these MCS. With a combination of biochemical, confocal imaging and electron microscopy approaches, I validated and identified parasite effector TgROP1 and ER proteins VAPA and VAPB [(vesicle-associated membrane protein-associated protein), collectively referred to as VAPs in this section] as required for mediating *Toxoplasma*-ER MCS (Fig. 4.1). This finding raises several questions which I will discuss in this section.

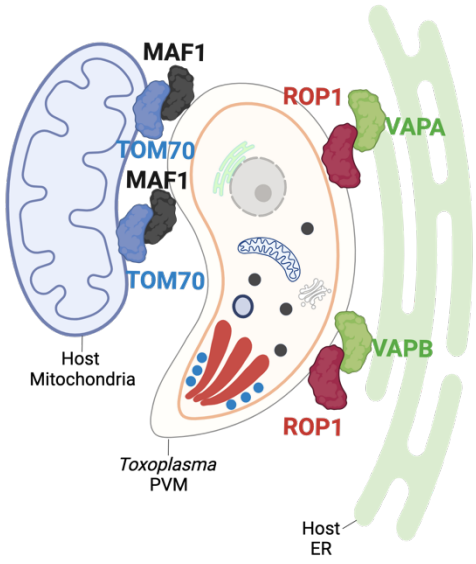

Fig. 4.1: The model of host organellar- *Toxoplasma* association. Host mitochondria MCS with the *Toxoplasma* vacuole are mediated by host OMM protein TOM70 and pathogen effector protein TgMAF1. Host ER-*Toxoplasma* MCS are mediated by effector protein TgROP1 and host VAPA and VAPB.

4.1 The molecular nature of the interaction between TgROP1 and VAPs

The host ER-*Toxoplasma* MCS tethers have remained unknown for over 60 years (Jones & Hirsch, 1972). Here, I identified host VAPs and TgROP1 as the main tethers mediating *Toxoplasma*-ER MCS. My work suggests that *Toxoplasma* exploits the MSP binding domain of VAPs as mutating key FFAT-binding residues in the major sperm protein (MSP) domains of either VAPA or VAPB reduced this interaction. One limitation of this is that all the VAP rescue experiments were performed with cells expressing the various constructs at the population level. In future experiments it may be important to sort the cells expressing the different VAP proteins for similar GFP expression and further assess MCS formation to consolidate our results.

Are the host ER-*Toxoplasma* MCS an example of molecular mimicry whereby *Toxoplasma* has evolved to express a eukaryotic host FFAT motif that enables interaction with host ER remains unknown. A direct way to test this would be to mutagenize the predicted FFAT motifs in TgROP1 and assess host ER association (hERa). In this context, in mammalian cells and for *Chlamydia* effector protein IncV, it was reported that amino acids phenylalanine (F) or a tyrosine residue at position 2 is critical for VAP binding (Murphy & Levine, 2016; Stanhope et al., 2017). According to our prediction TgROP1 contains a putative ExFxDAxE FFAT motif that is conserved across *Toxoplasma* strains with the following sequence: DDTFHDALQE. We can introduce single substitutions of F to an alanine amino acid to determine its role in ER association. This approach will also allow to exclude any indirect effects caused by the deletion of the entire motif or protein. Furthermore, the machinery that transports rhoptry proteins onto the *Toxoplasma* PVM remains unknown (Rastogi et al., 2019). Therefore, a limitation of the current study is the possibility of a pleiotropic effect that causes loss of ER association upon the deletion of TgROP1. This is corroborated by my data whereby loss of TgGRA45 indirectly results in no mitochondrial association because TgGRA45 is responsible for the PVM localization of TgMAF1 (Y. Wang et al., 2020). Therefore, confirming the presence of the FFAT motif in TgROP1 will: 1) provide the first evidence of molecular mimicry in a eukaryotic pathogen

and 2) exclude any pleiotropic effects and establish a direct role of TgROP1 in establishing MCS with host ER.

The immunoprecipitation and proteomics data suggest an interaction between VAPs and TgROP1. First, this IP was conducted once and needs to be repeated to support the current findings. Second, to further support this claim a GFP-IP between GFP-VAPA^{WT} and GFP-VAPA$^{K94D/M96D}$ cells infected with *Toxoplasma* will confirm whether the interaction is dependent on the MSP domain of VAPs. Last, to consolidate our findings and further validate the interaction between TgROP1 and VAPs, an *in vitro* system may be utilized. Briefly, FFAT binding MSP domain of VAPA can be expressed as a GST-tagged protein in *Escherichia coli* and incubated with lysates of TgROP1-expressing cells or lysates from cells infected with Δ*rop1:ROP1-HA* parasites.

Are TgROP1 and VAPs sufficient to mediate these MCS? Host mitochondrial association (HMA) in *Toxoplasma* is strain-dependent and previous work established TgMAF1 as sufficient for mediating HMA by expressing TgMAF1 in Type II parasites (Pernas et al., 2014). Given that all the strains of *Toxoplasma* associate with ER, it is not possible to test sufficiency with similar experiments. Interestingly, a close relative of the *Toxoplasma* species *Neospora caninum* was reported to attract ER but not physically tether it (Nolan et al., 2015). To test sufficiency, we could express TgROP1 in this species and assess whether this enables ER tethering.

The lack of either TgROP1 and/or VAPs does not completely abolish ER association with the parasite vacuole (PV) as a percentage of host ER remains associated with the PV. This is not surprising as during MCS formation it is common to observe redundancy meaning that several sets of tethers can maintain MCS. For example, in yeast the ER–plasma membrane contact sites are mediated by 3 sets of tethering proteins and changes in MCS formation are only observed upon loss of all the factors (Manford et al., 2012). This phenomenon of redundancy is also seen with *Chlamydia* where multiple tethers exist to form host ER-pathogen MCS (Vormittag, Ende, et al., 2023a). I observed a great reduction in ER-*Toxoplasma* MCS upon loss of VAP proteins or TgROP1 indicating that they are the main tethers for mediating these MCS; however, it is possible that there are either

additional tethers present or compensatory mechanisms that can mediate this contact in the absence of the main tethers.

4.2 What is the function of the host ER-*Toxoplasma* MCS- friend or foe?

The physiological relevance of host ER-*Toxoplasma* MCS and whether they benefit the host or pathogen are open questions. Given the versatile role of the ER in a cell, various possibilities that would benefit the parasite emerges. One obvious consideration is lipid scavenging. *Toxoplasma* replicates within host cells and thus requires a steady supply of lipids for its membranes that could be scavenged from the ER. It has been reported that the parasite acquires host-derived phospholipids (Charron & Sibley, 2002). It is well established that the ER is a hub for phospholipid metabolism and synthesis however whether the *Toxoplasma*-ER MCS directly transfer lipids to *Toxoplasma* is unknown (Osman et al., 2011). Given that both the ER and mitochondria associate with the PVM, to exclude a role of mitochondria and specifically assess ER-*Toxoplasma* MCS in mediating phospholipid transfer, future experiments can compare wild-type parasites and Δ*maf1* parasites that according to our data and previous work exhibit increased ER association but are HMA negative (Pernas et al., 2014). Briefly, we can incubate cells with phospholipid probes conjugated to BODIPY-FITC (green) and track host phospholipid incorporation in WT and Δ*maf1* parasites by flow cytometry and immunofluorescence. Pulse chase experiments can be further assessed in WT, VAP DKO and VAP DKO cells expressing either GFP-VAPA^{WT} or GFP-VAPA$^{K94D/M96D}$ infected with WT parasites. These experiments will provide insights into whether the ER-*Toxoplasma* MCS contact sites play a role in lipid transfer.

Another intriguing possibility is that instead of this MCS serving to directly transfer lipids, *Toxoplasma* may utilize VAP proteins to indirectly transfer lipids via increasing the interaction of VAP proteins with lipid transfer proteins (LTPs). Indeed, the MCS between *Chlamydia* and ER was proposed to be required for lipid transfer as effector protein IncD binds CERT which binds VAPs, and this axis was proposed to transfer lipids (Agaisse &

Derré, 2014; Derré et al., 2011; Elwell et al., 2011). Interestingly, our proteomics analysis in comparing uninfected and infected cells revealed increased interaction of key LTPs mainly belonging to the OSBP and OSBP-related (ORP/OSBPL) protein family with VAPA, upon infection with *Toxoplasma*. This preliminary analysis requires further validation to determine which LTPs interact with VAP proteins during infection and whether they mediate any lipid transfer. Notably, other intracellular pathogens such as *Salmonella typhimurium* and *Legionella pneumophila* were reported to recruit OSBP and ORPs to their pathogen vacuoles (Kolodziejek et al., 2019; Vormittag, Hüsler, et al., 2023).

The role of these MCS in supporting parasite survival can be further tested by assessing changes in growth upon *Toxoplasma* infection. If the ER is transferring lipids or other molecules or if these MCS are generally supporting parasite burden, then we would expect reduced growth in the absence of VAP proteins. This has been reported for *Chlamydia* whereby loss of host tethers CERT or VAPs decreases bacterial size (Derré et al., 2011; Elwell et al., 2011). In contrast, bacterial species *R. parkeri* that also tethers host ER via VAP proteins, does not exhibit a growth defect upon loss of these proteins (Acevedo-Sánchez et al., 2025). This suggests that the same host proteins can have different effects on pathogen burden, underscoring the importance of examining the role of VAPs in *Toxoplasma* growth.

It was reported that *in vitro* the loss of TgROP1 (Δ*rop1*) has no growth defect when their growth is assessed upon infection in human foreskin fibroblasts (Butterworth et al., 2022). In contrast, TgROP1 was shown to be essential for virulence *in vivo* upon infection of Type II Δ*rop1* parasites (Butterworth et al., 2022). Similarly, the HMA factor TgMAF1 has no growth advantage *in vitro* but outcompete *in vivo* upon infection with Type II parasites expressing this protein versus a strain that does not (Adomako-Ankomah et al., 2016; Pernas et al., 2014). It is possible that *in vitro* conditions are conducive to parasite replication and to observe a growth defect we may have to manipulate media conditions specially if we hypothesize that the ER transfers lipids to the parasite. To potentially observe a growth defect of Δ*rop1* parasites *in vitro*, we can manipulate serum/media conditions by testing *Toxoplasma* growth under normal and in nutrient scarce conditions in HeLa or ES-2 cells, which were the primary cells used in this thesis.

In a *Toxoplasma* CRISPR screen aimed at identifying *Toxoplasma* effector proteins conferring immune evasion from the host, TgROP1 emerged as a top hit (Butterworth et al., 2022). To confirm a role of TgROP1, the authors treated bone marrow-derived macrophages (BMDMs) with Interferon γ (IFNγ), the key cytokine known to control acute infection with *Toxoplasma* and infected these cells with *Toxoplasma*- Type I and Type II strains either WT or Δ*rop1* (Butterworth et al., 2022; Suzuki et al., 1988). Interestingly, Δ*rop1* parasites exhibited ~40% reduced survival in Type I and Type II strains upon IFNγ treatment but the mechanism by which this occurs remains elusive (Butterworth et al., 2022). Future experiments testing whether this is dependent or independent of the role of TgROP1 in mediating MCS with host ER will be intriguing to test. One straightforward approach to test this would be to treat BMDMs with IFNγ and infect them with TgROP1 FFAT-mutants that are unable to tether ER. Comparing the survival of these mutants to WT parasites would help determine whether the immune evasion phenotype of TgROP1 is linked to its role in tethering host ER.

Given the role of TgROP1 in mediating *Toxoplasma*-ER MCS, it is possible that they use the ER to shield themselves from being exposed to the host cell and thus mediate immune evasion. Alternatively, the ER is at the forefront of innate immunity and the MCS could be a way to hamper *Toxoplasma* existence in cells. The most common is the cytoplasmic pathogen-sensing cyclic GMP-AMP synthase (cGAS) that activates ER-resident protein stimulator of interferon (IFN) genes (STING), which then results in downstream signaling and immune responses (Cheng et al., 2020). Indeed, mice that are depleted for STING were reported to be more susceptible to *Toxoplasma* infection (P. Wang et al., 2019). The ER-*Toxoplasma* association may therefore enable close detection of the parasite and induce an innate immune defense against *Toxoplasma*. To view the formation of host-pathogen MCS from the lens of a defense strategy by the host is an emerging perspective. This is best illustrated by a recent study that demonstrated that the mitochondria-*Toxoplasma* MCS are a means of metabolic defense against the pathogen (Pernas et al., 2018). At early hours of infection, it was reported that the mitochondria fuse around the PV and increase their uptake of fatty acids, thereby limiting pathogen access and this in turn restricts parasite growth (Pernas et al., 2018).

Perturbations to ER protein homeostasis also result in a process called the unfolded protein response (UPR). Three key players of this pathway are: double-stranded RNA-activated protein kinase (PKR)-like endoplasmic reticulum kinase PERK, activating transcription factor 6 (ATF6), and inositol requiring kinase 1 (IRE1). They can activate the UPR in cells which, results in downstream changes to gene expression (Schröder & Kaufman, 2005). It has been reported that upon infection with *Chlamydiales* organism *Simkania negevensis*—that associates with host ER—the UPR is induced, and this process is suppressed by the pathogen for optimal growth. The mechanism by which this is achieved remains unknown. However, increased treatment with ER-stress inducing drugs decreases bacterial vacuole size and count (Mehlitz et al., 2014). Moreover, upon infection with *Toxoplasma* it was reported that several branches of the UPR are upregulated during infection, and this process supports migration of infected cells (Augusto et al., 2020). It remains to be tested however whether upregulation of UPR is an initial response by the host cell to inhibit growth that is later subverted by *Toxoplasma*.

4.3 Why are host MCS proteins targeted by pathogens?

As alluded to previously in most cases pathogens form MCS with host ER or host mitochondria. Furthermore, it is increasingly evident that similar sets of proteins are involved in this process. For MCS with ER, VAP proteins seem to be the universal choice by both host organelles and pathogens (Vormittag, Ende, et al., 2023a; H. Wu et al., 2018). Additionally, CERT and mitochondrial protein TOM70, are involved in mediating several MCS across species (Eisenberg-Bord et al., 2021; Filadi et al., 2018; Jiang et al., 2020; Vormittag, Ende, et al., 2023a; H. Wu et al., 2018). By targeting host proteins with key functions, pathogens can either exploit these functions for their benefit or subvert them for being used by the host. With VAPs and CERT, one obvious explanation is their ability to enable lipid transfer, which is lucrative for pathogen growth (Vormittag, Ende, et al., 2023a). In addition, recent work revealed that VAPs contribute to autophagy in cells by stabilizing the protein complex that supports autophagosome formation. (Scorrano et al., 2019; H. Wu et al., 2018). *Salmonella typhimurium* and *Mycobacterium tuberculosis* are two key examples of pathogens targeted for elimination via the process of autophagy, in

a process called xenophagy (Birmingham et al., 2006; J. Huang & Brumell, 2014). By sequestering MCS proteins such as VAPs, it is tempting to speculate that pathogens may decrease the pool of this protein available for cellular functions such as autophagy and benefit their survival. Most mitochondrial proteins are encoded in the cytoplasm and need to be imported in the mitochondria (Schmidt et al., 2010). TOM70 is important for mitochondrial protein import (Kreimendahl & Rassow, 2020). Thus, by targeting this protein pathogens may impede mitochondrial import and perturb mitochondrial homeostasis. Indeed, upon infection with *Toxoplasma* TOM70 is completely sequestered at the PVM via interaction with TgMAF1 (X. Li et al., 2022). This interaction impairs TOM70 import function and induces the remodelling of the outer mitochondrial membrane that further destabilizes mitochondrial integrity (X. Li et al., 2022).

4.4 Tug of war- hERa versus HMA

My data reveals that at early stages around 3-4 hours post infection (hpi), in the absence of the tethers such TgROP1 and TgMAF1 that tether the ER and the mitochondria, respectively, or host VAPS there is increased association with the other organelle. This poses the following questions: is ER and mitochondrial association with the parasite vacuole redundant? Is it simply a matter of space available for association with the PVM or do these organelles actively compete for binding with the parasite membrane? A simple experiment to understand this would be to engineer Type II parasites to express TgMAF1 and assess whether it is sufficient to displace ER-*Toxoplasma* contacts at early stages of infection.

To increase our understanding of these processes it will be important to understand whether host organellar-pathogen vacuole association is an active process. In a broader context- who is approaching whom during infection? Does *Toxoplasma* recruit host organelles? Or is it possible that host organelles traffic to the pathogen vacuole? If so, then how do they sense the presence of the parasite (Medeiros et al., 2021; Mehra & Pernas, 2023; Pernas, 2019)? In fact, for most host pathogen interactions, these questions remain unexplored. In this context, several scenarios emerge. Mitochondria are known to traffic within cells—for example mitochondria travel to the leading edge of cancer cells

to provide the ATP for migration (Cunniff et al., 2016). This suggests that to actively travel the organelles need a motive. Indeed, mitochondria are producers of cellular reactive oxygen species (ROS), and it was proposed that upon infection with pathogen *Staphylococcus aureaus*, ER-stress induced mitochondrial ROS is delivered via mitochondrial derived vesicles to the pathogen (Abuaita et al., 2018). This allows one to speculate that ER and mitochondria may actively seek proximity to pathogens to execute antimicrobial defenses. It was reported that upon treating *Toxoplasma*-infected cells with nocodazole, a microtubule depolymerizing drug, there was reduced HMA but hERA remained intact (Sinai et al., 1997) This suggests that mitochondrial positioning is influenced by host microtubules during infection but leaves the question of how ER targets *Toxoplasma* completely open-ended. Alternatively, given the versatile role of both these organelles in a cell, it can be envisioned that the pathogens would greatly benefit from interacting with these organelles and this implies a pro-parasite motive. While TgROP1 and TgMAF1 are the tethers that anchor host organelles to the PV, it is unknown whether *Toxoplasma* secretes additional effector proteins that facilitate the initial recruitment of host organelles, positioning them for subsequent tethering. Investigating this further will provide insights into the mechanisms that govern host-*Toxoplasma* interactions.

4.5 Can our host-microbe sensor be used to study MCS with other pathogens?

Here, I present a methodology that was applied to study both the mitochondria-*Toxoplasma* and ER-*Toxoplasma* MCS. Furthermore, I explored the versatility of this system with CRISPR libraries encompassing either genome-wide host sgRNAs or *Toxoplasma* effector protein targeted sgRNAs. A caveat of split-GFP systems is the forced reconstitution of GFP which stabilizes MCS formation (Scorrano et al., 2019). I tested MCS formation with the split-GFP system in the absence of the mitochondrial tethers to establish the system. Our data reveals upto 10-15% of forced MCS formation at later time points of infection with the mitochondrial split-GFP system. In future experiments, to

further characterize the ER-microbe split-GFP system we could express the split-GFP constructs in Δ*rop1* parasites and assess MCS formation.

For several intracellular microbes, mitochondria and ER are the two main organelles that establish host-pathogen MCS and yet in most cases either the pathogen or host tether remains unknown (Medeiros et al., 2021; Vormittag, Ende, et al., 2023a). Therefore, it is interesting to speculate that this system can be used to investigate the molecular tethers for other pathogens as well. An easy adaptation of the system can be envisioned with the bacterial species *Chlamydia*. Akin to *Toxoplasma*, *Chlamydia* exhibits strain-specificity in mediating HMA (Matsumoto et al., 1991). Therefore, the system can be easily adapted there utilizing this specificity.

For future adaptation and use in a screening approach of the host-microbe split-GFP systems it is important to keep in mind that if the MCS is characterized by redundancy, then the system will not be able to distinguish if only single genes are targeted. For example, the *Toxoplasma*-mitochondria MCS are mediated by single tethers and hence the system faithfully recapitulates the biology (Blank et al., 2021; X. Li et al., 2022; Pernas et al., 2014). In contrast, my work indicates that the *Toxoplasma*-ER MCS are facilitated by both VAPA and VAPB. This suggests that a similar host screen as was performed for the mitochondrial system would not work where only single genes are targeted. However, with the advent of CRISPR technologies utilizing a sgRNA library that targets paralogs will easily circumvent this limitation (Bock et al., 2022).

Overall, my study of the interaction between eukaryotic pathogen *Toxoplasma* and ER demonstrates that TgROP1 and VAPA and VAPB are required for establishing these MCS. Given the importance of host pathogen interactions in predicting the outcome of any infection, the field of trans-kingdom contact sites presents a new way to think about host defense and microbial exploitation of host organelles and pathways. From the pathogen perspective host-pathogen MCS either shields from immune detection or allows the siphoning of nutrients that supports pathogen growth (Vormittag, Ende, et al., 2023a). Alternatively, these MCS may be an avenue for the host to defend against microbes (Pernas et al., 2018). Formation of MCS is growing itself a niche in the field of host-

pathogen immunity. Studying this gives us a way to better understand co-evolution and adaptation of microbial and host defense strategies. Future work is required to delineate the precise functions mediated by the various host-pathogen membrane contact sites and their potential therapeutic implications, offering new avenues for intervention against pathogens.

5 List of abbreviations

ACBD5	Acyl-coenzyme A–binding domain protein 5
ALS	Amyotrophic lateral sclerosis
ANOVA	Analysis of variance
APEX	Ascorbate peroxidase
ATF6	Activating transcription factor 6
ATG2	Autophagy related gene 2
ATP	Adenosine triphosphate
BiC	Bimolecular complementation
BioID	Biotin identification
BMDM	Bone marrow-derived macrophages
BSA	Bovine serum albumin
CAMLG	Calcium modulating ligand
CAT	Chloramphenicol acetyltransferase
CERT	Ceramide transfer protein
cGAS	Cyclic GMP-AMP synthase
C. caviae	*Chlamydia caviae*
C. trachomatis	*Chlamydia trachomatis*
CRISPR	Clustered regularly interspaced short palindromic repeats
cDNA	Complementary deoxyribonucleic acid
C. burnetii	*Coxiella-burnetii*
ddFP	Dimerization dependent fluorescent protein
DRP1	Dynamin-related protein 1
E-Syt1	Extended synaptotagmin 1
EhSSP1	*E. hellem* sporoplasm surface protein 1
ELM	Eukaryotic linear motif
EM	Electron microscopy
ER	Endoplasmic reticulum
ERMES	ER-mitochondria encounter structure
ET	Electron tomography
FA	Fatty acid
FACS	Fluorescence-activated cell sorting
FBS	Fetal Bovine Serum
FFAT	Two phenylalanines (FF) in an acidic tract (AT)
FIB-SEM	Focused ion beam-scanning EM
FRET	Fluorescence resonance energy transfer
gDNA	Genomic deoxyribonucleic acid
GET4	Guided entry of tail anchored protein factor 4
GFP	Green fluorescent protein
GRP75	Glucose-regulated protein 75
hERa	Host ER association
HFF	Human foreskin fibroblasts
HMA	Host mitochondrial association
HXGPRT	Hypoxanthine-xanthine-guanine phosphoribosyl transferase
IFN	Interferon

Inc	Inclusion proteins
IP3R	Inositol-1,4,5-trisphosphate receptor
KO	Knockout
L. pneumophila	*Legionella pneumophila*
LCV	*L. pneumophila* -containing vacuole
LCVM	*L. pneumophila*-containing vacuole membrane
LTP	Lipid transfer proteins
MAM	Mitochondria associated membrane
MCS	Membrane contact sites
MCU	Mitochondrial Ca^{2+} uniporter
MFN	Mitofusin
Mmr1	Mitochondrial Myo2 receptor-related protein 1
MOSPD2	Motile sperm domain-containing protein 2
MPA	Mycophenolic Acid
MSP	Major sperm protein
NaCl	Sodium Chloride
NSP	Nonstructural protein
N-terminal	Amino terminal
OMM	Outer mitochondrial membrane
ORAI1	Calcium release-activated calcium channel protein 1
ORP	Oxysterol binding protein-related protein
ORP1L	Oxysterol binding protein-related protein 1 Long
OSBP	Oxysterol binding protein
OSBPL	Oxysterol binding protein-like protein
PBS	Phosphate buffered saline
PCR	Polymerase chain reaction
PFA	Paraformaldehyde
PH	Pleckstrin homology
PI	Phosphatidylinositides
PI4P	Phosphatidylinositol-4-phosphate
PLA	Proximity ligation assay
PM	Plasma membrane
PV	Parasite vacuole
PVM	Parasitophorous vacuole membrane
RE	Restriction enzymes
R. parkeri	*Rickettsia parkeri*
ROS	Reactive oxygen species
RRA	Robust rank aggregation
SAG1	Surface antigen one
SARS- CoV-2	Severe acute respiratory syndrome coronavirus 2
SERCA	Sarcoplasmic reticulum (SR)/ER Ca2+–adenosine triphosphatase
sgRNA	Single-guide ribonucleic acid
SD	Standard deviation
SOCE	Store-operated Ca^{2+} entry
SPOT	Structures positive for outer mitochondrial membrane
StART	Steroidogenic acute regulatory transfer
STIM1	Stromal interaction molecule 1

STING	Stimulator of interferon (IFN) genes
TgGRA	*Toxoplasma gondii* dense granule proteins
TgRON	*Toxoplasma gondii* rhoptry neck proteins
TgROP	*Toxoplasma gondii* rhoptry bulb proteins
TM	Transmembrane domain
TOM40	Translocase of outer mitochondrial membrane 40
TOM70	Translocase of the outer membrane 70
Toxoplasma	*Toxoplasma gondii*
UPR	Unfolded protein response
VAP	Vesicle-associated membrane protein (VAMP)-associated protein
VDAC	Voltage-dependent anion channel
VPS13	Vacuolar protein sorting 13
WT	Wild-type

Abbreviations of units

bp	Base pair
hpi	Hours post infection
kDa	Kilo Dalton
min	Minutes
nm	Nanometer
rpm	Rounds per minute
µg	Microgram
µM	Micrometer

6 References

Abuaita, B. H., Schultz, T. L., & O'Riordan, M. X. (2018). Mitochondria-Derived Vesicles Deliver Antimicrobial Reactive Oxygen Species to Control Phagosome-Localized Staphylococcus aureus. *Cell Host and Microbe*, *24*(5). https://doi.org/10.1016/j.chom.2018.10.005

Acevedo-Sánchez, Y., Woida, P. J., Anderson, C., Kraemer, S., & Lamason, R. L. (2025). Rickettsia parkeri forms extensive, stable contacts with the rough endoplasmic reticulum. *The Journal of Cell Biology*, *224*(3). https://doi.org/10.1083/jcb.202406122

Adomako-Ankomah, Y., English, E. D., Danielson, J. J., Pernas, L. F., Parker, M. L., Boulanger, M. J., & Boyle, J. P. (2016). Host mitochondrial association evolved in the human parasite Toxoplasma gondii via neofunctionalization of a gene duplicate. *Genetics*, *203*(1). https://doi.org/10.1534/genetics.115.186270

Agaisse, H., & Derré, I. (2014). Expression of the effector protein IncD in Chlamydia trachomatis mediates recruitment of the lipid transfer protein CERT and the endoplasmic reticulum-resident protein VAPB to the inclusion membrane. *Infection and Immunity*, *82*(5). https://doi.org/10.1128/IAI.01530-14

Agaisse, H., & Derré, I. (2015). STIM1 is a novel component of ER-Chlamydia trachomatis inclusion membrane contact sites. *PLoS ONE*, *10*(4). https://doi.org/10.1371/journal.pone.0125671

Alexander, D. L., Mital, J., Ward, G. E., Bradley, P., & Boothroyd, J. C. (2005). Identification of the moving junction complex of Toxoplasma gondii: A collaboration between distinct secretory organelles. *PLoS Pathogens*, *1*(2). https://doi.org/10.1371/journal.ppat.0010017

Amos, B., Aurrecoechea, C., Barba, M., Barreto, A., Basenko, E. Y., Bażant, W., Belnap, R., Blevins, A. S., Böhme, U., Brestelli, J., Brunk, B. P., Caddick, M., Callan, D., Campbell, L., Christensen, M. B., Christophides, G. K., Crouch, K., Davis, K., Debarry, J., … Zheng, J. (2022). VEuPathDB: The eukaryotic pathogen, vector and host bioinformatics resource center. *Nucleic Acids Research*, *50*(D1). https://doi.org/10.1093/nar/gkab929

Andrews, S., & others. (2019). FastQC: a quality control tool for high throughput sequence data. 2010. *Https://Www.Bioinformatics.Babraham.Ac.Uk/Projects/Fastqc/*.

Augusto, L., Martynowicz, J., Amin, P. H., Alakhras, N. S., Kaplan, M. H., Wek, R. C., & Sullivan, W. J. (2020). Toxoplasma gondii co-opts the unfolded protein response to enhance migration and dissemination of infected host cells. *MBio*, *11*(4). https://doi.org/10.1128/mBio.00915-20

Barazzuol, L., Giamogante, F., & Calì, T. (2021). Mitochondria Associated Membranes (MAMs): Architecture and physiopathological role. *Cell Calcium*, *94*. https://doi.org/10.1016/j.ceca.2020.102343

Barylyuk, K., Koreny, L., Ke, H., Butterworth, S., Crook, O. M., Lassadi, I., Gupta, V., Tromer, E., Mourier, T., Stevens, T. J., Breckels, L. M., Pain, A., Lilley, K. S., & Waller, R. F. (2020). A Comprehensive Subcellular Atlas of the Toxoplasma Proteome via hyperLOPIT Provides Spatial Context for Protein Functions. *Cell Host and Microbe*, *28*(5). https://doi.org/10.1016/j.chom.2020.09.011

Bateman, A., Martin, M. J., Orchard, S., Magrane, M., Ahmad, S., Alpi, E., Bowler-Barnett, E. H., Britto, R., Bye-A-Jee, H., Cukura, A., Denny, P., Dogan, T., Ebenezer, T. G., Fan, J., Garmiri, P., da Costa Gonzales, L. J., Hatton-Ellis, E., Hussein, A., Ignatchenko, A., … Zhang, J. (2023). UniProt: the Universal Protein Knowledgebase in 2023. *Nucleic Acids Research*, *51*(D1). https://doi.org/10.1093/nar/gkac1052

Baughman, J. M., Perocchi, F., Girgis, H. S., Plovanich, M., Belcher-Timme, C. A., Sancak, Y., Bao, X. R., Strittmatter, L., Goldberger, O., Bogorad, R. L., Koteliansky, V., & Mootha, V. K. (2011). Integrative genomics identifies MCU as an essential component of the mitochondrial calcium uniporter. *Nature*, *476*(7360). https://doi.org/10.1038/nature10234

Behnke, M. S., Fentress, S. J., Mashayekhi, M., Li, L. X., Taylor, G. A., & Sibley, L. D. (2012). The Polymorphic Pseudokinase ROP5 Controls Virulence in Toxoplasma gondii by Regulating the Active Kinase ROP18. *PLoS Pathogens*, *8*(11). https://doi.org/10.1371/journal.ppat.1002992

BERNHARD, W., & ROUILLER, C. (1956). Close topographical relationship between mitochondria and ergastoplasm of liver cells in a definite phase of cellular activity. *The Journal of Biophysical and Biochemical Cytology*, *2*(4, Suppl). https://doi.org/10.1083/jcb.2.4.73

Besteiro, S., Dubremetz, J. F., & Lebrun, M. (2011). The moving junction of apicomplexan parasites: A key structure for invasion. *Cellular Microbiology*, *13*(6). https://doi.org/10.1111/j.1462-5822.2011.01597.x

Birmingham, C. L., Smith, A. C., Bakowski, M. A., Yoshimori, T., & Brumell, J. H. (2006). Autophagy controls Salmonella infection in response to damage to the Salmonella-containing vacuole. *Journal of Biological Chemistry*, *281*(16). https://doi.org/10.1074/jbc.M509157200

Blader, I. J., Coleman, B. I., Chen, C. T., & Gubbels, M. J. (2015). Lytic Cycle of Toxoplasma gondii: 15 Years Later. In *Annual Review of Microbiology* (Vol. 69, Issue 1). https://doi.org/10.1146/annurev-micro-091014-104100

Blank, M. L., Xia, J., Morcos, M. M., Sun, M., Cantrell, P. S., Liu, Y., Zeng, X., Powell, C. J., Yates, N., Boulanger, M. J., & Boyle, J. P. (2021). Toxoplasma gondii association with host mitochondria requires key mitochondrial protein import machinery. *Proceedings of the National Academy of Sciences of the United States of America*, *118*(12). https://doi.org/10.1073/pnas.2013336118

Bock, C., Datlinger, P., Chardon, F., Coelho, M. A., Dong, M. B., Lawson, K. A., Lu, T., Maroc, L., Norman, T. M., Song, B., Stanley, G., Chen, S., Garnett, M., Li, W., Moffat, J., Qi, L. S., Shapiro, R. S., Shendure, J., Weissman, J. S., & Zhuang, X. (2022). High-content CRISPR screening. In *Nature Reviews Methods Primers* (Vol. 2, Issue 1). https://doi.org/10.1038/s43586-021-00093-4

Bougdour, A., Durandau, E., Brenier-Pinchart, M. P., Ortet, P., Barakat, M., Kieffer, S., Curt-Varesano, A., Curt-Bertini, R. L., Bastien, O., Coute, Y., Pelloux, H., & Hakimi, M. A. (2013). Host cell subversion by Toxoplasma GRA16, an exported dense granule protein that targets the host cell nucleus and alters gene expression. *Cell Host and Microbe*, *13*(4). https://doi.org/10.1016/j.chom.2013.03.002

Bougdour, A., Tardieux, I., & Hakimi, M. A. (2014). Toxoplasma exports dense granule proteins beyond the vacuole to the host cell nucleus and rewires the host genome expression. *Cellular Microbiology*, *16*(3). https://doi.org/10.1111/cmi.12255

Bradley, P. J., Ward, C., Cheng, S. J., Alexander, D. L., Coller, S., Coombs, G. H., Dunn, J. D., Ferguson, D. J., Sanderson, S. J., Wastling, J. M., & Boothroyd, J. C. (2005). Proteomic analysis of rhoptry organelles reveals many novel constituents for host-parasite interactions in Toxoplasma gondii. *Journal of Biological Chemistry*, *280*(40). https://doi.org/10.1074/jbc.M504158200

Braun, L., Brenier-Pinchart, M. P., Yogavel, M., Curt-Varesano, A., Curt-Bertini, R. L., Hussain, T., Kieffer-Jaquinod, S., Coute, Y., Pelloux, H., Tardieux, I., Sharma, A., Belrhali, H., Bougdour, A., & Hakimi, M. A. (2013). A Toxoplasma dense granule protein, GRA24, modulates the early immune response to infection by promoting a direct and sustained host p38 MAPK activation. *Journal of Experimental Medicine*, *210*(10). https://doi.org/10.1084/jem.20130103

Butterworth, S., Kordova, K., Chandrasekaran, S., Thomas, K. K., Torelli, F., Lockyer, E. J., Edwards, A., Goldstone, R., Koshy, A. A., & Treeck, M. (2023). High-throughput identification of Toxoplasma gondii effector proteins that target host cell transcription. *Cell Host and Microbe*, *31*(10). https://doi.org/10.1016/j.chom.2023.09.003

Butterworth, S., Torelli, F., Lockyer, E. J., Wagener, J., Song, O. R., Broncel, M., Russell, M. R. G., Moreira-Souza, A. C. A., Young, J. C., & Treeck, M. (2022). Toxoplasma gondii virulence factor ROP1 reduces parasite susceptibility to murine and human innate immune restriction. *PLoS Pathogens*, *18*(12). https://doi.org/10.1371/journal.ppat.1011021

Cabantous, S., Terwilliger, T. C., & Waldo, G. S. (2005). Protein tagging and detection with engineered self-assembling fragments of green fluorescent protein. *Nature Biotechnology*, *23*(1). https://doi.org/10.1038/nbt1044

Capitanio, C., Bieber, A., & Wilfling, F. (2023). How Membrane Contact Sites Shape the Phagophore. In *Contact* (Vol. 6). https://doi.org/10.1177/25152564231162495

Carruthers, V. B. (2002). Host cell invasion by the opportunistic pathogen Toxoplasma gondii. In *Acta Tropica* (Vol. 81, Issue 2). https://doi.org/10.1016/S0001-706X(01)00201-7

Charron, A. J., & Sibley, L. D. (2002). Host cells: Mobilizable lipid resources for the intracellular parasite Toxoplasma gondii. *Journal of Cell Science*, *115*(15). https://doi.org/10.1242/jcs.115.15.3049

Cheng, Z., Dai, T., He, X., Zhang, Z., Xie, F., Wang, S., Zhang, L., & Zhou, F. (2020). The interactions between cGAS-STING pathway and pathogens. In *Signal Transduction and Targeted Therapy* (Vol. 5, Issue 1). https://doi.org/10.1038/s41392-020-0198-7

Cheong, H. C., Lee, C. Y. Q., Cheok, Y. Y., Tan, G. M. Y., Looi, C. Y., & Wong, W. F. (2019). Chlamydiaceae: Diseases in primary hosts and zoonosis. In *Microorganisms* (Vol. 7, Issue 5). https://doi.org/10.3390/microorganisms7050146

Cho, N. H., Cheveralls, K. C., Brunner, A. D., Kim, K., Michaelis, A. C., Raghavan, P., Kobayashi, H., Savy, L., Li, J. Y., Canaj, H., Kim, J. Y. S., Stewart, E. M., Gnann, C., McCarthy, F., Cabrera, J. P., Brunetti, R. M., Chhun, B. B., Dingle, G., Hein, M. Y., … Leonetti, M. D. (2022). OpenCell: Endogenous tagging for the cartography of human cellular organization. *Science*, *375*(6585). https://doi.org/10.1126/science.abi6983

Chung, J., Torta, F., Masai, K., Lucast, L., Czapla, H., Tanner, L. B., Narayanaswamy, P., Wenk, M. R., Nakatsu, F., & De Camilli, P. (2015). PI4P/phosphatidylserine

countertransport at ORP5- and ORP8-mediated ER - Plasma membrane contacts. *Science*, *349*(6246). https://doi.org/10.1126/science.aab1370

Cieri, D., Vicario, M., Giacomello, M., Vallese, F., Filadi, R., Wagner, T., Pozzan, T., Pizzo, P., Scorrano, L., Brini, M., & Calì, T. (2018). SPLICS: A split green fluorescent protein-based contact site sensor for narrow and wide heterotypic organelle juxtaposition. *Cell Death and Differentiation*, *25*(6). https://doi.org/10.1038/s41418-017-0033-z

Clapham, D. E. (2007). Calcium Signaling. In *Cell* (Vol. 131, Issue 6). https://doi.org/10.1016/j.cell.2007.11.028

Clough, B., & Frickel, E. M. (2017). The Toxoplasma Parasitophorous Vacuole: An Evolving Host–Parasite Frontier. In *Trends in Parasitology* (Vol. 33, Issue 6). https://doi.org/10.1016/j.pt.2017.02.007

Cook, K. C., Tsopurashvili, E., Needham, J. M., Thompson, S. R., & Cristea, I. M. (2022). Restructured membrane contacts rewire organelles for human cytomegalovirus infection. *Nature Communications*, *13*(1). https://doi.org/10.1038/s41467-022-32488-6

Costello, J. L., Castro, I. G., Hacker, C., Schrader, T. A., Metz, J., Zeuschner, D., Azadi, A. S., Godinho, L. F., Costina, V., Findeisen, P., Manner, A., Islinger, M., & Schrader, M. (2017). ACBD5 and VAPB mediate membrane associations between peroxisomes and the ER. *Journal of Cell Biology*, *216*(2). https://doi.org/10.1083/jcb.201607055

Csordás, G., Várnai, P., Golenár, T., Roy, S., Purkins, G., Schneider, T. G., Balla, T., & Hajnóczky, G. (2010). Imaging Interorganelle Contacts and Local Calcium Dynamics at the ER-Mitochondrial Interface. *Molecular Cell*, *39*(1). https://doi.org/10.1016/j.molcel.2010.06.029

Cunniff, B., McKenzie, A. J., Heintz, N. H., & Howe, A. K. (2016). AMPK activity regulates trafficking of Mitochondria to the leading edge during cell migration and matrix invasion. *Molecular Biology of the Cell*, *27*(17). https://doi.org/10.1091/mbc.E16-05-0286

Dabrowski, R., Tulli, S., & Graef, M. (2023). Parallel phospholipid transfer by Vps13 and Atg2 determines autophagosome biogenesis dynamics. *Journal of Cell Biology*, *222*(7). https://doi.org/10.1083/jcb.202211039

Das, A., Nag, S., Mason, A. B., & Barroso, M. M. (2016). Endosome-mitochondria interactions are modulated by iron release from transferrin. *Journal of Cell Biology*, *214*(7). https://doi.org/10.1083/jcb.201602069

Delorme-Walker, V., Abrivard, M., Lagal, V., Anderson, K., Perazzi, A., Gonzalez, V., Page, C., Chauvet, J., Ochoa, W., Volkmann, N., Hanein, D., & Tardieux, I. (2012). Toxofilin upregulates the host cortical actin cytoskeleton dynamics, facilitating Toxoplasma invasion. *Journal of Cell Science*, *125*(18). https://doi.org/10.1242/jcs.103648

Derré, I., Pypaert, M., Dautry-Varsat, A., & Agaisse, H. (2007). RNAi screen in Drosophila cells reveals the involvement of the tom complex in Chlamydia infection. *PLoS Pathogens*, *3*(10). https://doi.org/10.1371/journal.ppat.0030155

Derré, I., Swiss, R., & Agaisse, H. (2011). The lipid transfer protein CERT interacts with the Chlamydia inclusion protein IncD and participates to ER-Chlamydia inclusion membrane contact sites. *PLoS Pathogens*, *7*(6). https://doi.org/10.1371/journal.ppat.1002092

Doench, J. G., Fusi, N., Sullender, M., Hegde, M., Vaimberg, E. W., Donovan, K. F., Smith, I., Tothova, Z., Wilen, C., Orchard, R., Virgin, H. W., Listgarten, J., & Root, D. E. (2016). Optimized sgRNA design to maximize activity and minimize off-target

effects of CRISPR-Cas9. *Nature Biotechnology*, *34*(2). https://doi.org/10.1038/nbt.3437

Dong, R., Saheki, Y., Swarup, S., Lucast, L., Harper, J. W., & De Camilli, P. (2016). Endosome-ER Contacts Control Actin Nucleation and Retromer Function through VAP-Dependent Regulation of PI4P. *Cell*, *166*(2). https://doi.org/10.1016/j.cell.2016.06.037

Dragan, A. L., & Voth, D. E. (2020). Coxiella burnetii: international pathogen of mystery. In *Microbes and Infection* (Vol. 22, Issue 3). https://doi.org/10.1016/j.micinf.2019.09.001

Dubremetz, J. F. (2007). Rhoptries are major players in Toxoplasma gondii invasion and host cell interaction. In *Cellular Microbiology* (Vol. 9, Issue 4). https://doi.org/10.1111/j.1462-5822.2007.00909.x

Eisenberg-Bord, M., Shai, N., Schuldiner, M., & Bohnert, M. (2016). A Tether Is a Tether Is a Tether: Tethering at Membrane Contact Sites. In *Developmental Cell* (Vol. 39, Issue 4). https://doi.org/10.1016/j.devcel.2016.10.022

Eisenberg-Bord, M., Zung, N., Collado, J., Drwesh, L., Fenech, E. J., Fadel, A., Dezorella, N., Bykov, Y. S., Rapaport, D., Fernandez-Busnadiego, R., & Schuldiner, M. (2021). CNM1 mediates nucleus–mitochondria contact site formation in response to phospholipid levels. *Journal of Cell Biology*, *220*(11). https://doi.org/10.1083/jcb.202104100

Elbaz-Alon, Y., Eisenberg-Bord, M., Shinder, V., Stiller, S. B., Shimoni, E., Wiedemann, N., Geiger, T., & Schuldiner, M. (2015). Lam6 Regulates the Extent of Contacts between Organelles. *Cell Reports*, *12*(1). https://doi.org/10.1016/j.celrep.2015.06.022

Elwell, C. A., Jiang, S., Kim, J. H., Lee, A., Wittmann, T., Hanada, K., Melancon, P., & Engel, J. N. (2011). Chlamydia trachomatis co-opts gbf1 and cert to acquire host sphingomyelin for distinct roles during intracellular development. *PLoS Pathogens*, *7*(9). https://doi.org/10.1371/journal.ppat.1002198

Escoll, P., Song, O. R., Viana, F., Steiner, B., Lagache, T., Olivo-Marin, J. C., Impens, F., Brodin, P., Hilbi, H., & Buchrieser, C. (2017). Legionella pneumophila Modulates Mitochondrial Dynamics to Trigger Metabolic Repurposing of Infected Macrophages. *Cell Host and Microbe*, *22*(3). https://doi.org/10.1016/j.chom.2017.07.020

Etheridge, R. D., Alaganan, A., Tang, K., Lou, H. J., Turk, B. E., & Sibley, L. D. (2014). The Toxoplasma pseudokinase ROP5 forms complexes with ROP18 and ROP17 kinases that synergize to control acute virulence in mice. *Cell Host and Microbe*, *15*(5). https://doi.org/10.1016/j.chom.2014.04.002

Evans, R., O'Neill, M., Pritzel, A., Antropova, N., Senior, A., Green, T., Žídek, A., Bates, R., Blackwell, S., Yim, J., Ronneberger, O., Bodenstein, S., Zielinski, M., Bridgland, A., Potapenko, A., Cowie, A., Tunyasuvunakool, K., Jain, R., Clancy, E., … Hassabis, D. (2022). Protein complex prediction with AlphaFold-Multimer. *BioRxiv*.

Feng, S., Sekine, S., Pessino, V., Li, H., Leonetti, M. D., & Huang, B. (2017). Improved split fluorescent proteins for endogenous protein labeling. *Nature Communications*, *8*(1). https://doi.org/10.1038/s41467-017-00494-8

Fentress, S. J., Behnke, M. S., Dunay, I. R., Mashayekhi, M., Rommereim, L. M., Fox, B. A., Bzik, D. J., Taylor, G. A., Turk, B. E., Lichti, C. F., Townsend, R. R., Qiu, W., Hui, R., Beatty, W. L., & Sibley, L. D. (2010). Phosphorylation of immunity-related GTPases by a toxoplasma gondii-secreted kinase promotes macrophage survival and

virulence. *Cell Host and Microbe*, *8*(6). https://doi.org/10.1016/j.chom.2010.11.005

Ferrel, A., Romano, J., Panas, M. W., Coppens, I., & Boothroyd, J. C. (2023). Host MOSPD2 enrichment at the parasitophorous vacuole membrane varies between Toxoplasma strains and involves complex interactions . *MSphere*, *8*(4). https://doi.org/10.1128/msphere.00670-22

Filadi, R., Leal, N. S., Schreiner, B., Rossi, A., Dentoni, G., Pinho, C. M., Wiehager, B., Cieri, D., Calì, T., Pizzo, P., & Ankarcrona, M. (2018). TOM70 Sustains Cell Bioenergetics by Promoting IP3R3-Mediated ER to Mitochondria Ca2+ Transfer. *Current Biology*, *28*(3). https://doi.org/10.1016/j.cub.2017.12.047

Franco, M., Panas, M. W., Marino, N. D., Lee, M. C. W., Buchholz, K. R., Kelly, F. D., Bednarski, J. J., Sleckman, B. P., Pourmand, N., & Boothroyd, J. C. (2016). A novel secreted protein, MYR1, is central to Toxoplasma's manipulation of host cells. *MBio*, *7*(1). https://doi.org/10.1128/mBio.02231-15

Frénal, K., Dubremetz, J. F., Lebrun, M., & Soldati-Favre, D. (2017). Gliding motility powers invasion and egress in Apicomplexa. In *Nature Reviews Microbiology* (Vol. 15, Issue 11). https://doi.org/10.1038/nrmicro.2017.86

Friedman, J. R., Lackner, L. L., West, M., DiBenedetto, J. R., Nunnari, J., & Voeltz, G. K. (2011). ER tubules mark sites of mitochondrial division. *Science*, *334*(6054). https://doi.org/10.1126/science.1207385

Giordano, F., Saheki, Y., Idevall-Hagren, O., Colombo, S. F., Pirruccello, M., Milosevic, I., Gracheva, E. O., Bagriantsev, S. N., Borgese, N., & De Camilli, P. (2013). XPI(4,5)P2-Dependent and Ca2+-Regulated ER-PM interactions mediated by the extended synaptotagmins. *Cell*, *153*(7). https://doi.org/10.1016/j.cell.2013.05.026

Gold, D. A., Kaplan, A. D., Lis, A., Bett, G. C. L., Rosowski, E. E., Cirelli, K. M., Bougdour, A., Sidik, S. M., Beck, J. R., Lourido, S., Egea, P. F., Bradley, P. J., Hakimi, M. A., Rasmusson, R. L., & Saeij, J. P. J. (2015). The Toxoplasma dense granule proteins GRA17 and GRA23 mediate the movement of small molecules between the host and the parasitophorous vacuole. *Cell Host and Microbe*, *17*(5). https://doi.org/10.1016/j.chom.2015.04.003

Griffith, M. B., Pearce, C. S., & Heaslip, A. T. (2022). Dense granule biogenesis, secretion, and function in Toxoplasma gondii. In *Journal of Eukaryotic Microbiology* (Vol. 69, Issue 6). https://doi.org/10.1111/jeu.12904

GUSTAFSON, P. V., AGAR, H. D., & CRAMER, D. I. (1954). An electron microscope study of Toxoplasma. *The American Journal of Tropical Medicine and Hygiene*, *3*(6). https://doi.org/10.4269/ajtmh.1954.3.1008

Hacker, C., Howell, M., Bhella, D., & Lucocq, J. (2014). Strategies for maximizing ATP supply in the microsporidian Encephalitozoon cuniculi: Direct binding of mitochondria to the parasitophorous vacuole and clustering of the mitochondrial porin VDAC. *Cellular Microbiology*, *16*(4). https://doi.org/10.1111/cmi.12240

Hamasaki, M., Furuta, N., Matsuda, A., Nezu, A., Yamamoto, A., Fujita, N., Oomori, H., Noda, T., Haraguchi, T., Hiraoka, Y., Amano, A., & Yoshimori, T. (2013). Autophagosomes form at ER-mitochondria contact sites. *Nature*, *495*(7441). https://doi.org/10.1038/nature11910

Han, B., Ma, Y., Tu, V., Tomita, T., Mayoral, J., Williams, T., Horta, A., Huang, H., & Weissa, L. M. (2019). Microsporidia interact with host cell mitochondria via

voltage-dependent anion channels using sporoplasm surface protein 1. *MBio*, *10*(4). https://doi.org/10.1128/mBio.01944-19

Hanada, K., Kumagai, K., Yasuda, S., Miura, Y., Kawano, M., Fukasawa, M., & Nishijima, M. (2003). Molecular machinery for non-vesicular trafficking of ceramide. *Nature*, *426*(6968). https://doi.org/10.1038/nature02188

Helle, S. C. J., Kanfer, G., Kolar, K., Lang, A., Michel, A. H., & Kornmann, B. (2013). Organization and function of membrane contact sites. In *Biochimica et Biophysica Acta - Molecular Cell Research* (Vol. 1833, Issue 11). https://doi.org/10.1016/j.bbamcr.2013.01.028

Horwitz, M. A. (1983). The legionnaires' disease bacterium (legionella pneumophila) inhibits phagosome-lysosome fusion in human monocytes. *Journal of Experimental Medicine*, *158*(6). https://doi.org/10.1084/jem.158.6.2108

Howe, D. K., & Sibley, L. D. (1995). Toxoplasma gondii comprises three clonal lineages: Correlation of parasite genotype with human disease. *Journal of Infectious Diseases*, *172*(6). https://doi.org/10.1093/infdis/172.6.1561

Hu, K., Mann, T., Striepen, B., Beckers, C. J. M., Roos, D. S., & Murray, J. M. (2002). Daughter cell assembly in the protozoan parasite Toxoplasma gondii. *Molecular Biology of the Cell*, *13*(2). https://doi.org/10.1091/mbc.01-06-0309

Huang, J., & Brumell, J. H. (2014). Bacteria-autophagy interplay: A battle for survival. In *Nature Reviews Microbiology* (Vol. 12, Issue 2). https://doi.org/10.1038/nrmicro3160

Huang, X., Jiang, C., Yu, L., & Yang, A. (2020). Current and Emerging Approaches for Studying Inter-Organelle Membrane Contact Sites. In *Frontiers in Cell and Developmental Biology* (Vol. 8). https://doi.org/10.3389/fcell.2020.00195

Hung, V., Lam, S. S., Udeshi, N. D., Svinkina, T., Guzman, G., Mootha, V. K., Carr, S. A., & Ting, A. Y. (2017). Proteomic mapping of cytosol-facing outer mitochondrial and ER membranes in living human cells by proximity biotinylation. *ELife*, *6*. https://doi.org/10.7554/eLife.24463

Huttlin, E. L., Ting, L., Bruckner, R. J., Gebreab, F., Gygi, M. P., Szpyt, J., Tam, S., Zarraga, G., Colby, G., Baltier, K., Dong, R., Guarani, V., Vaites, L. P., Ordureau, A., Rad, R., Erickson, B. K., Wühr, M., Chick, J., Zhai, B., … Gygi, S. P. (2015). The BioPlex Network: A Systematic Exploration of the Human Interactome. *Cell*, *162*(2). https://doi.org/10.1016/j.cell.2015.06.043

James, C., & Kehlenbach, R. H. (2021). The interactome of the VAP family of proteins: An overview. In *Cells* (Vol. 10, Issue 7). https://doi.org/10.3390/cells10071780

Janouškovec, J., Horák, A., Oborník, M., Lukeš, J., & Keeling, P. J. (2010). A common red algal origin of the apicomplexan, dinoflagellate, and heterokont plastids. *Proceedings of the National Academy of Sciences of the United States of America*, *107*(24). https://doi.org/10.1073/pnas.1003335107

Janouskovec, J., Paskerova, G. G., Miroliubova, T. S., Mikhaiiov, K. V., Birley, T., Aieoshin, V. V., & Simdyanov, T. G. (2019). Apicomplexan-like parasites are polyphyletic and widely but selectively dependent on cryptic plastid organelles. *ELife*, *8*. https://doi.org/10.7554/eLife.49662

Jiang, H. wei, Zhang, H. nan, Meng, Q. feng, Xie, J., Li, Y., Chen, H., Zheng, Y. xiao, Wang, X. ning, Qi, H., Zhang, J., Wang, P. H., Han, Z. G., & Tao, S. ce. (2020). SARS-CoV-2 Orf9b suppresses type I interferon responses by targeting TOM70. In *Cellular and*

Molecular Immunology (Vol. 17, Issue 9). https://doi.org/10.1038/s41423-020-0514-8

Joiner, K. A., & Roos, D. S. (2002). Secretory traffic in the eukaryotic parasite Toxoplasma gondii: Less is more. In *Journal of Cell Biology* (Vol. 157, Issue 4). https://doi.org/10.1083/jcb.200112144

Jones, T. C., & Hirsch, J. G. (1972). The interaction between toxoplasma gondii and mammalian cells: II. The absence of lysosomal fusion with phagocytic vacuoles containing living parasites. *Journal of Experimental Medicine*, *136*(5). https://doi.org/10.1084/jem.136.5.1173

Justis, A. V., Hansen, B., Beare, P. A., King, K. B., Heinzen, R. A., & Gilk, S. D. (2017). Interactions between the Coxiella burnetii parasitophorous vacuole and the endoplasmic reticulum involve the host protein ORP1L. *Cellular Microbiology*, *19*(1). https://doi.org/10.1111/cmi.12637

Kaiser, S. E., Brickner, J. H., Reilein, A. R., Fenn, T. D., Walter, P., & Brunger, A. T. (2005). Structural basis of FFAT motif-mediated ER targeting. *Structure*, *13*(7). https://doi.org/10.1016/j.str.2005.04.010

Kim, J. Y., Ahn, H. J., Ryu, K. J., & Nam, H. W. (2008). Interaction between parasitophorous vacuolar membrane-associated GRA3 and calcium modulating ligand of host cell endoplasmic reticulum in the parasitism of toxoplasma gondii. *Korean Journal of Parasitology*, *46*(4). https://doi.org/10.3347/kjp.2008.46.4.209

Kim, S., Wong, Y. C., Gao, F., & Krainc, D. (2021). Dysregulation of mitochondria-lysosome contacts by GBA1 dysfunction in dopaminergic neuronal models of Parkinson's disease. *Nature Communications*, *12*(1). https://doi.org/10.1038/s41467-021-22113-3

Kolodziejek, A. M., Altura, M. A., Fan, J., Petersen, E. M., Cook, M., Brzovic, P. S., & Miller, S. I. (2019). Salmonella Translocated Effectors Recruit OSBP1 to the Phagosome to Promote Vacuolar Membrane Integrity. *Cell Reports*, *27*(7). https://doi.org/10.1016/j.celrep.2019.04.021

Kornmann, B., Currie, E., Collins, S. R., Schuldiner, M., Nunnari, J., Weissman, J. S., & Walter, P. (2009). An ER-mitochondria tethering complex revealed by a synthetic biology screen. *Science*, *325*(5939). https://doi.org/10.1126/science.1175088

Kreimendahl, S., & Rassow, J. (2020). The mitochondrial outer membrane protein tom70—mediator in protein traffic, membrane contact sites and innate immunity. In *International Journal of Molecular Sciences* (Vol. 21, Issue 19). https://doi.org/10.3390/ijms21197262

Kumar, M., Michael, S., Alvarado-Valverde, J., Zeke, A., Lazar, T., Glavina, J., Nagy-Kanta, E., Donagh, J. Mac, Kalman, Z. E., Pascarelli, S., Palopoli, N., Dobson, L., Suarez, C. F., Van Roey, K., Krystkowiak, I., Griffin, J. E., Nagpal, A., Bhardwaj, R., Diella, F., … Gibson, T. J. (2024). ELM-the Eukaryotic Linear Motif resource-2024 update. *Nucleic Acids Research*, *52*(D1). https://doi.org/10.1093/nar/gkad1058

Kumar, N., Leonzino, M., Hancock-Cerutti, W., Horenkamp, F. A., Li, P. Q., Lees, J. A., Wheeler, H., Reinisch, K. M., & De Camilli, P. (2018). VPS13A and VPS13C are lipid transport proteins differentially localized at ER contact sites. *Journal of Cell Biology*, *217*(10). https://doi.org/10.1083/JCB.201807019

Lee, C. Y., Hubrich, D., Varga, J. K., Schäfer, C., Welzel, M., Schumbera, E., Djokic, M., Strom, J. M., Schönfeld, J., Geist, J. L., Polat, F., Gibson, T. J., Keller Valsecchi, C. I., Kumar, M., Schueler-Furman, O., & Luck, K. (2024). Systematic discovery of protein

interaction interfaces using AlphaFold and experimental validation. *Molecular Systems Biology*, *20*(2). https://doi.org/10.1038/s44320-023-00005-6

Lee, J. E., Cathey, P. I., Wu, H., Parker, R., & Voeltz, G. K. (2020). Endoplasmic reticulum contact sites regulate the dynamics of membraneless organelles. *Science*, *367*(6477). https://doi.org/10.1126/science.aay7108

Lentini, G., Dos Santos Pacheco, N., & Burleigh, B. A. (2018). Targeting host mitochondria: A role for the Trypanosoma cruzi amastigote flagellum. *Cellular Microbiology*, *20*(2). https://doi.org/10.1111/cmi.12807

Li, W., Xu, H., Xiao, T., Cong, L., Love, M. I., Zhang, F., Irizarry, R. A., Liu, J. S., Brown, M., & Liu, X. S. (2014). MAGeCK enables robust identification of essential genes from genome-scale CRISPR/Cas9 knockout screens. *Genome Biology*, *15*(12). https://doi.org/10.1186/s13059-014-0554-4

Li, X., Straub, J., Medeiros, T. C., Mehra, C., Den Brave, F., Peker, E., Atanassov, I., Stillger, K., Michaelis, J. B., Burbridge, E., Adrain, C., Münch, C., Riemer, J., Becker, T., & Pernas, L. F. (2022). Mitochondria shed their outer membrane in response to infection-induced stress. *Science*, *375*(6577). https://doi.org/10.1126/science.abi4343

Liou, J., Kim, M. L., Won, D. H., Jones, J. T., Myers, J. W., Ferrell, J. E., & Meyer, T. (2005). STIM is a Ca2+ sensor essential for Ca2+-store- depletion-triggered Ca2+ influx. *Current Biology*, *15*(13). https://doi.org/10.1016/j.cub.2005.05.055

Loewen, C. J. R., Roy, A., & Levine, T. P. (2003). A conserved ER targeting motif in three families of lipid binding proteins and in Opi1p binds VAP. *EMBO Journal*, *22*(9). https://doi.org/10.1093/emboj/cdg201

Manford, A. G., Stefan, C. J., Yuan, H. L., MacGurn, J. A., & Emr, S. D. (2012). ER-to-Plasma Membrane Tethering Proteins Regulate Cell Signaling and ER Morphology. *Developmental Cell*, *23*(6). https://doi.org/10.1016/j.devcel.2012.11.004

Marino, N. D., Panas, M. W., Franco, M., Theisen, T. C., Naor, A., Rastogi, S., Buchholz, K. R., Lorenzi, H. A., & Boothroyd, J. C. (2018). Identification of a novel protein complex essential for effector translocation across the parasitophorous vacuole membrane of Toxoplasma gondii. *PLoS Pathogens*, *14*(1). https://doi.org/10.1371/journal.ppat.1006828

Matsumoto, A., Bessho, H., Uehira, K., & Suda, T. (1991). Morphological studies of the association of mitochondria with chlamydial inclusions and the fusion of chlamydial inclusions. *Journal of Electron Microscopy*, *40*(5). https://doi.org/10.1093/oxfordjournals.jmicro.a050908

McCune, B. T., Tang, W., Lu, J., Eaglesham, J. B., Thorne, L., Mayer, A. E., Condiff, E., Nice, T. J., Goodfellow, I., Krezel, A. M., & Virgin, H. W. (2017). Noroviruses co-opt the function of host proteins VAPA and VAPB for replication via a phenylalanine–phenylalanine- acidic-tract-motif mimic in nonstructural viral protein NS1/2. *MBio*, *8*(4). https://doi.org/10.1128/mBio.00668-17

Medeiros, T. C., Mehra, C., & Pernas, L. (2021). Contact and competition between mitochondria and microbes. In *Current Opinion in Microbiology* (Vol. 63). https://doi.org/10.1016/j.mib.2021.07.014

Mehlitz, A., Karunakaran, K., Herweg, J. A., Krohne, G., van de Linde, S., Rieck, E., Sauer, M., & Rudel, T. (2014). The chlamydial organism Simkania negevensis forms ER vacuole contact sites and inhibits ER-stress. *Cellular Microbiology*, *16*(8). https://doi.org/10.1111/cmi.12278

Mehra, C., & Pernas, L. (2023). Contact sites between host organelles and pathogens: boon or bane? *MSphere*, *8*(6). https://doi.org/10.1128/msphere.00448-23

Mesmin, B., Bigay, J., Moser Von Filseck, J., Lacas-Gervais, S., Drin, G., & Antonny, B. (2013). XA four-step cycle driven by PI(4)P hydrolysis directs sterol/PI(4)P exchange by the ER-Golgi Tether OSBP. *Cell*, *155*(4). https://doi.org/10.1016/j.cell.2013.09.056

Michelucci, A., Cordes, T., Ghelfi, J., Pailot, A., Reiling, N., Goldmann, O., Binz, T., Wegner, A., Tallam, A., Rausell, A., Buttini, M., Linster, C. L., Medina, E., Balling, R., & Hiller, K. (2013). Immune-responsive gene 1 protein links metabolism to immunity by catalyzing itaconic acid production. *Proceedings of the National Academy of Sciences of the United States of America*, *110*(19). https://doi.org/10.1073/pnas.1218599110

Mondino, S., Schmidt, S., Rolando, M., Escoll, P., Gomez-Valero, L., & Buchrieser, C. (2020). Legionnaires' Disease: State of the Art Knowledge of Pathogenesis Mechanisms of Legionella. In *Annual Review of Pathology: Mechanisms of Disease* (Vol. 15). https://doi.org/10.1146/annurev-pathmechdis-012419-032742

Moustaqim-barrette, A., Lin, Y. Q., Pradhan, S., Neely, G. G., Bellen, H. J., & Tsuda, H. (2014). The amyotrophic lateral sclerosis 8 protein, VAP, is required for ER protein quality control. *Human Molecular Genetics*, *23*(8). https://doi.org/10.1093/hmg/ddt594

Murphy, S. E., & Levine, T. P. (2016). VAP, a Versatile Access Point for the Endoplasmic Reticulum: Review and analysis of FFAT-like motifs in the VAPome. *Biochimica et Biophysica Acta - Molecular and Cell Biology of Lipids*, *1861*(8). https://doi.org/10.1016/j.bbalip.2016.02.009

Nascimbeni, A. C., Giordano, F., Dupont, N., Grasso, D., Vaccaro, M. I., Codogno, P., & Morel, E. (2017). ER –plasma membrane contact sites contribute to autophagosome biogenesis by regulation of local PI 3P synthesis . *The EMBO Journal*, *36*(14). https://doi.org/10.15252/embj.201797006

Nicolle, C., & Manceaux, L. H. (1908). Sur une infection à corps de Leishman (ou organismes voisins) du gondi. *Comptes Rendus Hebdomadaires Des Séances de l'Académie Des Sciences*, *147*.

Nishimura, Y., Hayashi, M., Inada, H., & Tanaka, T. (1999). Molecular cloning and characterization of mammalian homologues of vesicle-associated membrane protein-associated (VAMP-associated) proteins. *Biochemical and Biophysical Research Communications*, *254*(1). https://doi.org/10.1006/bbrc.1998.9876

Nolan, S. J., Romano, J. D., & Coppens, I. (2017). Host lipid droplets: An important source of lipids salvaged by the intracellular parasite Toxoplasma gondii. *PLoS Pathogens*, *13*(6). https://doi.org/10.1371/journal.ppat.1006362

Nolan, S. J., Romano, J. D., Luechtefeld, T., & Coppens, I. (2015). Neospora caninum recruits host cell structures to its parasitophorous vacuole and salvages lipids from organelles. *Eukaryotic Cell*, *14*(5). https://doi.org/10.1128/EC.00262-14

Nolte, H., MacVicar, T. D., Tellkamp, F., & Krüger, M. (2018). Instant Clue: A Software Suite for Interactive Data Visualization and Analysis. *Scientific Reports*, *8*(1). https://doi.org/10.1038/s41598-018-31154-6

Obara, C. J., Nixon-Abell, J., Moore, A. S., Riccio, F., Hoffman, D. P., Shtengel, G., Xu, C. S., Schaefer, K., Pasolli, H. A., Masson, J. B., Hess, H. F., Calderon, C. P., Blackstone, C., & Lippincott-Schwartz, J. (2024). Motion of VAPB molecules reveals ER–

mitochondria contact site subdomains. *Nature*, *626*(7997). https://doi.org/10.1038/s41586-023-06956-y

Olkkonen, V. M., & Ikonen, E. (2024). Getting to Grips with the Oxysterol-Binding Protein Family – a Forty Year Perspective. In *Contact* (Vol. 7). SAGE Publications Inc. https://doi.org/10.1177/25152564241273598

Osman, C., Voelker, D. R., & Langer, T. (2011). Making heads or tails of phospholipids in mitochondria. In *Journal of Cell Biology* (Vol. 192, Issue 1). https://doi.org/10.1083/jcb.201006159

Park, C. Y., Hoover, P. J., Mullins, F. M., Bachhawat, P., Covington, E. D., Raunser, S., Walz, T., Garcia, K. C., Dolmetsch, R. E., & Lewis, R. S. (2009). STIM1 Clusters and Activates CRAC Channels via Direct Binding of a Cytosolic Domain to Orai1. *Cell*, *136*(5). https://doi.org/10.1016/j.cell.2009.02.014

Peretti, D., Dahan, N., Shimoni, E., Hirschberg, K., & Lev, S. (2008). Coordinated lipid transfer between the endoplasmic reticulum and the golgi complex requires the VAP proteins and is essential for Golgi-mediated transport. *Molecular Biology of the Cell*, *19*(9). https://doi.org/10.1091/mbc.E08-05-0498

Pernas, L. (2019). mSphere of Influence: Finding a Direction—How Do Mitochondria Know Where To Go? *MSphere*, *4*(4). https://doi.org/10.1128/msphere.00321-19

Pernas, L., Adomako-Ankomah, Y., Shastri, A. J., Ewald, S. E., Treeck, M., Boyle, J. P., & Boothroyd, J. C. (2014). Toxoplasma Effector MAF1 Mediates Recruitment of Host Mitochondria and Impacts the Host Response. *PLoS Biology*, *12*(4). https://doi.org/10.1371/journal.pbio.1001845

Pernas, L., Bean, C., Boothroyd, J. C., & Scorrano, L. (2018). Mitochondria Restrict Growth of the Intracellular Parasite Toxoplasma gondii by Limiting Its Uptake of Fatty Acids. *Cell Metabolism*, *27*(4). https://doi.org/10.1016/j.cmet.2018.02.018

Pietraszewska-Bogiel, A., & Gadella, T. W. J. (2011). FRET microscopy: From principle to routine technology in cell biology. *Journal of Microscopy*, *241*(2). https://doi.org/10.1111/j.1365-2818.2010.03437.x

Poupel, O., Boleti, H., Axisa, S., Couture-Tosi, E., & Tardieux, I. (2000). Toxofilin, a novel actin-binding protein from Toxoplasma gondii, sequesters actin monomers and caps actin filaments. *Molecular Biology of the Cell*, *11*(1). https://doi.org/10.1091/mbc.11.1.355

R Core Computing Team. (2017). R: A Language and Environment for Statistical Computing. *R Foundation for Statistical Computing, Vienna, Austria*, *0*.

Rastogi, S., Cygan, A. M., & Boothroyd, J. C. (2019). Translocation of effector proteins into host cells by Toxoplasma gondii. In *Current Opinion in Microbiology* (Vol. 52). https://doi.org/10.1016/j.mib.2019.07.002

Raychaudhuri, S., & Prinz, W. A. (2010). The diverse functions of oxysterol-binding proteins. In *Annual Review of Cell and Developmental Biology* (Vol. 26). https://doi.org/10.1146/annurev.cellbio.042308.113334

Ritchie, M. E., Phipson, B., Wu, D., Hu, Y., Law, C. W., Shi, W., & Smyth, G. K. (2015). Limma powers differential expression analyses for RNA-sequencing and microarray studies. *Nucleic Acids Research*, *43*(7). https://doi.org/10.1093/nar/gkv007

Rizzuto, R., Pinton, P., Carrington, W., Fay, F. S., Fogarty, K. E., Lifshitz, L. M., Tuft, R. A., & Pozzan, T. (1998). Close contacts with the endoplasmic reticulum as determinants of mitochondrial Ca2+ responses. *Science*, *280*(5370). https://doi.org/10.1126/science.280.5370.1763

Robert-Gangneux, F., & Dardé, M. L. (2012). Epidemiology of and diagnostic strategies for toxoplasmosis. In *Clinical Microbiology Reviews* (Vol. 25, Issue 2). https://doi.org/10.1128/CMR.05013-11

Rocha, N., Kuijl, C., Van Der Kant, R., Janssen, L., Houben, D., Janssen, H., Zwart, W., & Neefjes, J. (2009). Cholesterol sensor ORP1L contacts the ER protein VAP to control Rab7-RILP-p150Glued and late endosome positioning. *Journal of Cell Biology*, *185*(7). https://doi.org/10.1083/jcb.200811005

Rostovtseva, T. K., & Bezrukov, S. M. (1998). ATP transport through a single mitochondrial channel, VDAC, studied by current fluctuation analysis. *Biophysical Journal*, *74*(5). https://doi.org/10.1016/S0006-3495(98)77945-7

Rowland, A. A., Chitwood, P. J., Phillips, M. J., & Voeltz, G. K. (2014). ER contact sites define the position and timing of endosome fission. *Cell*, *159*(5). https://doi.org/10.1016/j.cell.2014.10.023

Ryter, S. W., Cloonan, S. M., & Choi, A. M. K. (2013). Autophagy: A critical regulator of cellular metabolism and homeostasis. In *Molecules and Cells* (Vol. 36, Issue 1). https://doi.org/10.1007/s10059-013-0140-8

Saeij, J. P. J., Boyle, J. P., & Boothroyd, J. C. (2005). Differences among the three major strains of Toxoplasma gondii and their specific interactions with the infected host. In *Trends in Parasitology* (Vol. 21, Issue 10). https://doi.org/10.1016/j.pt.2005.08.001

Saeij, J. P. J., Coller, S., Boyle, J. P., Jerome, M. E., White, M. W., & Boothroyd, J. C. (2007). Toxoplasma co-opts host gene expression by injection of a polymorphic kinase homologue. *Nature*, *445*(7125). https://doi.org/10.1038/nature05395

Schmidt, O., Pfanner, N., & Meisinger, C. (2010). Mitochondrial protein import: From proteomics to functional mechanisms. In *Nature Reviews Molecular Cell Biology* (Vol. 11, Issue 9). https://doi.org/10.1038/nrm2959

Schröder, M., & Kaufman, R. J. (2005). The mammalian unfolded protein response. In *Annual Review of Biochemistry* (Vol. 74). https://doi.org/10.1146/annurev.biochem.73.011303.074134

Scorrano, L., De Matteis, M. A., Emr, S., Giordano, F., Hajnóczky, G., Kornmann, B., Lackner, L. L., Levine, T. P., Pellegrini, L., Reinisch, K., Rizzuto, R., Simmen, T., Stenmark, H., Ungermann, C., & Schuldiner, M. (2019). Coming together to define membrane contact sites. *Nature Communications*, *10*(1). https://doi.org/10.1038/s41467-019-09253-3

Shalem, O., Sanjana, N. E., & Zhang, F. (2015). High-throughput functional genomics using CRISPR-Cas9. In *Nature Reviews Genetics* (Vol. 16, Issue 5). https://doi.org/10.1038/nrg3899

Sinai, A. P., & Joiner, K. A. (2001). The Toxoplasma gondii protein ROP2 mediates host organelle association with the parasitophorous vacuole membrane. *Journal of Cell Biology*, *154*(1). https://doi.org/10.1083/jcb.200101073

Sinai, A. P., Webster, P., & Joiner, K. A. (1997). Association of host cell endoplasmic reticulum and mitochondria with the Toxoplasma grondii parasitophorous vacuole membrane: A high affinity interaction. *Journal of Cell Science*, *110*(17). https://doi.org/10.1242/jcs.110.17.2117

Smirnova, E., Griparic, L., Shurland, D. L., & Van der Bliek, A. M. (2001). Dynamin-related protein Drp1 is required for mitochondrial division in mammalian cells. *Molecular Biology of the Cell*, *12*(8). https://doi.org/10.1091/mbc.12.8.2245

Söderberg, O., Gullberg, M., Jarvius, M., Ridderstråle, K., Leuchowius, K. J., Jarvius, J., Wester, K., Hydbring, P., Bahram, F., Larsson, L. G., & Landegren, U. (2006). Direct observation of individual endogenous protein complexes in situ by proximity ligation. *Nature Methods*, *3*(12). https://doi.org/10.1038/nmeth947

Splendore, A. (1908). Un nuovo protozoa parassita deconigli incontrato nelle lesioni anatomiche d'une malattia che ricorda in molti punti il Kala-azar dell'uoma. Nota preliminare pel. *Rev Soc Sci Sao Paulo*, *3*.

Stanhope, R., Flora, E., Bayne, C., & Derré, I. (2017). IncV, a FFAT motif-containing Chlamydia protein, tethers the endoplasmic reticulum to the pathogen-containing vacuole. *Proceedings of the National Academy of Sciences of the United States of America*, *114*(45). https://doi.org/10.1073/pnas.1709060114

Su, C., Evans, D., Cole, R. H., Kissinger, J. C., Ajioka, J. W., & Sibley, L. D. (2003). Recent expansion of Toxoplasma through enhanced oral transmission. *Science*, *299*(5605). https://doi.org/10.1126/science.1078035

Suss-Toby, E., Zimmerberg, J., & Ward, G. E. (1996). Toxoplasma invasion: The parasitophorous vacuole is formed from host cell plasma membrane and pinches off via a fission pore. *Proceedings of the National Academy of Sciences of the United States of America*, *93*(16). https://doi.org/10.1073/pnas.93.16.8413

Suzuki, Y., Orellana, M. A., Schreiber, R. D., & Remington, J. S. (1988). Interferon-γ: The major mediator of resistance against Toxoplasma gondii. *Science*, *240*(4851). https://doi.org/10.1126/science.3128869

Swayne, T. C., Zhou, C., Boldogh, I. R., Charalel, J. K., McFaline-Figueroa, J. R., Thoms, S., Yang, C., Leung, G., McInnes, J., Erdmann, R., & Pon, L. A. (2011). Role for cER and Mmr1p in anchorage of mitochondria at sites of polarized surface growth in budding yeast. *Current Biology*, *21*(23). https://doi.org/10.1016/j.cub.2011.10.019

Szabadkai, G., Bianchi, K., Várnai, P., De Stefani, D., Wieckowski, M. R., Cavagna, D., Nagy, A. I., Balla, T., & Rizzuto, R. (2006). Chaperone-mediated coupling of endoplasmic reticulum and mitochondrial Ca2+ channels. *Journal of Cell Biology*, *175*(6). https://doi.org/10.1083/jcb.200608073

Tubbs, E., & Rieusset, J. (2016). Study of endoplasmic reticulum and mitochondria interactions by in situ proximity ligation assay in fixed cells. *Journal of Visualized Experiments*, *2016*(118). https://doi.org/10.3791/54899

Valm, A. M., Cohen, S., Legant, W. R., Melunis, J., Hershberg, U., Wait, E., Cohen, A. R., Davidson, M. W., Betzig, E., & Lippincott-Schwartz, J. (2017). Applying systems-level spectral imaging and analysis to reveal the organelle interactome. In *Nature* (Vol. 546, Issue 7656). https://doi.org/10.1038/nature22369

Valverde, D. P., Yu, S., Boggavarapu, V., Kumar, N., Lees, J. A., Walz, T., Reinisch, K. M., & Melia, T. J. (2019). ATG2 transports lipids to promote autophagosome biogenesis. *Journal of Cell Biology*, *218*(6). https://doi.org/10.1083/JCB.201811139

Vance, J. E. (1990). Phospholipid synthesis in a membrane fraction associated with mitochondria. *Journal of Biological Chemistry*, *265*(13). https://doi.org/10.1016/s0021-9258(19)39106-9

Vance, J. E., & Shiao, Y. J. (1996). Intracellular trafficking of phospholipids: Import of phosphatidylserine into mitochondria. *Anticancer Research*, *16*(3 B).

Voeltz, G. K., Sawyer, E. M., Hajnóczky, G., & Prinz, W. A. (2024). Making the connection: How membrane contact sites have changed our view of organelle biology. In *Cell* (Vol. 187, Issue 2). https://doi.org/10.1016/j.cell.2023.11.040

Vormittag, S., Ende, R. J., Derré, I., & Hilbi, H. (2023a). Pathogen vacuole membrane contact sites - Close encounters of the ffth kind. In *MicroLife* (Vol. 4). https://doi.org/10.1093/femsml/uqad018

Vormittag, S., Ende, R. J., Derré, I., & Hilbi, H. (2023b). Pathogen vacuole membrane contact sites - Close encounters of the ffth kind. In *MicroLife* (Vol. 4). https://doi.org/10.1093/femsml/uqad018

Vormittag, S., Hüsler, D., Haneburger, I., Kroniger, T., Anand, A., Prantl, M., Barisch, C., Maaß, S., Becher, D., Letourneur, F., & Hilbi, H. (2023). Legionella - and host-driven lipid flux at LCV-ER membrane contact sites promotes vacuole remodeling . *EMBO Reports*, *24*(3). https://doi.org/10.15252/embr.202256007

Wang, P., Li, S., Zhao, Y., Zhang, B., Li, Y., Liu, S., Du, H., Cao, L., Ou, M., Ye, X., Li, P., Gao, X., Wang, P., Jing, C., Shao, F., Yang, G., & You, F. (2019). The GRA15 protein from Toxoplasma gondii enhances host defense responses by activating the interferon stimulator STING. *Journal of Biological Chemistry*, *294*(45). https://doi.org/10.1074/jbc.RA119.009172

Wang, Y., Sangaré, L. O., Paredes-Santos, T. C., Hassan, M. A., Krishnamurthy, S., Furuta, A. M., Markus, B. M., Lourido, S., & Saeij, J. P. J. (2020). Genome-wide screens identify Toxoplasma gondii determinants of parasite fitness in IFNγ-activated murine macrophages. *Nature Communications*, *11*(1). https://doi.org/10.1038/s41467-020-18991-8

Weber-Boyvat, M., Kentala, H., Lilja, J., Vihervaara, T., Hanninen, R., Zhou, Y., Peränen, J., Nyman, T. A., Ivaska, J., & Olkkonen, V. M. (2015). OSBP-related protein 3 (ORP3) coupling with VAMP-associated protein A regulates R-Ras activity. *Experimental Cell Research*, *331*(2). https://doi.org/10.1016/j.yexcr.2014.10.019

Weiss, L. M., & Dubey, J. P. (2009). Toxoplasmosis: A history of clinical observations. In *International Journal for Parasitology* (Vol. 39, Issue 8). https://doi.org/10.1016/j.ijpara.2009.02.004

Wilking, H., Thamm, M., Stark, K., Aebischer, T., & Seeber, F. (2016). Prevalence, incidence estimations, and risk factors of Toxoplasma gondii infection in Germany: A representative, cross-sectional, serological study. *Scientific Reports*, *6*. https://doi.org/10.1038/srep22551

Wilson, E. L., Yu, Y., Leal, N. S., Woodward, J. A., Patikas, N., Morris, J. L., Field, S. F., Plumbly, W., Paupe, V., Chowdhury, S. R., Antrobus, R., Lindop, G. E., Adia, Y. M., Loh, S. H. Y., Prudent, J., Martins, L. M., & Metzakopian, E. (2024). Genome-wide CRISPR/Cas9 screen shows that loss of GET4 increases mitochondria-endoplasmic reticulum contact sites and is neuroprotective. *Cell Death and Disease*, *15*(3). https://doi.org/10.1038/s41419-024-06568-y

Wolf, a, Cowen, D., & Paige, B. H. (1939). Toxoplasmic encephalomyelitis: III. A new case of granulomatous encephalomyelitis due to a protozoon. *The American Journal of Pathology*, *15*(6).

Wolf, A., Cowen, D., & Paige, B. (1939). Human toxoplasmosis: Occurrence in infants as an encephalomyelitis verification by transmission to animals. *Science*, *89*(2306). https://doi.org/10.1126/science.89.2306.226

Wu, H., Carvalho, P., & Voeltz, G. K. (2018). Here, there, and everywhere: The importance of ER membrane contact sites. *Science*, *361*(6401). https://doi.org/10.1126/science.aan5835

Wu, M. M., Buchanan, J. A., Luik, R. M., & Lewis, R. S. (2006). Ca2+ store depletion causes STIM1 to accumulate in ER regions closely associated with the plasma membrane. *Journal of Cell Biology*, *174*(6). https://doi.org/10.1083/jcb.200604014

Young, J., Dominicus, C., Wagener, J., Butterworth, S., Ye, X., Kelly, G., Ordan, M., Saunders, B., Instrell, R., Howell, M., Stewart, A., & Treeck, M. (2019). A CRISPR platform for targeted in vivo screens identifies Toxoplasma gondii virulence factors in mice. *Nature Communications*, *10*(1). https://doi.org/10.1038/s41467-019-11855-w

Zhang, S. L., Yeromin, A. V., Zhang, X. H. F., Yu, Y., Safrina, O., Penna, A., Roos, J., Stauderman, K. A., & Cahalan, M. D. (2006). Genome-wide RNAi screen of Ca2+ influx identifies genes that regulate Ca2+ release-activated Ca2+ channel activity. *Proceedings of the National Academy of Sciences of the United States of America*, *103*(24). https://doi.org/10.1073/pnas.0603161103

Zhang, S. L., Yu, Y., Roos, J., Kozak, J. A., Deerinck, T. J., Ellisman, M. H., Stauderman, K. A., & Cahalan, M. D. (2005). STIM1 is a Ca2+ sensor that activates CRAC channels and migrates from the Ca2+ store to the plasma membrane. *Nature*, *437*(7060). https://doi.org/10.1038/nature04147

Zhou, Y., Srinivasan, P., Razavi, S., Seymour, S., Meraner, P., Gudlur, A., Stathopulos, P. B., Ikura, M., Rao, A., & Hogan, P. G. (2013). Initial activation of STIM1, the regulator of store-operated calcium entry. *Nature Structural and Molecular Biology*, *20*(8). https://doi.org/10.1038/nsmb.2625